General Disclaimer

One or more of the Following Statements may affect this Document

- This document has been reproduced from the best copy furnished by the organizational source. It is being released in the interest of making available as much information as possible.

- This document may contain data, which exceeds the sheet parameters. It was furnished in this condition by the organizational source and is the best copy available.

- This document may contain tone-on-tone or color graphs, charts and/or pictures, which have been reproduced in black and white.

- This document is paginated as submitted by the original source.

- Portions of this document are not fully legible due to the historical nature of some of the material. However, it is the best reproduction available from the original submission.

NASA TECHNICAL MEMORANDUM NASA TM-77413

MICROSCOPIC ASPECTS OF THE EFFECT OF FRICTION REDUCERS AT THE LUBRICATION LIMIT

J.-L. Mansot

Translation of "Aspects microscopiques de l'action des réducteurs de frottement en lubrification limite", Lyon Ecole Centrale, Lyon, France, Doctor of Engineering Thesis, 1982, pp. 1-140.

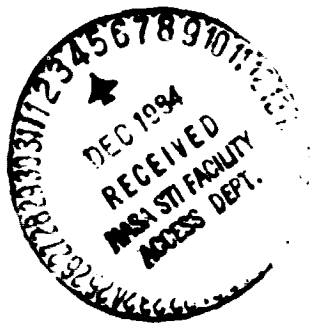

NATIONAL AERONAUTICS AND SPACE ADMINISTRATION
WASHINGTON, D.C. 20546 JUNE 1984

STANDARD TITLE PAGE

1. Report No. NASA TM-77413	2. Government Accession No.	3. Recipient's Catalog No.
4. Title and Subtitle: Microscopic aspects of the effect of friction reducers at the lubrication limit.		5. Report Date: June 1984 6. Performing Organization Code
7. Author(s): J.-L. Mansot.		8. Performing Organization Report No. 10. Work Unit No.
9. Performing Organization Name and Address: Leo Kanner Associates, Redwood City, California 94063		11. Contract or Grant No. NASw-3541 13. Type of Report and Period Covered: Translation
12. Sponsoring Agency Name and Address: National Aeronautics and Space Administration, Washington, D.C. 20546		14. Sponsoring Agency Code

15. Supplementary Notes

"Aspects microscopiques de l'action des réducteurs de frottement en lubrification limite", Lyon Ecole Centrale, Lyon, France, Doctor of Engineering Thesis, 1982, pp. 1-140.

16. Abstract

An attempt is made to analytically model the physico-chemical properties of lubricants and their capacity to reduce friction. A technique of frozen fracturing of the lubricants was employed to study the dispersion of additives throughout a lubricant. Adsorption was observed at the liquid-solid interface, which was the region where the solid and lubricant met, and the molecular dispersion of the additive enhanced the effectiveness of the lubricant. The electrically conductive characteristics of the lubricant at the friction interface indicated the presence of tunneling effects. The Bethe model was used to examine the relationship between the coefficient of friction and the variation of interface thickness. The electron transport permitted an inelastic tunnel electron spectroscopic investigation of the molecular transformations undergone by the additive during friction episodes.

17. Key Words (Selected by Author(s))	18. Distribution Statement: "Unclassified-Unlimited"

19. Security Classif. (of this report)	20. Security Classif. (of this page)	21. No. of Pages	22.
"Unclassified"	"unclassified"	97	

Foreword

The present work has been carried out at the Surfaces Technology Laboratory of the Central School of Lyon.

I would like to express all my gratitude to Mr. Moiroux, School Director, for having accepted me into his institution.

I would particularly like to express my sincere gratitude to Professor J. M. Georges, the person responsible for the Surfaces Technology Laboratory, for the interest which he has shown in my work and for having allowed me to conduct them with the best conditions.

I am very appreciative of the honor which Professor Gobin has given to me by agreeing to preside over the Jury of this thesis.

My very deep gratitude goes to Mrs. L. Ter Minassian Saraga, Research Director at CNRS, for the interest which she has shown in the nature of my work; I thank her for having agreed to participate on the Jury.

I thank Professor O. Paulmier, who has done me the honor of examining this thesis and has agreed to be a member of this Jury.

I would like to thank Mr. S. J. Candan for the assistance which he has given to me during this work, as well as the enthusiasm which he has imparted to me.

I thank the PCUK Society for having procured for us the product which is at the origin of this study, and more particularly M. Eudeline of C.A.L. who agreed to participate on this Jury. My gratitude goes most particularly to Mr. J. M. Martin, Teaching Assistant, for the constant attention which he has shown in my work, as well as the assistance which he has never ceased to lavish during the entire duration of this work.

During this study, we have made contacts with the manufacturers concerned by our problems, and in particular the ELF Aquitaine Society and the Renault Corporation. On this occasion, allow me to thank Mr. Constant (ELF) and Mr. Daignes (RNUR) for the constructive discussions which we have had.

May my comrades of the Laboratory find here the expression of my sincere thanks for the assistance and friendship which they have given to me during these past two years at the Laboratory. I could not forget all those who have contributed from near and far to the presentation of this thesis, and more particularly to Miss S. Ferlay who was assigned the tedious friction work.

Regarding members of the Surface Technology Laboratory, I would like to thank the General Commission of Scientific and Technical Research for the financial assistance and confidence which it has granted me during the entire duration of these studies.

General Outline of the Thesis Pages /1*

*Numbers in the margin indicate pagination in the foreign text.

MICROSCOPIC ASPECTS OF THE EFFECT OF FRICTION REDUCERS AT THE LUBRICATION LIMIT

J.-L. Mansot
L'Ecole Centrale De Lyon
Lyon, France

Chapter 0 /2

Introduction

0-1. Some Reminders on Lubricants

0-1.1. Role of the Lubricant

0-1.2 Classification of Lubricants

0-11. Objective of the Work

Chapter 0 /3

Introduction

Although lubrication has a long history, conception of present-day lubricants still depends largely on empiricism. However, during these last few years, a significant effort has been undertaken in a large number of research laboratories in order to study the basic mechanisms in the action of these products and in order to better conceive lubricants, that is to say to discover the formulations best adapted to the applications for which they are designed. It is thus necessary today to deal with the lubricants at the same time as the materials constituting the surfaces of frictional contact.

0-1. Some Reminders on Lubricants

0.1.1. Role of the Lubricant

The lubricant function consists of reducing destructive interactions (friction, wear) at the time of relative shifting of surfaces in contact within machinery.

To this short definition, it is necessary to add several remarks of significance:
-The "anti-wear" lubricant (A.U.) does not necessarily procure low values of the coefficient of friction; in other words the basic mechanisms of friction and wear are certainly different; /4
-The wear of a part is more difficult to quantify than the coefficient of friction which is associated with it. Indeed, it can correspond to an effective loss in weight of the piece considered, but often it occurs in the form of a deterioration of the surfaces in frictional contact through processes of plastic deformation, adhesion, or transfer

without necessarily implying a weight loss;
-The majority of present-day lubricants are multi-functional, that is to say that besides their proper lubricating function, they can fulfil a certain number of also very important other functions.

As an example, table 0.1 presents, in the case of motor oils, the properties necessary for good functionning of internal combustion engines.

TABLE 0.1. PROPERTIES NECESSARY IN A LUBRICATING OIL FOR GOOD FUNCTIONNING OF INTERNAL COMBUSTION ENGINES.

Mechanical properties	Physico-chemical properties
-reduction of friction forces	-thermal and oxidation stability
-protection against all types of wear	-detergency/dispersion (elimination of impurities, gums, and deposits)
-ease of starting (pour point depressant)	-anti-foam
	-anti-corrosion, anti-rust

Thus, lubricants are often complex mixtures of chemical products with perhaps ten different compounds.

0.1.2. Classification of Lubricants /5

A certain number of classifications of lubricants have been defined in the literature (Schilling, 1972), these being able to be classified according to their function, their capacity to reduce energy losses through friction, or also their tendency to reduce wear in certain machinery. It is nevertheless convenient to define them according to the physico-chemical state in which they occur. Table 0.2 presents such a classification of the principal lubricants currently encountered.

The characterization of lubricants presented in table 0.2 appears /6
to be relatively simple. Nevertheless, taking into consideration the number of properties which a lubricant must satisfy, it is not rare, particularly in the case where the continuous phase is liquid, to encounter several physico-chemical states within the lubricant (true solution + colloidal solution + suspension).

To this very simple classification of lubricants, it is necessary to add another which demonstrates, according to the lubrication regime implicated, what the physical and/or chemical properties are which have made a contribution. Table 0.3 presents such a classificaiton for liquid lubricants.

TABLE 0.2. CLASSIFICATION OF THE MOST STANDARD LUBRICANTS, BASED ON THEIR PHYSICO-CHEMICAL STATE.

Nature of the continuous phase	Nature of the dispersed phase	Nature of the mixture	Example of application
gas	—	gas	gas bearings
	liquid	aerosol	oil mists
	solid	aerosol	powdery solid lubricant
liquid	liquid	true or colloidal solution	—
		microcrenulation or emulsion	fluids of layer put into shape
	solid	true or colloidal solution	—
		suspension	graphite oils greases
solid	liquid	solid emulsion	porous impregnated materials
	solid	solid earth	autolubricating materials

0.2. Objective of the Work /7

The work will only concern the realm of lubrication limits where empiricism still largely governs the formulation of lubricants.

We have thus proposed, within the framework of this thesis, to study the relationships existing between the physico-chemical properties of lubricant models and their capacity to reduce friction.

TABLE 0.3. PROPERTIES OF THE LUBRICANT OPERATING ACCORDING TO THE LUBRICATION REGIME IMPLICATED

Lubrication regime	$\frac{h}{R_a}$	$\frac{h}{h_m}$	Characteristics put into play by the lubricant	Role of the lubricant
Hydrodynamics	6.7	100	Physical and macroscopic: viscosity of the base	Separation of the surfaces by interaction through a thick oil film
Elasto-hydrodynamics	2-3	30-80	Physical and macroscopic: viscosity of the base	Separation of the surfaces by a thick oil film
Mixed	0.8	10-30	Physical and physico-chemical: viscosity of the base, action of the additives	Separation of the surfaces by interaction through an oil film, protection of the surfaces by slow formation of a tribochemical film
Boundary	0.08	1-10	Physico-chemical action of the additive	Protection of surfaces by rapid formation of a tribochemical film due to the degradation of the anti-wear additives

h = thickness of the interface separating the surfaces

R_a = equivalent rugosity of the two surfaces

h_m = molecular weight of the additive present in the oil

Chapter I /8

Application of the Freezing Fracturing Technique to the Study of Lubricants

I-1. Presentation of the Freezing Fracturing Technique

I-2. Description of the Technique

I-2.1. Block Diagram of Sample Preparation

I-2.2. Diagram of the Apparatus Used

I-3. Detailed Description of Different Stages in Sample Preparation

I-3.1. Freezing of Samples

I-3.2. Fracturing of Samples

I-3.3. Replication of Surfaces

I-3.4. Recovery and Cleaning of Replicates

I-4. Examination of Replicates by Electron Microscopy

I-5. Application of the Freezing Fracturing Technique in the Anhydrous Environment Constituted by Lubricants

I-5.1. Experimental Conditions

I-5.2. Selection of the Paraffin Reference Base

I-5.3. Study of the Paraffin/Detergent System

I-5.4. Study of a Paraffin/Index of Viscosity Improvement System

I-5.5. Application of the Freezing Fracturing Technique to the Study of Completely Formulated Oils

I-5.5.1. Unused Oil /9

I-5.5.2. Used Oil

I-5.6. Application of the Freezing Fracturing Technique to the Study of Greases

I-6. Conclusion

Chapter I /10

Application of the Freezing Fracturing Technique to the Study of Lubricants

As we have seen previously, the majority of continuous phase liquid lubricants occur in the form of more or less complex dispersions, where for obvious reasons the droplet or aggregate particles have sizes unable to exceed several microns.

In order to study the structure of this type of dispersion, a certain number of techniques has already been placed into operation. The principal ones are grouped in table I.1. In the discussion of these, we have to note the important place occupied by electron microscopy techniques in the study of dispersions, and more particularly cryoscouring and freezing fracturing, which allow us to obtain a significant amount of data on the structure of the product studied (size, distribution of size, form, internal and/or external structure of the particles, arrangement of these within the continuous phase, ...). The advantages of these two techniques are nevertheless counterbalanced by the numerous possibilities of artifacts (freezing, fracturing, contamination) capable of leading to serious errors of interpretation. The freezing fracturing technique having been selected as the method for investigation in order to study the structure of lubricants, we will see during the following paragraphs how to identify and/or avoid the inherent artifacts of this method.

I.1. Presentation of the Freezing Fracturing Technique /12

Freezing fracturing is a method which allows us to study in situ the particles of a dispersion by transmission electron microscopy (T.E.M.). This technique has particularly been developed to study the biological environment where it allows us to obtain data on the external and/or internal structure of micro-organisms, according to which the fracturing unrolls at the surface or through these (E. L. Benedetti and P. Favard, 1973). In the case of more standard dispersions, this method allows us to estimate besides the size, the form and structure of the dispersed particles, their arrangement within the continuous phase (in the case where there is no freezing artifact) (S. Jöstrand, 1979). This chapter has the objective of presenting the cryo-fracturing technique, its possibilities and its limitations, as well as its applicability to the study of lubricants.

I.2. Description of the Freezing Fracturing Technique

I.2.1. Block Diagram of Sample Preparation

The following process to prepare the sample is presented in figure I.1. The different steps will be described in detail in the following paragraphs.

TABLE I.1. PRINCIPAL TECHNIQUES USED TO STUDY DISPERSIONS /11

	Technique	Data obtained	Dispersion to which technique applies	Problems Connected with technique
Optical Techniques	Standard light diffusion	Mass and form of particles	All dispersions	Dispersions must not be very absorbent or else dilution with the possibility of perturbation of the original structure
	Quasi-elastic light diffusion	Size of particles	All dispersions	
	Turbidimetry	Size of particles	All dispersions	
	Optical microscopy	Size and form of particles	Only suspensions	
Mechanical Techniques	Ferrography	Size of particles	Suspensions of ferromagnetic particles	
	Fractional centrifugation			
Conductometric Techniques	Coulter counter	Size of particles	All dispersions	Perturbation of original structure by dilution with electrolyte
Chromatographic techniques	Gel Permeation	Mass of Particles	Particularly polymeric dispersions	
Scanning, and transmission and Electron Microscopy Techniques	Deposit of dispersion on grill, elimination of continuous phase. Direct examination by MET or MEB	Size and form of particles	Suspensions	Destruction of structure of dispersion artifact of aggregation
	Ultramicrotomy after replacement of continuous phase by polymerizable binder	Size and form of particles	Suspensions	Perturbation of structure by replacement of continuous phase by a binder

TABLE I.1. (CONT.)

	Technique	Data obtained	Dispersion to which technique applies	Problems Connected with technique
Scanning and Transmission Electron Microscopy Techniques (cont.)	Freezing fracturing Cryo-scouring	Size, form, distribution within continuous phase, external and/or internal structure	All dispersions	Artifacts of freezing, plastic deformation, contamination

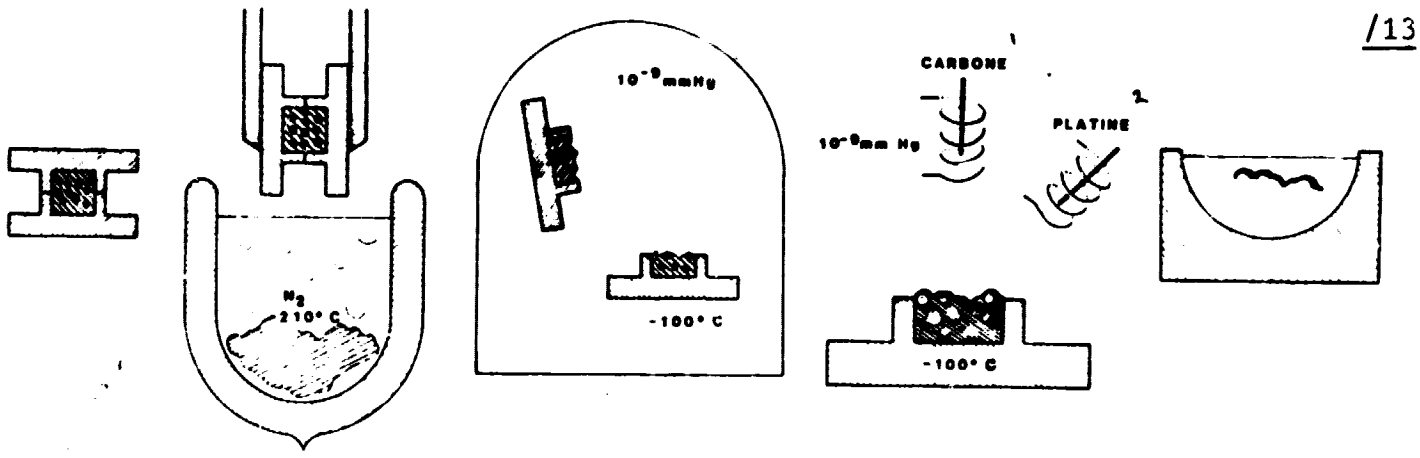

Figure I.1. Freezing Fracturing Technique.

Key: 1-Carbon; 2-Platinum

I.2.2. Diagram of the Apparatus Used

The apparatus which we use is a freezing fracturing assembly constructed by the Balzers S.A. Society equipped, in our case, to operate under ultra-high vacuum.

Figure I.2 presents the different components of the appartus.

/14

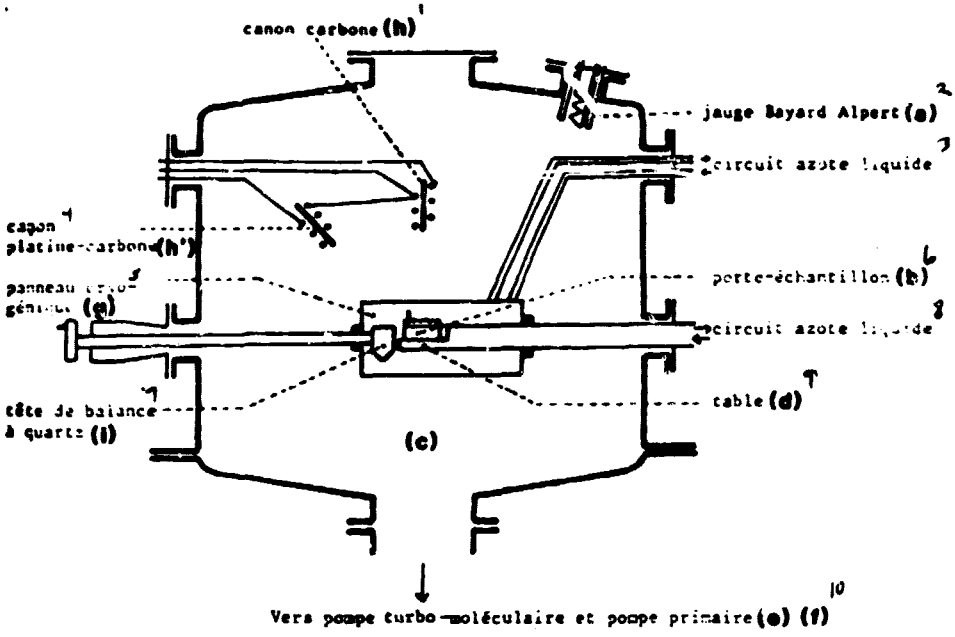

Figure I.2. Diagram of the chamber used.

Key: 1-carbon cannon;2-Bayard Alpert gauge;(a) 3- Liquid nitrogen circuit;4-platinum-carbon cannon (h'); 5-cryogenic panel (g);6-sample entrance (b); 7-quartz balance head (i);8-liquid nitrogen circuit;9-table (d);10-toward turbo-molecular pump and primary pump (e) (f)

I.3. Detailed Description of Different Stages in Sample Preparation /15

I.3.1. Freezing of samples

Inorder to solidify the sample (liquid or gel), it is necessary to freeze it. However, in the case of polyphasic compounds (dispersions), freezing must not produce any perturbation of structure (crystallization of the continuous phase inducing segregations of the dispersed phase through migration of this to the borders of the growing crystals).

It is thus necessary that freezing be an actual hardening of the system fixing the original structure of the dispersion (vitrification). To obtain such a result, it is necessary to use very high speeds of freezing, on the order of several thousandths of degrees per second. This necessitates on one hand the use of small samples having a particular shape (the spherical shape being the best), so that freezing within

the sample is carried out at a speed on the same order as at the surface of the sample, and on the other hand, the use of a very low temperature refrigerating agent, the speeds of cooling being a function of the difference in sample/refrigerating agent temperature. Table I.2 presents the different methods of freezing used and gives an approximation of the speeds of cooling obtained with each of them. The low speed of freezing obtained with liquid nitrogen is connected to the phenomenom of calefaction being produced in this refrigerating agent (formation of an insulating gaseous sheath at the surface of the sample).

TABLE I-2. DIFFERENT TECHNIQUES OF FREEZING.

Technique	Refrigerating Agent	Size and Shape of Sample	Speed of Freezing
Standard technique of immersion of the sample in the refrigerating agent	Liquid nitrogen 77 K	1 mm^3 cylindrical	100 K/s
	molten nitrogen 63K	1 mm^3 cylindrical	1000 to 5000 K/s
	Molten freon 93 K	1 mm^3 cylindrical	1000 to 5000 K/s
Cryojet: the sample is cooled by a stream of propane	liquid propane 83 K	1 mm^3 cylindrical	10^3 to 10^4 K/s
Spray freezing: the sample is pulverized in the liquid propane	liquid propane 83 K	spheres of 30 m diameter	$2 \cdot 10^4$ K/s
Projection of droplets against a cooled copper plate	liquid helium 4.3 K	droplets of 30 m diameter	$4 \cdot 10^4$ K/s
Freezing under pressure	vitrification is obtained by lowering of the melting point and the critical temperature of supercooling of the sample, in order to reduce the margin of temperature between the start of crystallization and the point of recrystallization. The speeds of freezing depend on the refrigerating agent.		

To understand the advantage of high speeds of cooling, we are going to take as an example the freezing of water. This has been studied

in extensive fashion, taking into account the very great application of the technique of cryofracturing in biology (J. E. Rash and C. S. Hudson, 1979). Thus, when we cool pure water below the fusion point of ice (273 K), it can have supercooling until impurities present in the liquid make the processes of cyrstallization start by serving as crystal nuclei (heterogeneous nucleation). /17

If no impurities exist within the water, thi, can thus be maintained in supercooling up to the temeprature of 233 K (E. L. Benedetti and P. Favard, 1973). Beyond, the water molecules themselves act as crystallization nuclei (homogeneous nucleation) and the processes of growing of ice crystals starts.

The diagram presented in figure I.3, obtained by Riehle, demonstrates, in the case of pure water, the development of the speed of growing of ice crystals as a function of the temperature.

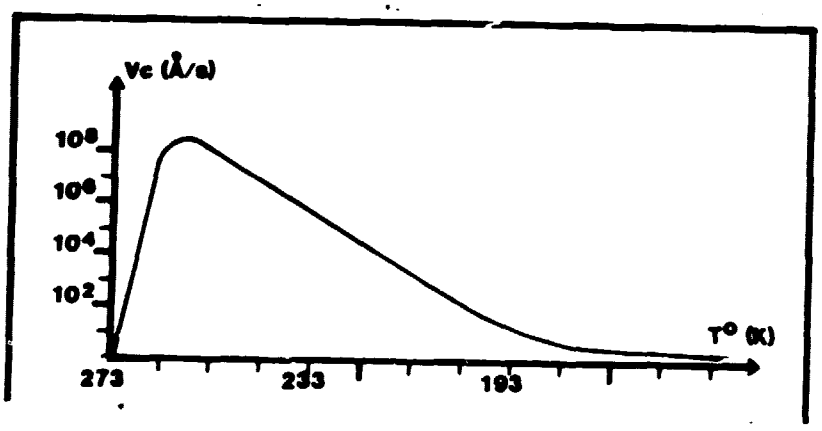

Figure I.3. Developemnt of the speed of growing of ice crystals as a function of the temperature in the case of pure water (Riehle, 1968).

This curve shows us that the speed of growing of crystals, zero at the fusion point of ice, passes through a maximum ($V_c > 10^8$ Å/s) in the vicinity of 263 K then decreases gradually (this being due to the increase of viscosity of the mixture inhibiting molecular rearrangements to form crystallites) until negligible speeds ($V_c < 1$ Å/s) at the temperature of 143 K (temperature of recrystallization of pure water). /18

These remarks thus simplify the necessity of passing very rapidly from the temperature at which the processes of crystallization start to that of recrystallization, in order that the size of crystals is negligible ($\leq$ 100 A) and consequently only perturb very slightly, if at all, the original structure of the dispersion studied. The diagram presented in figure I.4 illustrates this by demonstrating the development of the size of the ice crystals obtained as a function of speeds of freezing.

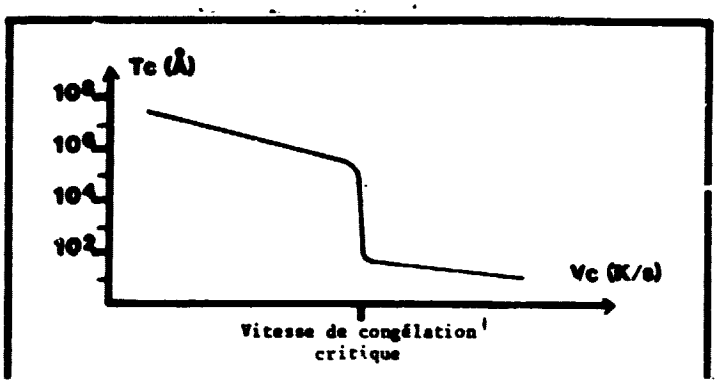

Figure I.4. Development of the weight (T_c) of ice crystals as a function of speeds of freezing (V_c) (Riehle, 1968).

Key: 1-Critical speed of freezing.

The critical speed of freezing allowing us, in the case of pure water, to obtain crystallites of size less than 100 Å has been estimated by Riehle (1968) at 10^6 K/s.

In the majority of samples which have been studied, the continuous phase constituted by water containing some percent of products in solution (alcohols, surfactants, ...) modifying its properties in relation to the phenomenon of freezing. In these cases, the literature points out to us (Moor, 1964) that speeds of freezing on the order of $2 \cdot 10^4$ K/s are sufficient to vitrify in satisfactory fashion the sample and that the temperature of recrystallization, below which the dispersion must be maintained in order to prevent it from developing, is readjusted up to approximately 193 K. /19

In the majority of our tests, relating to anhydrous environments, the sample to be frozen occurs in the form of a cylindrical droplet of approximately 1 mm^3 volume (figure I.1) maintained through capillary attraction in a sample holder constituted of two capsules, perforated in their center, of gold nickel alloy (good thermal conductor and chemically inert in relation to the products studied). Freezing is carried out by immersion of the sample capsule into molten nitrogen (63 K) prepared by storage of liquid nitrogen under primary vacuum.

In certain particular cases (continuous phase emulsion), we will be induced to use the "spray freezing" technique in order to obtain sufficient speeds to well vitrify this type of sample ($2 \cdot 10^4$ K/s). The principle of this method is detailed in figure I.5.

I.3.2. Fracturing of Samples

The samples, frozen in good condition, are then placed in a holder capsule (figure I.2.b.) maintained at the temperature of 77 K by immer-

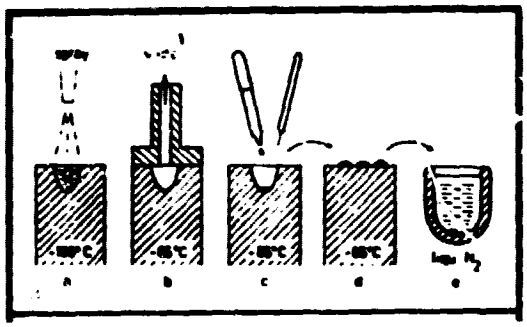

Figure I.5. Spray freezing techniques of freezing.

a) projection of the product in the form of droplets into the liquid propane
b) evaporation of the propane
c) addition of the binder
d) introduction of the droplet and binder mixture into the sample portions
e) transfer of the sample portions into the liquid nitrogen

Key: 1-Vacuum.

sion in liquid nitrogen. The holder capsule is then introduced into the vacuum chamber (figure I.2.c.), then scoured by very pure gaseous nitrogen (nitrogen U furnished by Liquid Air), then deposited on the operating table (figure I.2.d.) refrigerated at 223 K by circulation of liquid nitrogen.

The chamber is then placed under vacuum with the assistance of a pumping group constituted of a primary blade pump and a turbomolecular pump (figure I.2.e. and I.2.f.). When the pressure on the inside of the chamber is on the order of $5 \cdot 10^{-6}$ mmHg, the cryogenic panel (figure I.2.g.) is cooled up to 77 K by circulation of liquid nitrogen. The holder capsule is then reheated up to 153 K, then opened mechanically. The sample is then fractured by separation of the capsule constituting the sample holder (figure I.1.c.). The new surfaces generated by fracturing are representative of the internal structure of the dispersion studied. /21

The temperature difference maintained between the table and the cryogenic panel has two roles:
-Allowing the revelation of relief on the surfaces appearing at the time of fracturing through sublimation of the continuous phase (when this is sublimable).
-Protecting the sample from contamination.

Indeed, it is necessary to note that at low temperature the new surface generated by the fracturing processes can be contaminated very quickly by contaminants present in the chamber (at $P=10^{-6}$ mmHg), the principal constituents of the atmosphere are H_2O, CO, CO_2, H_2, and hydrocarbon vapors in the case where the secondary vacuum is obtained

with the assistance of an oil diffusion pump (Moor, 1971).

Contamination occurs according to two processes:

-Condensation of Contaminants at the Surface of the Sample

In the case of hydrocarbon vapors, the panel maintained at 77 K suffices to protect the sample by condensing the majority of these.

In the case of water vapor, the speed of contamination depends on /22
the temperature of the sample and the prevailing pressure in the chamber.

The diagrams presented in figure I.6.a. and I.6.b. demonstrate that with our experimental conditions (turbomolecular pump, cryogenic panel maintained at 77 K, sample at 153 or 173 K, P=5 10^{-8}), the risks of contamination by condensation are very limited.

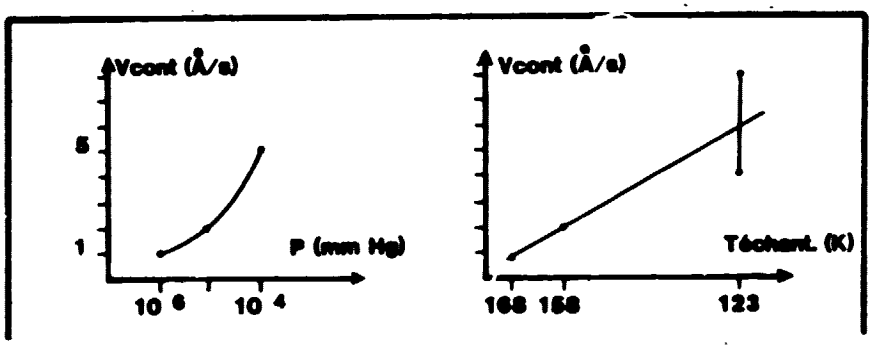

Figure I.6. Speed of contamination (V_{cont}) by condensation of water vapor of one surface.

A-at the temperature of 168 K as a function of the prevailing pressure in the chamber (J. E. Rash and S. Hudson, 1979)
B-under a pressure of 10^{-6} mmHg as a function of the temperature of the sample (J. E. Rash and S. Hudson, 1979).

-Contamination by Adsorption of Molecules Present in the Chamber (H_2O,..)

This type of contamination is practically inevitable, the surface then covering one or several layers of molecules having the disadvantage of softening of the relief and thus overestimation of the size of /23
the big particles and underestimation of that of the small ones. However, Moor (1971) points out that for a pressure of 10^{-6} mmHg and a sample temperature of 173 K, the first monolayer is established in approximately one second, and that the thickness of the adsorbed layer at

the end of one minute can be estimated at 10 or 20 Å, the speeds of adsorption decreasing as a function of the thickness of the layer. With our conditions, this type of contamination can be considered as negligible.

I.3.3. Replication of Surfaces

In the case where fracturing is followed by sublimation, replication is carried out at the time of the end of this operation. In other cases, replication is carried out immediately after fracturing of the sample in such a fashion to avoid the establishment of the replica on a surface contaminated in too significant a fashion.

The replication operation diagrammed on figure I.1 is carried out in the following fashion: two layers, one of 25 Å of platinum, the other of 300 Å of carbon, are deposited at the surface of the sample according to a respective incidence of 45° (shade) and 90° in relation to the mean plane of the surface. The deposits are carried out with the assistance of electron beam evaporators (figure I.2.h), the thickness of the layers is determined by weight with the assistance of a quartz balance set in the vicinity of the sample. The granulometry of the platinum particles allows a point by point resolution by M.E.T. of 15 to 20 Å. The platinum and carbon deposits are only separated by a few seconds, in order to avoid the establishment of a layer of contamination between them which could induce cleavage of the replica at the time of later operations thus rendering it unuseable.

I.3.4. Recovery and Cleaning of Replicates /24

The material constituting the sample is dissolved (figure I.1.e.) in a system of appropriate solvents. The replicate is then rinsed in different very pure solvents (R.P.E. solvent Carlo Erba, bidistilled water, ...) then arranged on a grid of T.E.M.

I.4. Examination of Replicates By Electron Microscopy

Figure I.7 presents the principle of transmission electron microscopy examination of a platinum carbon replicate. A schematic representation of the plate obtained, as well as the standard utilization which is made of it are presented in figure I.7.b. and I.7.c. It is necessary to note that at the time of a T.E.M. examination, the replicate can be damaged. In particular, at very strong magnifications, recrystallization of the platinum under electron beams softens the contours of shaded objects.

I.5. Application of Freezing Fracturing Technique to the Anhydrous Environment Constituted by Lubricants

In this paragraph, we present examples of applications of the

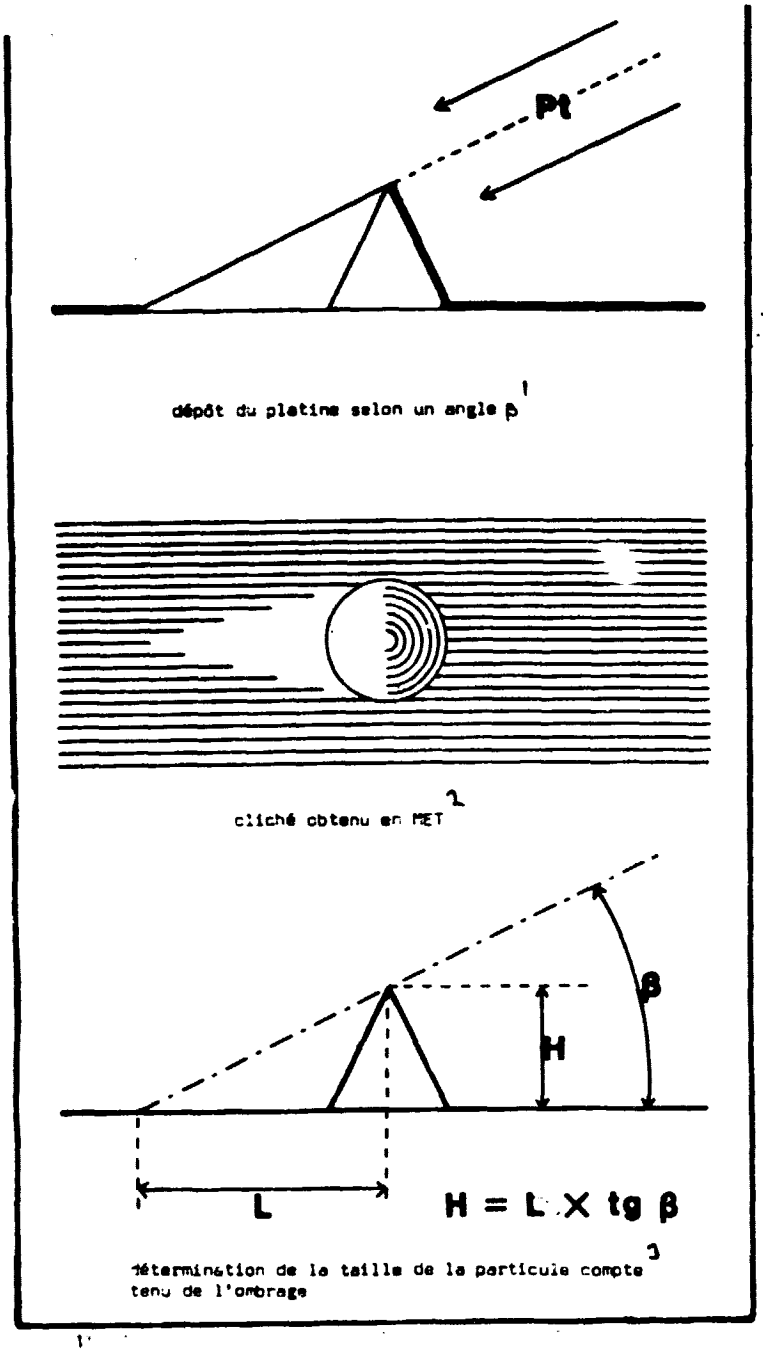

Figure I.7. Principle of examination of a replicate by transmission electron microscopy (TEM).

Key: 1-Deposit of platinum according to an angle β; 2-plate obtained by TEM;3-determination of the size of the particle, taking into account shading.

freezing fracturing technique to the study of liquid lubricants without detailing them completely, the objective being to demonstrate the pros-

pects opened by this method.

I.5.1. Experimental Conditions

In all the tests which we present here, the experimental conditions are identical and are presented in table I.3.

TABLE I.3. EXPERIMENTAL CONDITIONS AT THE TIME OF FREEZING FRACTURING TESTS. /26

Refrigerating agent	: Liquid nitrogen (63 K)
Pressure before fracturing	: $5 \cdot 10^{-8}$ mmHg
Temperature of fracturing	: 153 K
Angle of the platinum shading	: 45^{o}
Thickness of the platinum layer	: 30 Å
Thickness of the carbon layer	: 300 Å

I.5.2. Selection of the Paraffin Reference Base

Before studying the dispersions of certain additives within a base, it is necessary for us to select this in such a fashion to have a well-defined continuous phase. Our selection is based on a pure paraffin, n-dodecane, used in another connection to test additives in the laboratory (Martin, 1978).

Figure I.8 presents a transmission electron microscopy plate (MET) obtained on a cryofractured replicate of dodecane. Fracturing at this spot is smooth and we do not observe any dispersed particles within the base (base granulometry is that of the carbon particles of the replicate). We thus can end with good freezing of the sample.

At the time of the next tests, the presence of dispersed particles within the continuous phase could thus be attributed to additives previously added to the dodecane.

I.5.3. Study of the Paraffin/Detergent System

In all present-day thermal engines, lubricating oils contain detergent agents (or dispersants) whose objective is to avoid flocculation of particles due to fuel combustion and oxidation of the oil in both the hot and cold parts of the engine.

When the fuel used is a low desulfurized petroleum product, combustion is accompanied by formation of sulfur oxidation compounds (SO_2,

SO_3, ...) inducing wear by corrosion (Desportes). In this case, the oil, besides its lubricating action, must neutralize the corrosive agents before they can come into contact with the metallic walls. The lubricant is then activated with "superalkalinized detergents" containing a significant proportion of a basic agent, calcium carbonate, whose role is to salify the sulfuric acid formed at the time of fuel combustion. /28

Figure I.9 demonstrates the microscopic structure of three detergents dispersed to 20% with dodecane. Plates I.9.a. and I.9.b correspond to calcium sulfonates of the form $(CH_3-(CH_2)_n-\emptyset-SO_3-(Ca)_{1/2}$ with $25 \leq n \leq 30$ containing different quantities of excess calcium carbonate.

/27

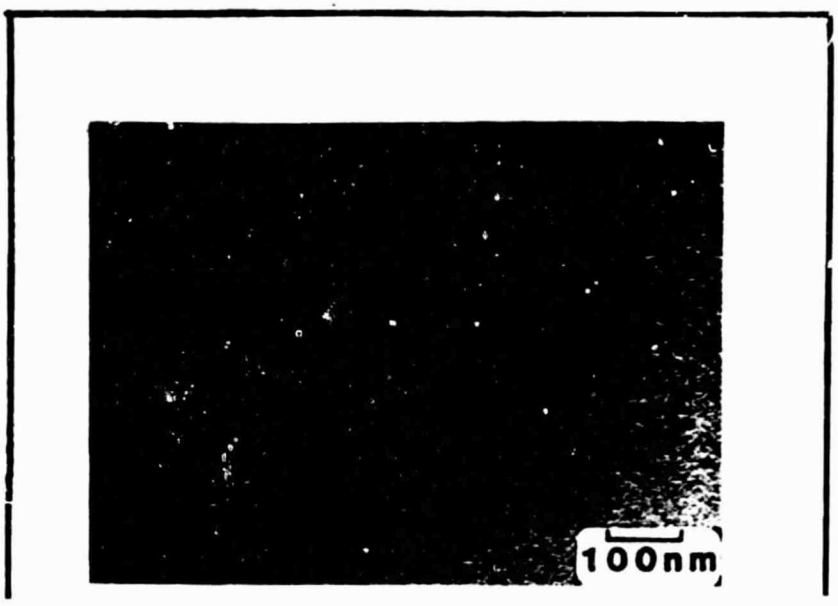

Figure I.8. TEM plate carried out on a replicate obtained by cryofracturing of pure dodecane.

Plate I.9.b corresponds to a calcium phenolate of complex formula and strongly superalkalinized.

In the case of slightly superalkalinized sulfonates (figure I.9.a) we note, within the continuous phase, the presence of small particles, approximately spherical, whose diameter is on the order of 100 Å (corresponding to approximately two times the theoretical length of sulfonate molecules) corresponding to the micellar dispersion of the detergent in the dodecane.

The plate relating to very superalkalinized sulfonate (figure I.9. b.) demonstrates spheroidal dispersed particles whose diameter may be estimated at approximately 300 Å. These aggregates could correspond to

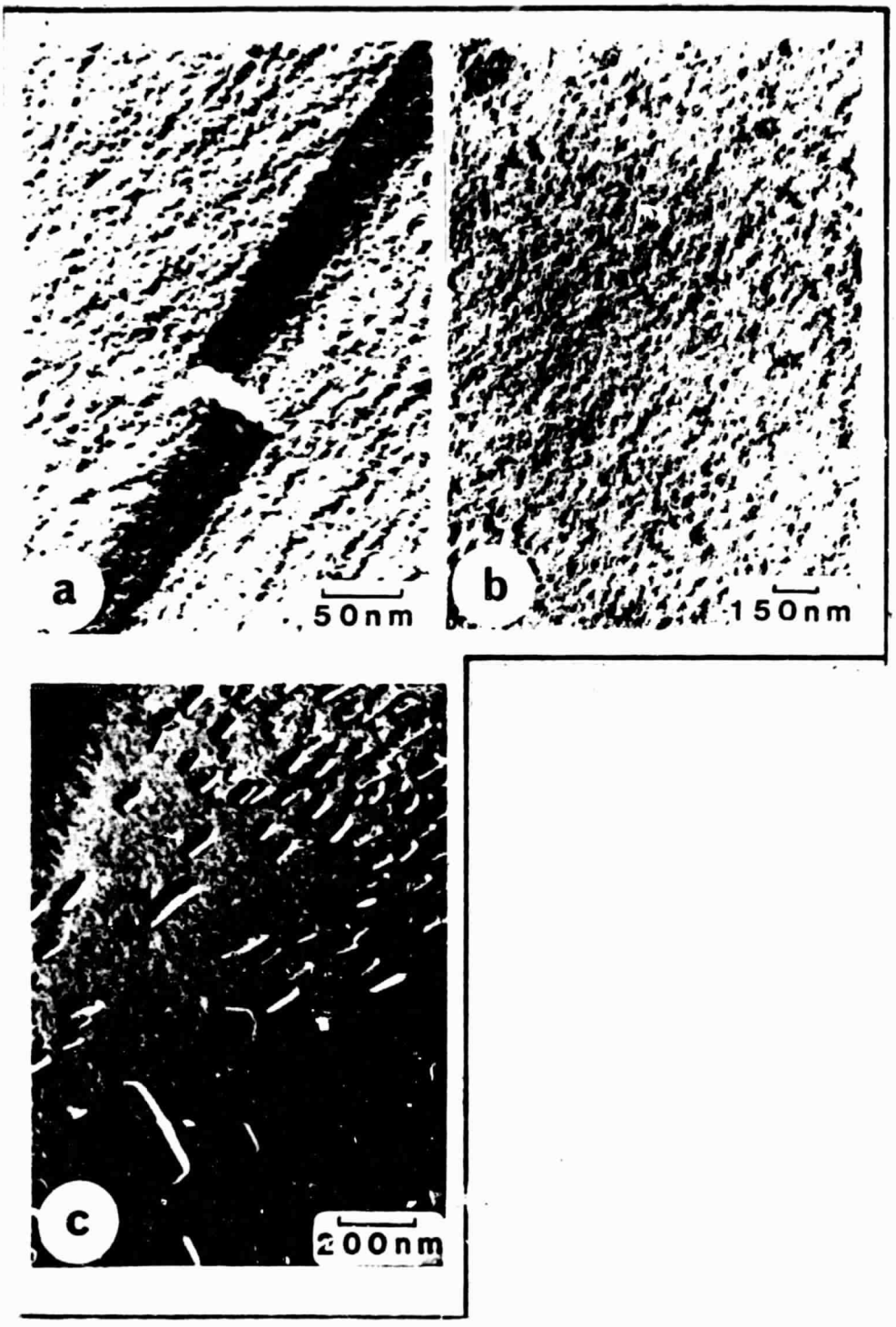

Figure I.9. TEM plates obtained on replicates prepared by cryofracturing of detergent/dodecane dispersions.

a) slightly superalkalinized calcium sulfonate
b) strongly superalkalinized calsium sulfonate
c) strongly superalkalinized calcium phenolate

the particles of calcium carbonate dispersant in the form of micella by the molecules of detergents, these already having been seen in the literature (Watkins, 1972).

In the case of strongly superalkalinized phenolate (figure I.9.c), the particles of calcium carbonate have sizes largely greater than the preceding ones. They have the shape of platelets of 300 Å thickness and 500 to 1000 Å of length and width.

Cryofracturing provides us here with significant data on superbasic detergents (state of dispersion, size and shape of dispersed particles). Taking into account the insolubility of calcium carbonate in oil, neutralization of the sulfuric acid produced at the time of combustion will be a heterogeneous phase reaction. In this case, the speed of neutralization will be limited by the specific surface of the reactive phases, and in particular, of basic particles. The specific surface will be optimum for spherical particles of small size. In this exact case, the freezing fracturing technique allow us to perceive these parameters and thus prejudge the reactivity of these additives. /30

I.5.4. Study of a Paraffin/Index of Viscosity Improvement System

The additives improving viscosity, of polymeric type, are introduced into the bases in such a fashion to render the oils multigrade, that is to say in order to reduce the variations of oil viscosity at high and low temperature.

Figure I.10 represents the dispersion of a methyl polymethacrylate of mass 100,000 within dodecane. The plate demonstrates the presence of a great number of spherical particles of average diameter 150 Å corresponding to molecules, this having been confirmed by the light diffusion technique (hydrodynamic diameter=180 Å; mass of particles= 100,000). We observe the presence of spheres of very different sizes (of diameter going from 50 A to 350 Å), this resulting in the polydispersity of the polymer. Dodecane not being a good solvent of methyl polymethacrylate, the spherical particles which we see on the plate (I.10) correspond to dense spheres and not to a polymer molecule in the form of statistical balls in solvent θ. It is undoubtedly for this reason that we perceive very well the dispersed additive within the base.

I.5.5. Application of the Freezing Fracturing Technique to the Study of Completely Formulated Oils /32

I.5.5.1. Unused Oil

In the case of unused detergent oil presented in figure I.11, the cryofracturing technique allows us to detect the presence of spherical particles of diameter comprised between 100 and 300 Å capable of corresponding both to superbasic detergent additives and viscosity additives. It is a question here of a limitation of the technique. However, an

Figure I.10. TEM plate obtained from a replicate prepared by cryofracturing of a polymetacrylate dispersion of methyl/dodecane.

/33

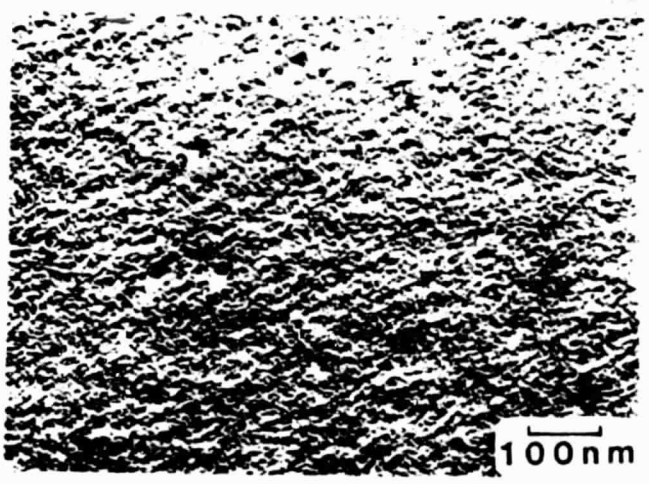

Figure I.11. TEM plate obtained from a replicate prepared by cryofracturing of unused Agip detergent oil.

additional artifice is then necessary to cancel this indetermination. Indeed, it suffices to not dissolve the particles confined in the repli-

cate (figure I.12) and to analyze them by Dispersive Energy x-ray Spectroscopy (DES) under electron beams. On the other hand, through electron micro-diffraction on these same particles, we have a measure of distinguishing the state of the additive (crystallized or amorphous), giving information on its reactivity. It is important to note that for small size aggregates, it is necessary to use a high performance microscope. We have been able to verify that these techniques were feasible in the case of the dispersion of calcium carbonate presented in figure I.12, I.12, a qualitative DES analysis having revealed the presence of calcium in the particles (JEOL 100 C PCUK microscope).

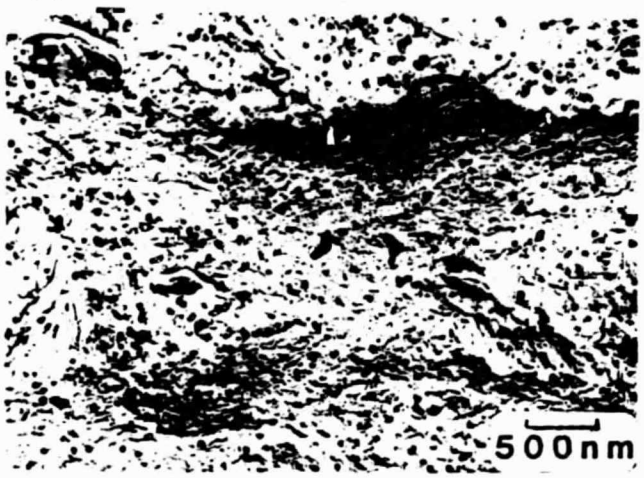

Figure I.12. TEM plate obtained on a replicate prepared by cryofracturing of a superalkalinized sulfonate dispersion/dodecane.

The black non-shaded particles are due to the presence of calcium carbonate mounted in the replicate.

I.5.5.2. Used Oil

The electron microscopy plates presented in figure I.13 demonstrate the structure of the oil previously having functionned in a thermal engine. Fracturing revealed the presence of numerous particles within the continuous phase. Certain ones, black and not shaded, are of grains of calamine which remained stuck to the replicate. The droplets in the shape of spheres or "raspberries" were connected with the presence of emulsified water in the oil. On the other hand, we note that the polyphasic nature of certain drops can correpsond to complex emulsion structures (oil/water/oil for example. These particles, carried /35
permanently in the oil, are due either to fuel combustion or oxidation of the oil and can give rise to abrasive wear in the case of calamines or corrosive wear in the case of water droplets, thus being able to carry corrosive products (H_2SO_4).

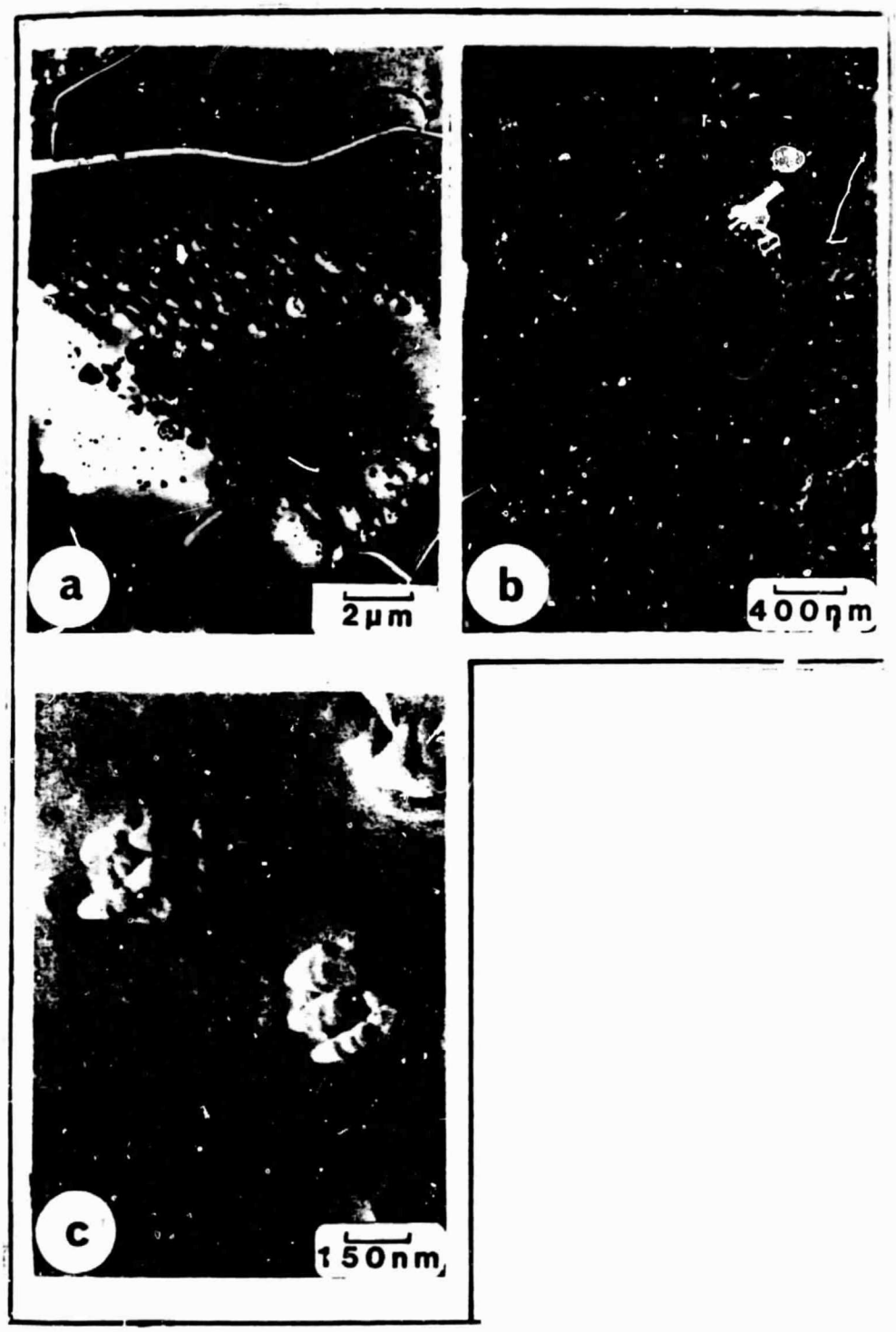

Figure I.13. Different microscopic aspects of a used Agip detergent oil

a) low magnification emulsified appearance;
b) spherical droplets undoubtedly constituted by water;
c) particles in the shape of raspberries capable of being attributed to the existence of an inverted emulsion of oil/water/oil.

I.5.6. Application of the Freezing Fracturing Technique to the Study of Greases

The word grease employed during this paragraph is not used in the sense that it is assigned by official nomenclature (lipids, ...). Here it designates a class of industrial lubricants which occur in the form of gels and are constituted by a soap dispersion (lithium stearate,...) with a mineral oil additive. This type of product serves to permanently lubricate machinery such as ball bearings.

Numerous authors have already studied the microscopic structure of greases, in particular those whose soap is hydroxy-12 lithium stearate (Anderson, Nelson and Farley, 1967; Peyrot and DuParquet, 1976). The methods used until now are standard techniques of transmission electron microscopy; a fine layer of grease is deposited on a microscope grid, the oil is dissolved with the assistance of a solvent, the remaining soap fibers are examined by TEM either directly or after platinum shading (Peyrot and DuParquet, 1976). In all cases, the dispersion structure had been destroyed. Watkins (1972) has demonstrated that cryoscouring (fracturing is induced by a knife) was applicable to this type of lubricant.

The plates which we show in figures I.15 and I.16 present different aspects of the dispersion constituted by a hydroxy-12 lithium stearate grease revealed by the cryofracturing technique. Figure I.17 demonstrates soap fibers seen by TEM on one hand by the technique developed by DuParquet (figure I.16a) and on the other hand, through the intermediary of the freezing fracturing technique (figure I.16b and c).

In the first case, we had access to the length of the fibers; in the second case, the fracturing according to which develops at the surface or through the fibers, we get information on their shape (coiled, figure I.16b) and their internal structure (the fibers are constituted of hydroxy-12 lithium stearate platelets, figure I.16c). /37

I.6. Conclusion

During this chapter, we have seen that the freezing fracturing technique can be applied to the study of dispersions constituted by lubricants. It gives us a significant amount of information on the size, shape, structure, and distribution of the dispersed phase within the continuous phase. However, the possibility of artifacts (segregation, contamination, ...) as well as the impossibility of identifying the nature of the particles within a mixture including more than two compounds necessitates the use of complementary techniques such as light diffusion or XES microanalyses (dispersive energy x-ray spectroscopy).

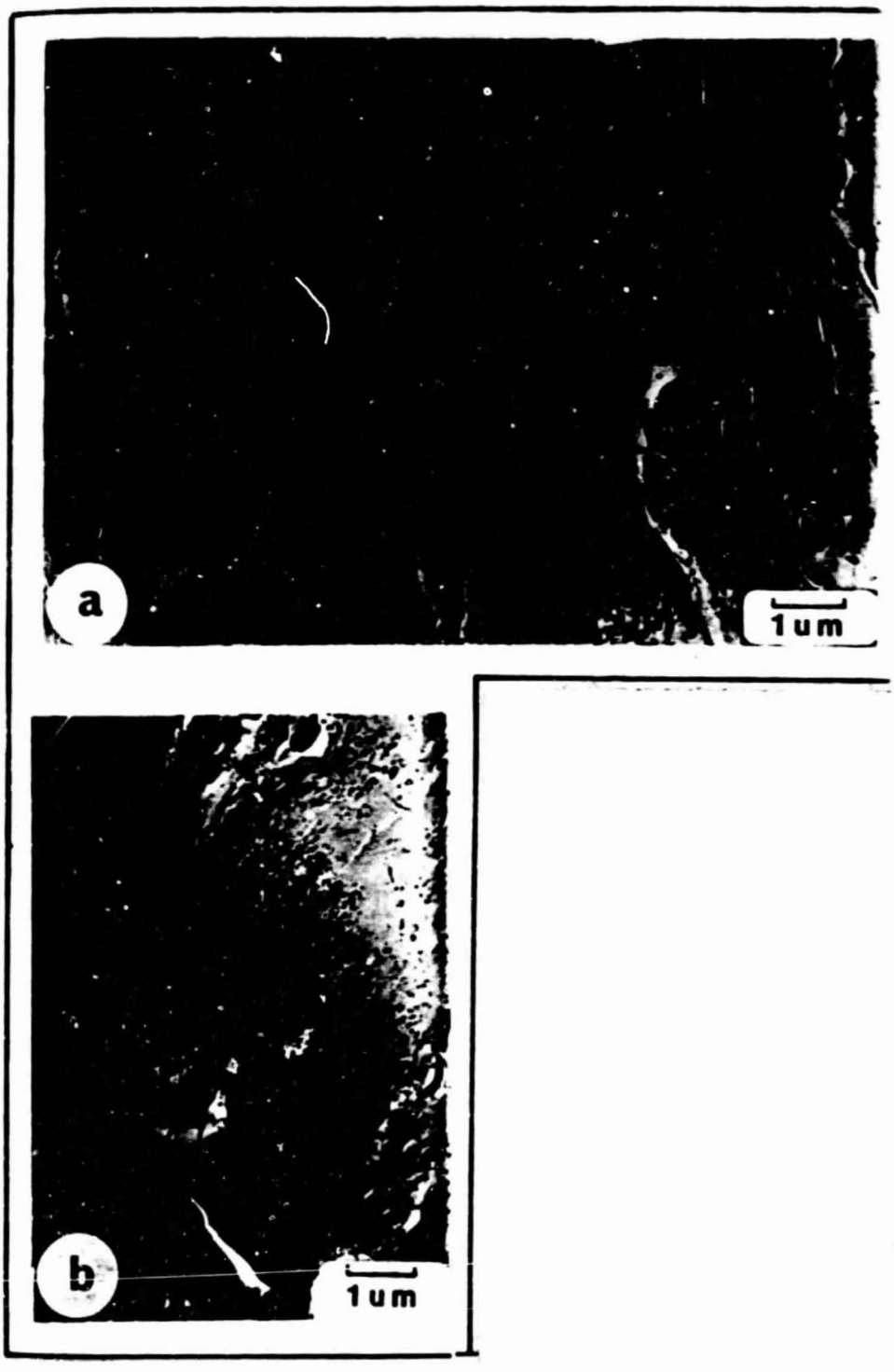

Figure I.15. Two principal microscopic appearances of the dispersion constituted by a hydroxy-12 lithium stearate lubricating grease.

a) dispersion of soap in the oil in the shape of fibers;
b) soap agglomerate.

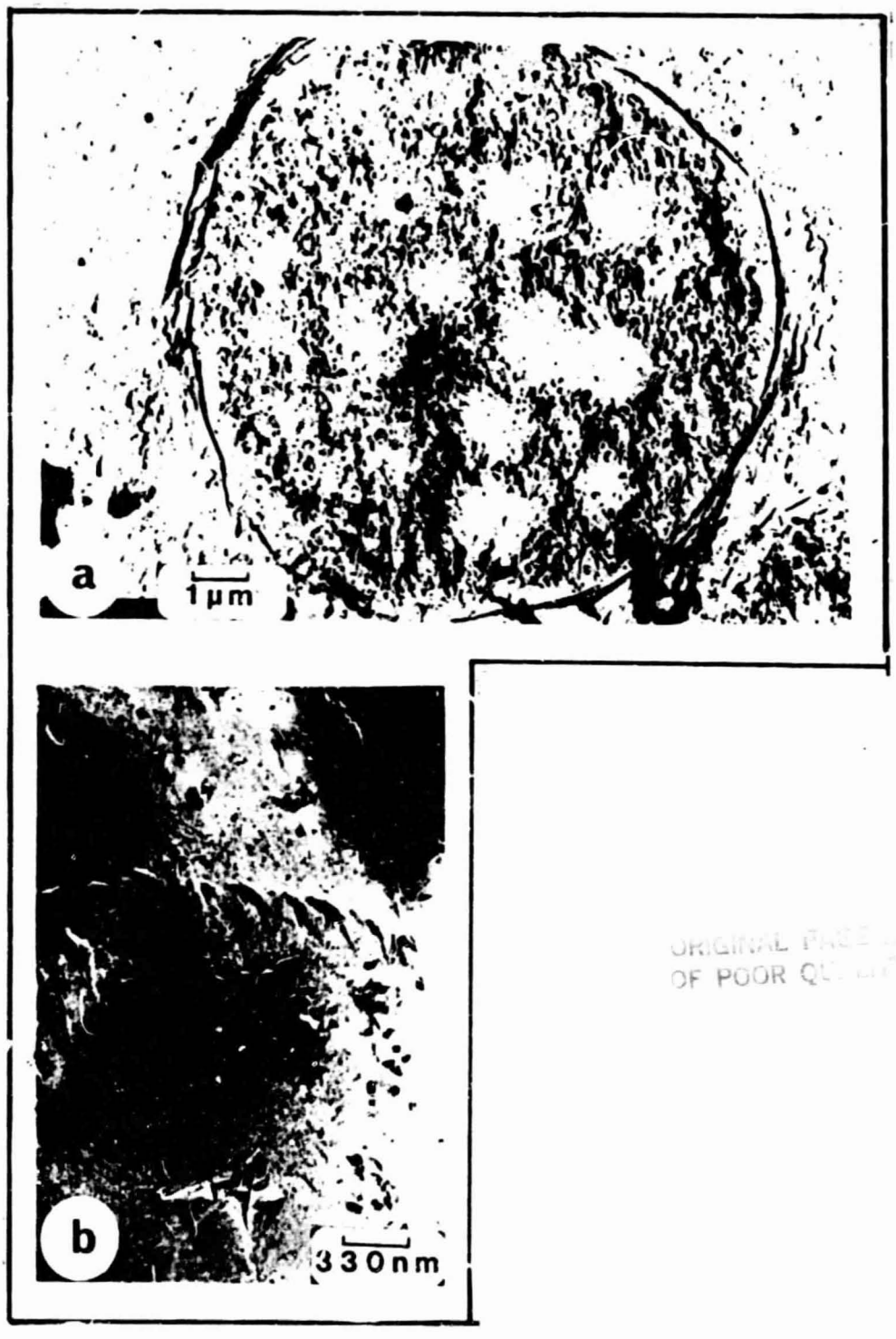

Figure I.16. Microscopic aspects of the dispersion constituted by a hydroxy-12 lithium stearate lubricating grease.

a) soap agglomerate in which oil drops are imprisoned;
b) coiled soap fibers.

/38

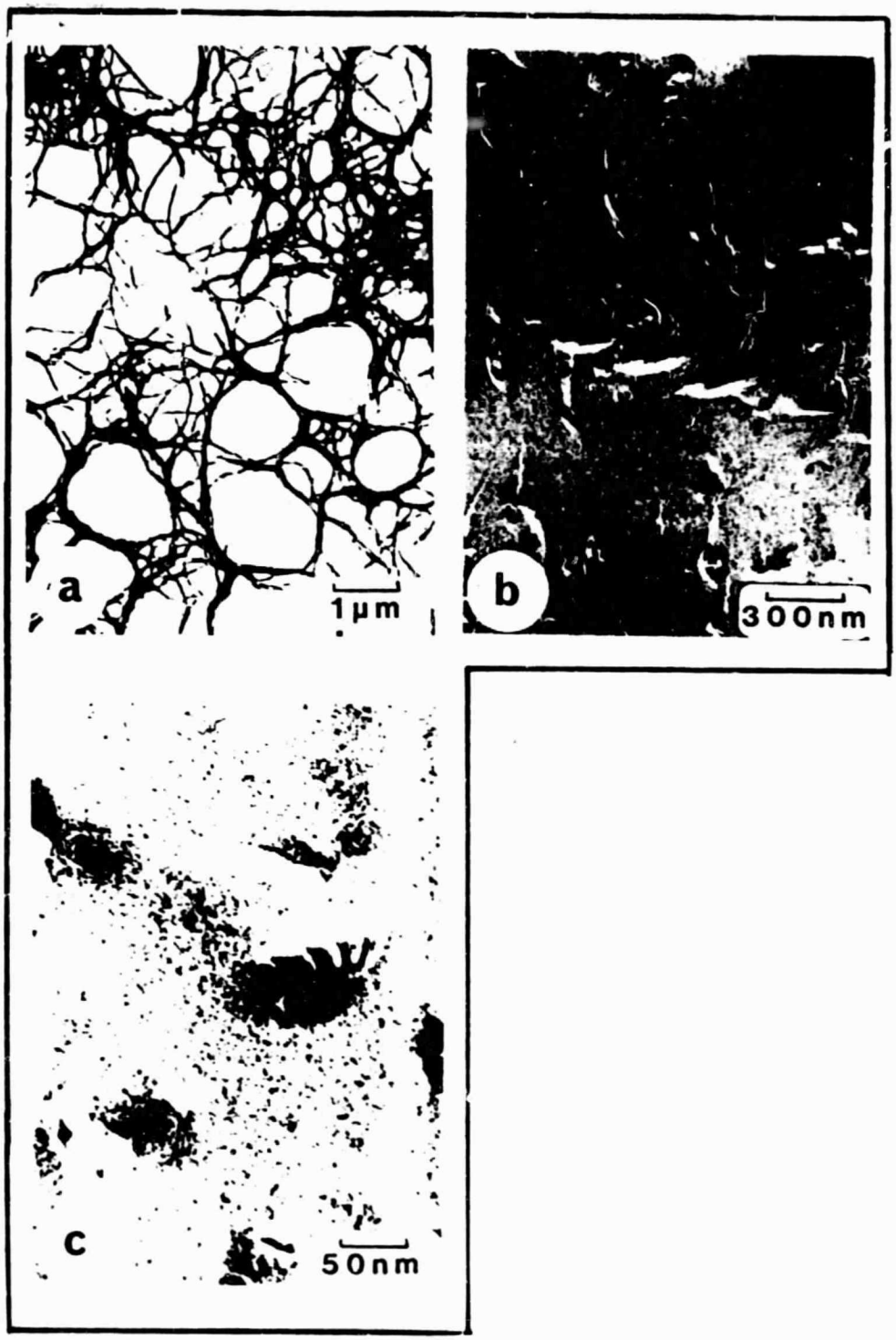

Figure I.17. Comparison of TEM plates obtained.

a) by the method developed by DuParquet (DuParquet photo);
b) and c) by the freezing fracturing technique ;
b) coiled appearance of a fiber ;
c) section of a soap fiber revealing its structure in platelets.

Chapter II /40

Contribution of the Molecular Structure of the Lubricant to the Reduction of Friction

II-1. Introduction

II-2. Reactive Conditions with Hertzian Contact with Pure Sliding

II-2.1. Elastic Static Contact with Pure Normal Load

II-2.1.1. Hertz Theory

II-2.1.2. Case of Rough Surfaces

II-2.2. Influences of the Presence of an Interfacial Film within the Sphere-Contact on the Hertz Theory

II-2.3. Transitory State of Contact

II-2.4. Dynamic Contact with Normal Load $\vec{W}$ and Tangential Force $\vec{T}$

II-2.5. Conditions of Our Tests

II-3. Selection of Reagent

II-4. Study of the Conditions of the Supply of Contact

II-4.1. Study of Pure Ester

II-4.2. Study with the Assistance of the Freezing Fracturing Technique of the n-Dodecane/Ester Solution

II-4.3. Study of the n-Dodecane/Ester Solution by Light Diffusion

II-4.3.1. Reminders Concerning the Measurement of the Mean Diffused Intensity

II-4.3.2. Measurement of Correlation Times

II-4.3.3. Experimental Device and Conditions

II-4.3.4. Results and Discussion /41

II-4.3.4.1. Measurements of Diffused Intensity

II-4.3.4.2. Quasi-Elastic Diffusion

II-4.3.4. Conclusion on the Results

II-4.4. Study of the Adsorption of the Additive at a Solid-Liquid Interface

Chapter II /42

Contribution of the Molecular Structure of the Lubricant to the Reduction of Friction

II.1. Introduction

A test of friction on a sphere-plane simulator in the presence of a lubricant can, from a physico-chemical point of view, break down into several stages. Figure II.1 presents the physico-chemical development of a friction reducer additive (R.F.) during this type of test, as well as the recommended techniques for the study of each stage.

II.2. Reactive Conditions with Hertzian Contact with Pure Sliding /43

We find a situation in the hypothesis of sphere/plane contact considered as a chemical reactor where lubricant molecules can be subjected to transformations at the time of shearing of the interface by sliding of the sphere on the plane. Such processes can be decomposed chronologically into four stages (figure II.2).

The geometrical, metallurgical, and mechanical parameters of contact lead to particular physical conditions:

-high hydrostatic pressures ($\simeq$1 GPa)

-very low quantity of reagent (0.1 nanogram)
-high rate of shearing (10^5 s^{-1} in the dynamic case)

We are going to examine these different points in more detailed fashion by restating the principal results of contact theories. /44

II.2.1. Elastic Static Contact with Pure Normal Load (Called Static Case in the Following Text)

II.2.1.1. Hertz Theory (1881)

In the case of ideally smooth surfaces and purely elastic contact, the Hertz theory allows us to determine the actual contact surface, the distribution of pressures on it, and the distribution of stresses within materials (see figure II.3).

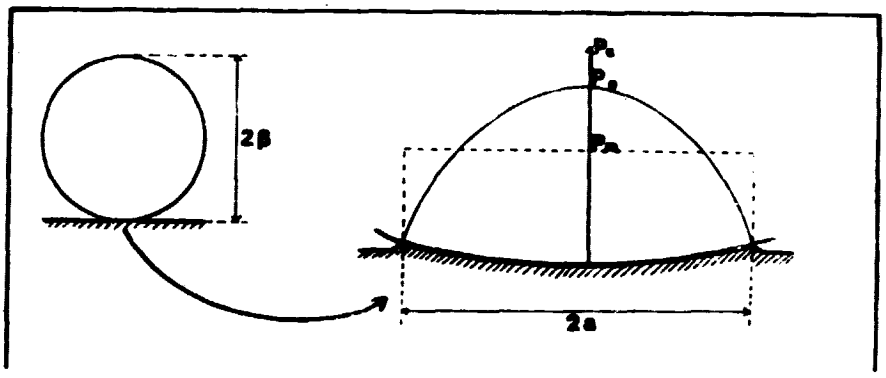

Figure II.3. Diagram representing a plane sphere Hertzian contact.

a=radius of the contact zone; P_o=maximum pressure in the contact; P_m=mean pressure in the contact; β=radius of the sphere

Hertz obtains the following relationships (Timoshenko, 1951):

$$\begin{cases} a = \left[\frac{3}{4} E' \beta\right]^{-1/3} W^{1/3} & (2\text{-}1) \\ P_m = \frac{1}{\pi}\left[\frac{4}{3} E' \beta\right]^{1/3} W^{1/3} = \frac{W}{\pi a^2} & (2\text{-}2) \\ P_o = \frac{3}{2} P_m & (2\text{-}3) \end{cases}$$

with: β =radius of curvature of the sphere /45
E' such that $\frac{1}{E'} = \frac{1-\nu_1^2}{E_1} + \frac{1-\nu_2^2}{E_2}$

ν_1 and ν_2=respective Poisson coefficients of the materials constituting the sphere and the plane
E_1 and E_2=Young units of the materials constituting the sphere and the plane

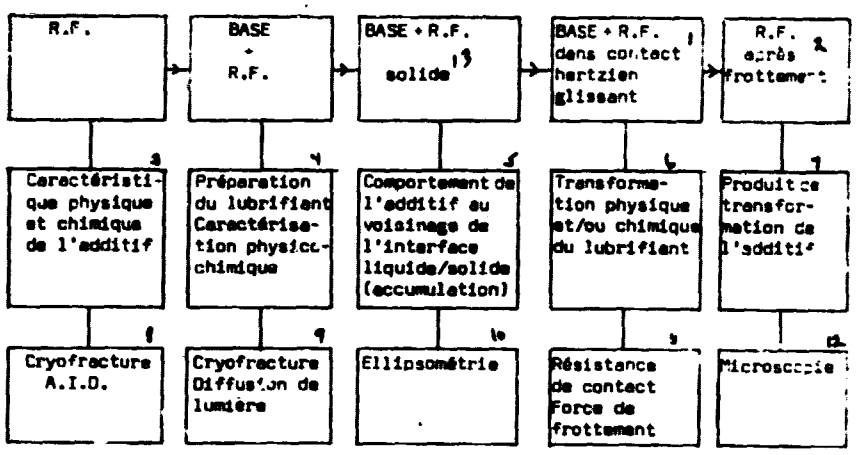

Figure II.1. Diagram of the different stages followed by a friction reducer agent R.F. during a tribological test.

Key: 1-BASE+R.F. in sliding hertzian contact; 2-R.F. after friction; 3-Physical and chemical characteristics of the additive; 4-Preparation of the lubricant; physico-chemical characterization; 5-Behavior of the additive in the vicinity of the liquid/solid interface (accumulation); 6-Physical and/or chemical transformation of the lubricant; 7-Transformation product of the additive; 8-A.I.D. cryofracturing; 9-Cryofracturing height diffusion; 10-Ellipsometry; 11-Resistance of contact; force of friction; 12-Microscopy; 13-Solid.

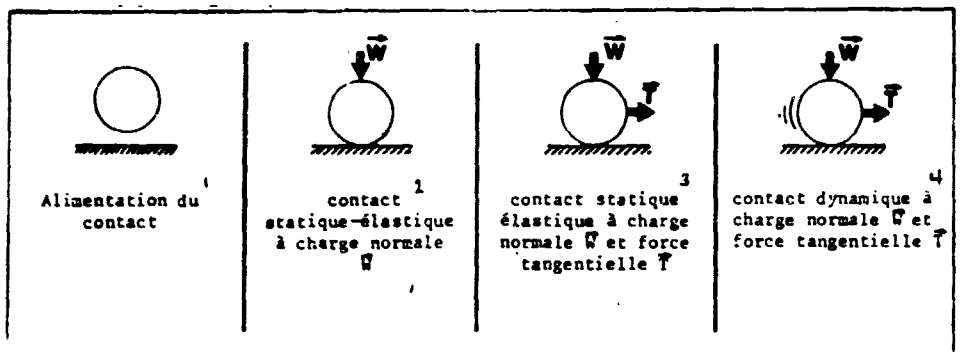

Figure II.2. Different stages of the development of contact.

Key: 1-Supply of contact; 2-Static-elastic contact with normal load $\vec{W}$; 3-Static-elastic contact with normal load $\vec{W}$ and tangential force $\vec{T}$; 4-Dynamic contact with normal load $\vec{W}$ and tangential force $\vec{T}$.

a=radius of the contact zone
P_m=mean pressure in the contact
P_c=maximum pressure in the contact
W=normal load applied on the contact

The limit of the elastic realm is attained when P_m is equal to 0.4 H, H being the hardness of the softest material constituting the substances in contact, which leads to a limit value of the theoretical pressures prevailing with such a contact on the order of several gigapascals.

II.2.1.2. Case of Rough Surfaces

The Hertz model can be extended to cases of rough surfaces (models of multiple contacts of Archard, 1957 and Greenwood and Tripp, 1971).

However, in the case of very polished surfaces ($\sigma_s \leq 10$ nm), we can reasonably make the hypothesis that the actual contact area coincides with the Hertzian area (Tabor, 1972).

II.2.2. Influence of the Pressure of an Interfacial Film Within the Sphere-Plane Contact on the Hertz Theory

/46

The friction properties of thin films within a hyperpolished sphere-film contact have been widely studied up to now (Wilson, 1955; Courtinex-Pratt, 1955; Zisman, 1957; Israelachvili, 1973; Briscoe, 1974; ...).

In the case of very thin films present within the interface ($e \leq 50$ nm), these authors have acknowledged that the calculations developed by Hertz and his contemporaries remain valuable.

II.2.3. Transitory State of Contact

This stage is characterized by the annular propagation of sliding of the periphery of the contact up to the center of this. The phenomena occurring at the interface during this period have been very widely studied (Mindlin, 1950).

Figure II.4 demonstrates the distribution of shearing stresses on a circular contact area determined by a normally loaded spere-plane contact ($\vec{W}$) subjected to a tangential force ($\vec{T}$). To treat this problem the authors have considered that the Hertz calculations remain variable even in the presence of a tangential force.

II.2.4. Dynamic Contact with Normal Load $\vec{W}$ and Tangential Force $\vec{T}$

When the contact zone is completely sliding, the tangential force $\vec{T}$ takes at each instant a value which is connected to $\vec{W}$ by the relationship:

$\vec{T}=\mu\vec{W}$ where μ is the instantaneous coefficient of friction.

The average pressure with the contact is then near the value found in the static case, but it is no longer hydrostatic. Courtney-Pratt et al. have demonstrated (1955) that at the time of sliding, in the case of soft materials, the contact area was much higher than that corresponding to the static case. In our case (100C6/100C6 metallurgy), the increase of the contact area is at most on the order of 10% when we pass it from the static state to the dynamic state. /48

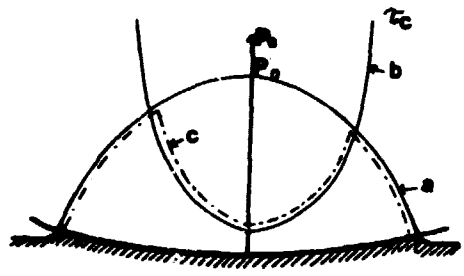

Figure II.4. Distribution of shearing pressures and stresses with a normally loaded sphere-plane contact (W) subjected to a tangential force (T).

a) curve of distribution of pressures within the contact zone
b) curve of distribution of shearing stresses without sliding
c) curve of distribution of shearing stresses by considering the sliding of an annular zone

II.2.5. Conditions of Our Tests

The tribological conditions of our tests are grouped in table II.1.

These different parameters allow us to estimate the physical and chemical conditions prevailing with the reactor constituted by the sphere/plane hertzian contact subjected to a shearing stress. These are grouped in table II.2.

With such conditions, we can expect that the lubricant molecules undergo multiple degradations.

TABLE II.1. GROUPING OF THE TRIBOLOGICAL PARAMETERS OF OUR TESTS

Materials	: 100C6 treated steel H_V=880
Normal Load	: W=1 daN
Radius of Curvature of the Sphere	: R=6 x 10^{-3} m
Equivalent Roughness of the Surfaces	: $\sigma_a \leq 10$ nm
Sliding Velocity	: v=5 x 10^{-5} m/s
Temperature	: 298 K

TABLE II.2. GROUPING OF THE PHYSICAL AND CHEMICAL CONDITIONS PREVAILING WITH THE CONTACT /49

Contact area	: 2 x 10^{-8} m^2
Volume of Material	: $< 10^{-16}$ m^2
Mean Pressure Prevailing With the Contact	: 10^8 to 10^9 Pa
Shearing Rate	: $\frac{v}{h} > 10^3$ s^{-1}
Overtemperature of Contact (Macroscopic)	: θ negligible
Possible Catalytic Effect With Contact of the Native Material	
Duration of the Stress on the Interface	: 3 s

II.3. Selection of Reagent

A great number of studies have already been carried out on the reduction of friction (Bowden and Leben, 1939; Zisman, 1957) and have brought out the anti-friction activity of amphiphilic molecules (such as fatty acids for example). Such molecules can be represented by the standard diagram below (figure II.5).

Non-polar portion (lipophilic) — Polar portion (hydrophilic)

Figure II.5. Diagram of an amphiphilic molecule.

The simple compounds studied most, and consequently the best known, are fatty acids (oleic stearic acid, ...) and their derivatives (ester, salt, ...). /50

The additives which we have selected to successfully conduct our study is a sequence copolymer (of complex ester type) of molecular mass 4300 answering a complex expanded formula which we diagram in the following fashion:

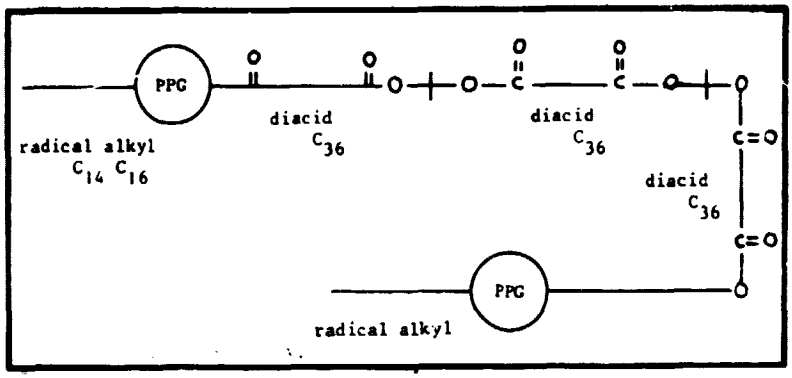

The formula of different constituents of the molecule:
allsyl radical
P.P.G.: Polyoxypropylene glycol, such that the mass of this fragment is 1500
Diacid in C_{36}:

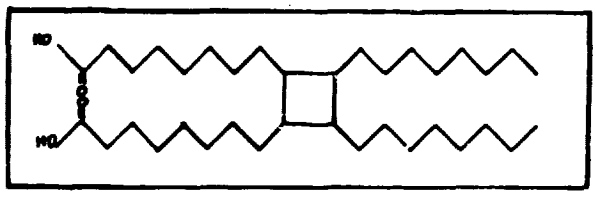

The additive, which we will call ester in the rest of this work, is an amphiphilic compound which we can diagram in the following fashion:

/51

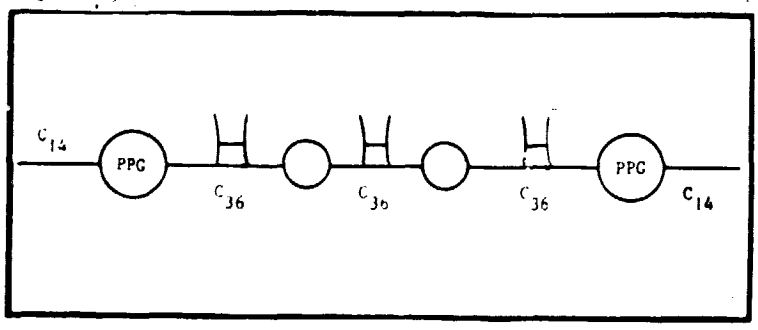

This compound, already used in industrial and multipurpose oils:
-Improves the viscosity index

-Anti-wear
-Reduces friction.

Table II.3 presents these characteristics. The selection of such a molecule, despite its apparent structural complexity, presents certain advantages:

-Better possibility of "molecular" following through electron microscopy due to the fact of its non-negligible size

-Interesting model proposed by Furey (1973) in the literature to explain the action of such additives (in situ polymerization,...)

-Industrially useable additive.

TABLE II.3. CHARACTERISTICS OF THE COMPLEX ESTER /52

Characteristics	Units	Values
Molecular mass		
by number	$\overline{M}$	7200
by weight	$\overline{M}^n$	12100
by Z	$\overline{M}_z^p$	17100
Volume mass at 20°C	g/ml	0.964
ASTM color		<2
Viscosities		
at 37.8°C	cSt	1554
at 98.9°C	cSt	155.9
Viscosity index	VI_E	223
Melting point	°C	-24
Flash point v.o.	°C	282
Conradson carbon	% weight	0.15
Ester index	function/kg	1.40
Hydroxyl index	function/kg	0.04
Acid index	function/kg	0.06
Non-saturation	double bond/kg	0.82

II.4. Study of the Conditions of the Supply of Contact

II.4.1. Study of Pure Ester

A preliminary study of the behavior of the ester as a function of temperature, under atmospheric pressure, has been carried out by differential thermal analysis (DTA). Figure II.6 represents the thermogram obtained for this product with normal pressure conditions

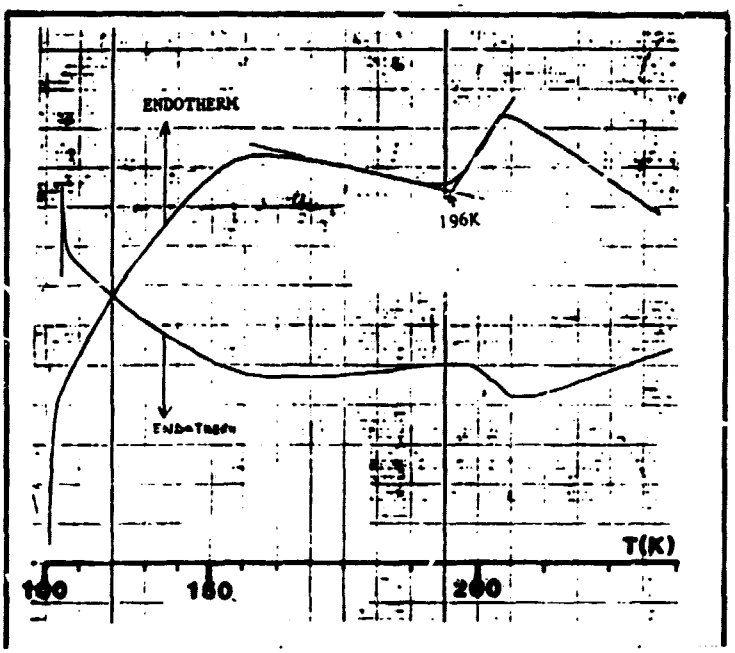

/54

Figure II.6. Thermogram obtained by differential thermal analysis for pure ester.

Recording conditions:
- -cooling of the ester from 300 K to 100 K with a speed of 360 K/mn
- -maintenance for 5 mn at 100 K
- -reheating with a speed of 10 K/mn

(1 bar). We observe vitreous transition at approximately the temperature of -78°C, but we do not observe crystallization. This indicates to us the possibility of good vitrification at the time of freezing-fracturing.

Figure II.7 is an assemblage of transmission electron microscope plates obtained from platinum carbon replicates of pure ester prepared by the freezing fracturing technique (c.f. chapter I) with the same conditions as in chapter I (table I.2). We observe in the first instance the good vitrification of the system, obtained at the time of freezing, characterized by the facies of the fracture developing within the material (branched appearance of the fractures) obtained classically at the time of cleavage of a vitrified medium. /53

A finer observation of the plates reveals the granular appearance of the surface, the product appearing to be composed of aggregates whose diameter is estimated at 10 mm and whose arrangement does not demonstrate any organization at moderate or long distance.

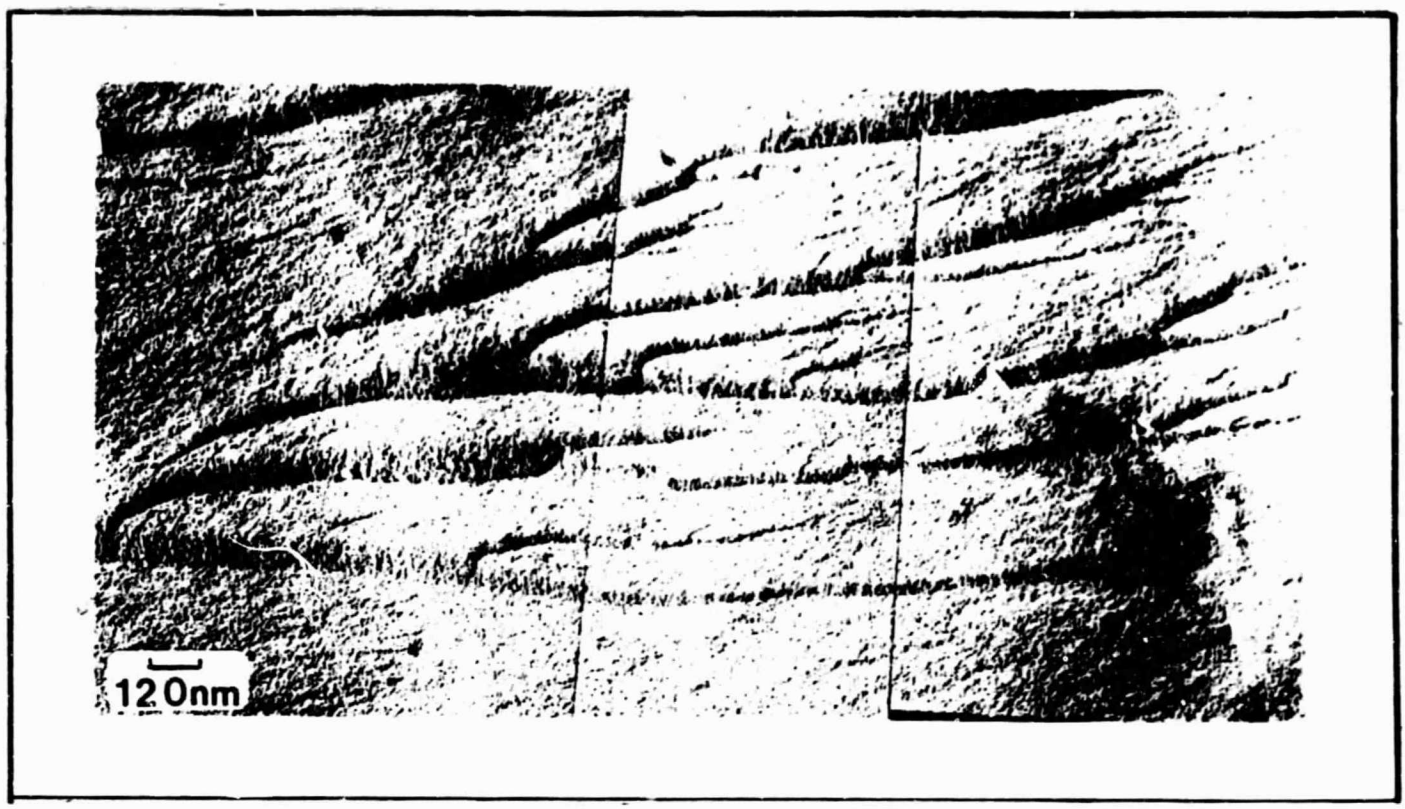

Figure II.7. Transmission electron microscopy plate obtained on a platinum carbon replicate of pure ester prepared by the freezing fracturing method: /55

-"channeled" aspect of the fractures;
-presence of spheres of 100 Å diameter.

II.4.2. Study with the Assistance of the Freezing Fracturing Technique of the n-Dodecane/Ester Solution

The good vitrification noted at the time of freezing of the n-dodecane (c.f. I.5.2) allows us to imagine just as good vitrification of the n-dodecane/ester solutions. Several tests have been carried out on solutions of different concentrations of ester, the conditions of freezing fracturing manipulations being identical to that concerning the study of the pure ester.

We only present here the results obtained with a 10% solution of ester in the n-dodecane, the different aspects observed on this sample being completely representative of those presented by solutions of concentrations between 1 and 10% ester.

Figure II.8 presents the three aspects encountered in the solution at the time of examination by transmission electron microscopy of the replicates obtained by cryofracturing of the sample. The three plates reveal the biphasic constitution of the solution at the microscopic

/57

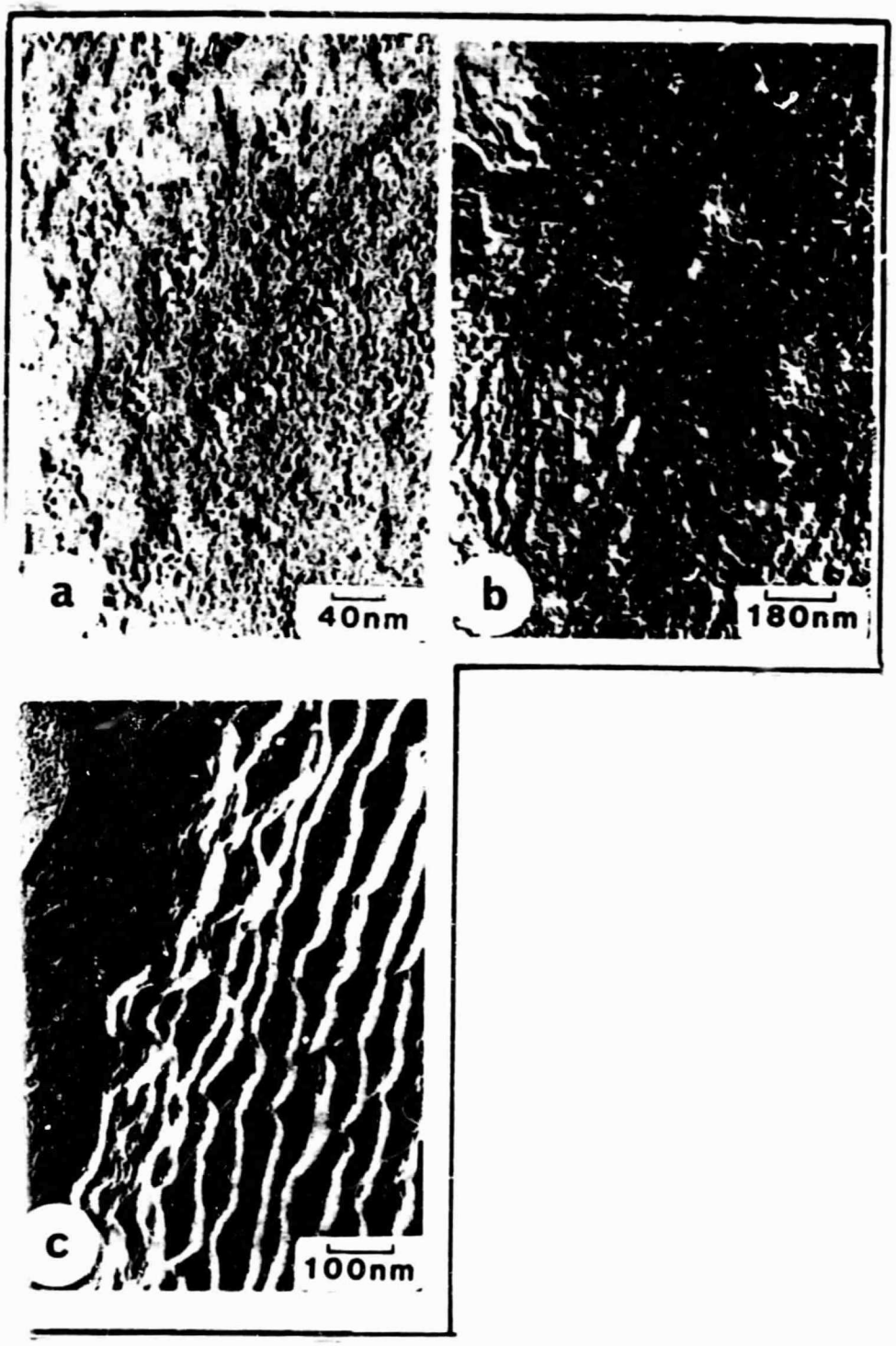

Figure II.8. Different microscopic aspects of the n-dodecane/ester solution.

a) 60-80 Å spheres traced at random within the continuous phase
b) 60-80 Å spheres traced in regular fashion in beads within the continuous phase
c) coexistence of a structure platelets and 60-80 Å diameter spheres

level and clearly demonstrating the existence of spheroidal particles whose diameter is estimated at 60-80 Å, dispersed within the continuous phase. While photograph II.8a shows us a random distribution of these particles, plates II.8b show us an organization into beads and platelets, the latter capable of being connected with the existence of a smectite-type mesophase within the solution. However, if this type of organization existed at ambient temperature, the solution would be double-cooling (in the case of the existence of a smectite). Now, we have been able to verify that this was not the case. On the other hand if, with the same conditions, the particles were aligned within the solution, this would result in quasi-elastic diffusion of light, through a function of autocorrelation composed of two exponentials, the time constant corresponding to the second being very large in relation to the first (Pusey, 1978; Grüner and Lehmann, 1980), which is not the case as we will see in the following paragraph. /56

The formation of these organized phases thus can not be due only to freezing. Indeed, it is imaginable that at the time of cooling of the sample, certain zones of this undergoing phase transitions such as this have already been observed in the case of microemulsions (Candau, 1979). We will thus deduce from these tests the existence of spherical particles of 60-80 Å diameter constituted by the additive. However, it is necessary to note that contrarily to the gaussian pellets formed by certain polymers (polystyrene in cyclohexane) which to our knowledge have not yet been demonstrated by the freezing fracturing technique, the particles which we see within the dodecane are more solid and more compact than the static pellets and would correspond to micellar type molecular aggregates.

II.4.3. Study of the n-Dodecane/Ester Solution by Light Diffusion

The first theories, taking into account the diffusion of light by small particles in front of the wave length, due to Einstein (1910) and Smoluchowsky (1912) have allowed us to express the intensity of the different fields from local fluctuations of the dielectric constant. today, light diffusion techniques are up to date in laboratories and largely described in the literature (Strazielle). In the macromolecular realm which interests us here, we can distinguish two developments of these. The first is illustrated by the measurement techniques of different intensity which lead to the determination of the mass and the dimensions of the macromolecules. The second more recent development concerns spectroscopy allowing us to tackle dynamic studies (determination of the radius of hydrodynamic gyration for example, ...) of the molecules in solution from the analysis of the spectral distribution of the diffused field and from calculation of the different correlation functions associated with fluctuations of the physical parameters of the medium.

II.4.3.1. Reminders Concerning the Measurement of the Average Diffused Intensity

The excess of diffusion due to a suspension of small particles in

front of the wave length of the incident polarized beam within a vertical plane is given by the equation:

$$\Delta R_\theta = \frac{4\pi^2 n^2}{\lambda^4}\left(\frac{\partial n}{\partial c}\right)^2 k_B T \chi \qquad (2\text{-}4)$$

where ΔR_θ is the difference between the Rayleigh ratio of the solution and the solvent

$\frac{\partial n}{\partial c}$ is the increment of the index of the solution in relation to to the solvent (in g cm^{-3})

k_B is the Boltzmann constant

n is the refraction index of the solution /59

λ is the wave length of the incident beam

T is the temperature in K

χ is the osmotic compressibility of the solution, where χ has the expression:

$$\chi = c\left(\frac{\partial \pi}{\partial c}\right)^{-1} \qquad (2\text{-}5)$$

π is the osmotic pressure of the solution.

For dilute solutions, the value of osmotic pressure can be obtained with the assistance of an approximation, the concentration being expressed in the form of a second degree polynomial.

Thus the dependence of ΔR_θ as a function of the concentration can be rewritten in the form:

$$\frac{c}{\Delta R_\theta} = k\left(\frac{1}{M_w} + 2A_2 c\right) \qquad (2\text{-}6)$$

with

$$k = \left(\frac{4\pi^2 n^2}{\lambda^4}\left(\frac{\partial n}{\partial c}\right)^2\right)^{-1} \mathcal{N} \qquad (2\text{-}7)$$

where M_w is the mean particular mass by weight

A_2 is the second coefficient of virial of the osmotic pressure

$\mathcal{N}$ is the Avogadro number.

The relative intensities I and I_3 diffused at 90° through the solution and the solvent are converted into Rayleigh ratios by using as a reference value the intensity I_{B2} diffused through benzene tri-distilled and filtered on 0.2 μm millipore. The Rayleigh ratio then has for expression:

$$\Delta R_\theta = \frac{4\pi^2 n^2}{\lambda^4} \times \frac{I_{B2}}{I - I_3} \times c\left(\frac{\partial n}{\partial c}\right)^2 \qquad (2\text{-}8)$$

II.4.3.2. Measurement of Correlation Times /60

The quasi-elastic diffusion of light is a technique which uses the temporal fluctuations of the diffused light, in order to measure the coefficient of diffusion by movement of the macromolecules in solution.

These temporal fluctuations are produced by Brownian movement of the macromolecules and can be detected by measuring the function of autocorrelation of the diffused intensity.

The correlation values of the diffused intensity are analyzed by the standard method of accumulants (Koppel, 1972; Pusey, 1975) in order to obtain the mean value of the time constant $\bar{\Gamma}$ and the variance υ. This latter measures the width of the distribution of the time constant. It is given by the expression:

$$\upsilon = (\bar{\Gamma}^2 - \bar{\Gamma}^2) / \bar{\Gamma}^2 \qquad (2\text{-}9)$$

$\bar{\Gamma}^2$ is the second order moment of the distribution. The coefficient of diffusion is determined from the mean value of the time constant in agreement with the relationship:

$$\bar{\Gamma} = 2k^2 D \qquad (2\text{-}10)$$

The amplitude of the vector of diffusion k is given by the expresion:

$$k = \left[\frac{4\pi n \sin\theta}{2} \right] \times \lambda^{-1} \qquad (2\text{-}11)$$

where θ is the angle of diffusion, λ the wave length of the incident light in the vacuum, and n the refraction index of the diffusing medium.

The variation of D with the particle concentration is generally well described, in the case of solutions of very dilute solutions of spherical particles by the linear relationship (Cazabat and Langevin, 1980):

$$D = D_0 (1 + \gamma c) \qquad (2\text{-}12)$$

where γ is a coefficient of virial taking into account the volume excluded and the hydrodynamic interactions. Within the limit of very low concentrations, D is given by the relationship of Stokes-Einstein:

$$D_{c \to 0} = D_0 = \frac{k_B T}{6\pi \eta_0 R_{Hy}}$$

where k_B is the Boltzmann constant
T the absolute temperature
η_0 the viscosity of the solvent
R_{Hy} the hydrodynamic radius of the diffusing particles. /61

II.4.3.3. Experimental Device and Conditions

The device presented in figure II.9 allows the measurement of the mean diffused intensity, the current leaving the photomultiplier (P.M.) being proportional to the intensity of light received on the P.M. cath-

ode. If we send the electrical signal leaving the P.M. onto a discriminator + correlator system, the assemblage allows us to analyze the temporal fluctuations of the diffused intensity.

The optical source used is a Spectra-Physics laser with ionized argon operating at 488 nm. The diffused light is collected according to a predetermined angle by the intermediary of a system of lenses and focused on the P.M. cathode (I.T.T., F.W. 130). For the applications of quasi-elastic diffusion of light, the function of correlation of the diffused intensity depending on the time is derived with the assistance of a 48 channel digital correlator (Precision Devices and Malvern Systems Ltd.). /62

The polymer solutions are vacuum-cleaned by centrifugation of the diffusion cells at 10000 t/mn for one hour.

The solutions presenting a fluorescence phenomenon when they are illuminated by a light beam of 488 nm wavelength, we have arranged an interferential filter in front of the P.M. in such a fashion to reduce the contribution of the fluorescent intensity detected. With these conditions, the intensity due to fluorescence is negligible compared to the signal due to diffusion. This has moreover been confirmed by experiments carried out at a wavelength of 632.8 nm (by using a Helium-neon laser) which does not induce fluorescence in the samples. The increment of the index of the solution in relation to the solvent is measured on a Debye type differential refractometer sold commercially by Brice Phoenix.

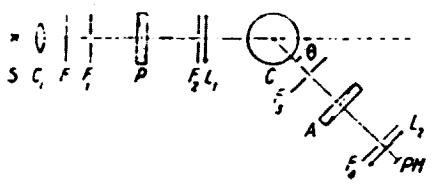

Figure II.9. Principle of a measurement apparatus of diffused intensity

F1, F2, F3, F4: slits; L1, L2: convergent lenses; S: light source; c: condenser; P: polarizer; C: measurement cell; A: analyzer; F: interferential filter; PM: photomultiplier.

II.4.3.4. Results and Discussion

A) Measurements of Diffused Intensity

The values presented in table II.4 are calculated from measurements of diffused intensity by the solvent (I_s) and by the different solutions

(I) at an angle of 90° in relation to the direction of propagation of the incident beam.

TABLE II.4 /63

Ester/hexane concentration en g/cm³	$\frac{I-I_s}{I_s} = i$	$10^3 \frac{c}{i}$	$\frac{I-I_s}{I_{Bz}}$	$10^6 \frac{\partial \Pi}{RT \partial c}$	$10^{-7} D$
$3,3\ 10^{-4}$	0,03 ±0,01	11	0,021		
$6,6\ 10^{-4}$	0,03 ±0,01	22	0,021	239	
$9\ 10^{-4}$	0,045 ±0,005	20	0,032	217,4	
$3,3\ 10^{-3}$	0,27 ±0,05	12,2	0,19	132,7	
$6,6\ 10^{-3}$	0,6 ±0,05	11	0,43	119,6	24,1
$1,33\ 10^{-2}$	1,38 ±0,05	9,7	0,981	105,5	23,6
$2,67\ 10^{-2}$	2,51 ±0,05	10,6	1,80	115,3	23
$4,04\ 10^{-2}$	3,70 ±0,05	10,9	2,64	118,5	21,5
$5,4\ 10^{-2}$	4,96 ±0,05	11,1	3,47	120,7	20,5
$6,8\ 10^{-2}$	5,8 ±0,2	11,6	4,18	126,2	19,9
$1,00\ 10^{-1}$	7,2 ±0,2	14,7	4,85	159,9	15,8
$1,20\ 10^{-1}$	7,2 ±0,2	16,8	5,70	182,7	17,2
$1,41\ 10^{-1}$	7,3 ±0,1	19,3	5,20	209,9	16,7
$1,60\ 10^{-1}$	7,2 ±0,1	22,1	5,18	240,3	16,8
$1,80\ 10^{-1}$	7 ±0,1	25,7	5,00	279,5	16,4
$2,20\ 10^{-1}$	6,4 ±0,1	34,4	4,55	374,1	16

I_{BZ} is the intensity diffused by benzene which we have selected as reference substance.

The ratio I_{BZ}/I_S is in our case equal to 1.4.

The value of the ester/hexane increment measured with the assistance of a Debye type differential refractometer is 0.1068 from 546 and 632.8 nm.

With a view of measuring the mass of the dispersed particles, /65 we have reported in figure II.10 the values of the ratio c/i as a function of the concentration. In the case of benzene, as reference substance, the equation (2-8) becomes:

$$0.681 \frac{I_{Bz}}{I_s} \times \frac{c}{i} \times \left(\frac{\partial n}{\partial c}\right)^2 = \frac{1}{M_w} + 2A_2 c \qquad (2\text{-}14)$$

We then have:

$$\lim_{c \to 0} \frac{c}{i} = \frac{1}{M_w}$$

The curve $\frac{c}{i} = f(c)$ presented in figure II.10 demonstrates a very clear change in behavior in the vicinity of the concentration of 1.

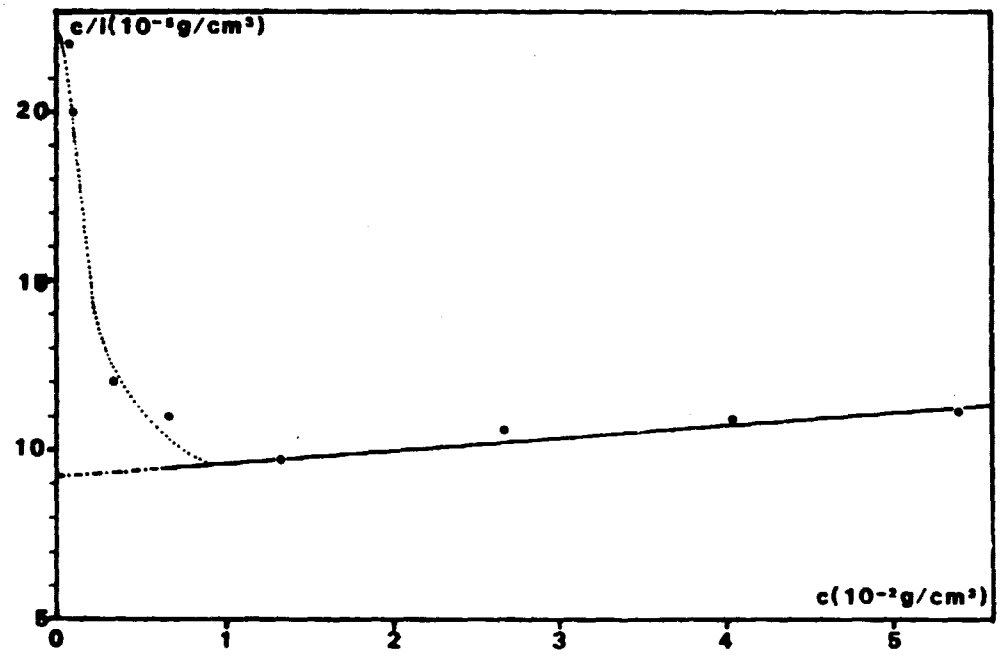

Figure II.10. Development of the ratio c/i as a function of the concentration of ester solutions in hexane.

This transition leads to variations of the structure and mass of the particles in solution and can be reconciled with the phenomenon of critical micellar concentration observed in solutions of amphiphilic compounds (Mittal, 1977).

From measurements carried out in the concentration zone of $10^{-2} \leq c \leq 7 \cdot 10^{-2}$ g/cm^3, it is possible to determine a particular mass through extrapolation to zero concentration. We obtain:

$$\lim_{c \to 0} \frac{c}{i} = 9.2 \text{ where } M_w = 10000 \pm 500.$$

In the realm of very low concentrations, we can estimate the molecular mass by working out the mean of the two values of the ratio c/i corresponding to the lowest concentrations. The mass thus obtained is 4300, corresponding well enough to the theoretical molecular mass of the polymer.

Thus, in the zone of concentrations less than 10^{-2} g/cm^3, the aqueous solution was molecularly dispersed within the hexane, whereas at higher concentrations the value of the particular mass , 2 or 3 times higher than the molecular mass, shows the existence of molecular associations of micellar type, including two or three principal molecules (the presence of micella including a higher number of molecules was probably more in the minority).

The slope of the straight line obtained in the zone of concentration of $10^{-2} \rightarrow 7 \cdot 10^{-2}$ g/cm^3 reveals the existence of a second non-zero coefficient of virial and thus interparticular interactions. /67

Taking into account the polymolecular structure of the dispersed particles, it appears reasonable to assume that these indications are of hard sphere type. This is confirmed besides by the aspect of the curve:

$$\frac{I - I_s}{I_{Bz}} = F(c)$$

presented on figure II.11 demonstrating a maximum in the vicinity of $1.5 \cdot 10^{-1}$ g/cm^3. This value of the concentration is very close to that provided by the hard sphere model developed by Vrij (1970). Similar results have been obtained in the case of micro-emulsions (Cazabat, 1980), suspensions of latex or particles of silica (A.K. Van Helden, 1980). We have thus taken the model of Vrij et al. to analyze the results of diffused intensity as a function of the concentration.

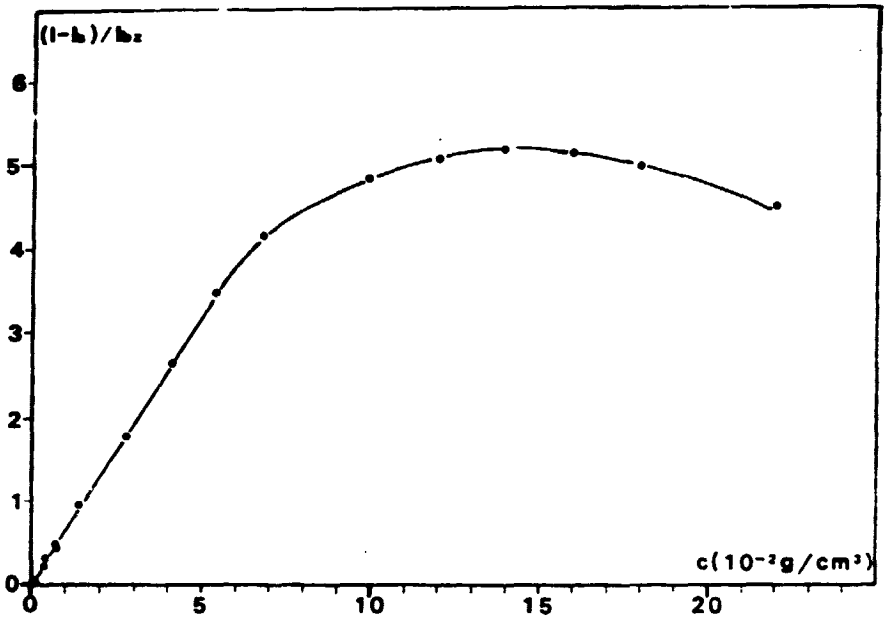

Figure II.11. Development of the ratio $\frac{I - I_s}{I_{Bz}}$ as a function of the concentration of ester solutions in hexane.

For hard spheres, the mean interaction potential, of repellent type $V(r)$, is given by the following relationship:

$$V(r) = \begin{cases} \infty & r \leq \sigma_{HS} \\ 0 & r > \sigma_{HS} \end{cases} \qquad (2\text{-}16)$$

where Γ is the distance between the centers and σ_{Hs} the diameter of the hard spheres.

Thiele (1963) has been able to solve the equation P_y for such interaction potentials and has found two somewhat slightly different analytical expressions of the osmotic pressure according to the methods adopted to link the statistical theory with thermodynamics, a very exact expression has been found by combining the two solutions of equation P_y. This expression proposed by Carnahan and Starling (1969) has the following form:

$$\pi = (cRT/M)\, F_{(c)} \qquad (2\text{-}17)$$

$$F_{(c)} = (1 + qc + q^2c^2 - q^3c^3)(1-qc)^{-3}$$

where $R = \mathcal{N}k$ and $q = \pi \sigma_{Hs}^3 \mathcal{N} / 6M$

with $\mathcal{N}$ = Avogadro number
k = Boltzmann constant
σ_{Hs} = hard sphere diameter
M = mass of particles.

/68

By deriving (2.17), we obtain:

$$\frac{\partial \pi}{RT\partial c} = \frac{1}{M}\left(\frac{\partial}{\partial c}\, c \cdot F_{(c)}\right) = \frac{1}{M}\left[F_{(c)} + \frac{\partial F_{(c)}}{\partial c} \times c\right]$$

with all calculations made:

$$\frac{\partial \pi}{RT\partial c} = \frac{1}{M}\,\frac{(1+2qc)^2 - q^3c^3(4-qc)}{(1-qc)^4} \qquad (2\text{-}18).$$

Here figure II.12 represents a network of curves composed of the experimental curve:

$$\frac{\partial \pi}{RT\partial c} = F\ (c)$$

and those calculated from relationship (2-18) for different values of σ_{Hs}.

The experimental curve presents, in the zone of concentration of $10^{-2} \leq c \leq 7 \cdot 10^{-2}$ g/cm^3, a linear portion, whose extrapolation to zero concentration allows us to discover the mass of the particles and whose slope allows us to calculate the second coefficient of virial. Indeed:

$$\frac{\partial \pi}{RT\partial c} = \frac{1}{M} + \frac{2\mathcal{N}bc}{M^2} \qquad (2\text{-}19)$$

where

$$b = \tfrac{1}{2}\int_0^{\infty}\left[1 - \exp\left(\frac{V(r)}{RT}\right)\right] 4\pi r^2\, dr \qquad (2\text{-}20)$$

Here the experimental value of the second coefficient of virial is thus equal to:

$$b = 3.56 \cdot 10^{-20}\ \text{cm}^3.$$

Then knowing the form of the hard sphere potential (2-16), we obtain:

$$b = \frac{1}{2}\int_0^{\sigma_{Hs}} 4\pi r^2\, dr = 2\pi\sigma_{Hs}^3 \qquad (2\text{-}21)$$

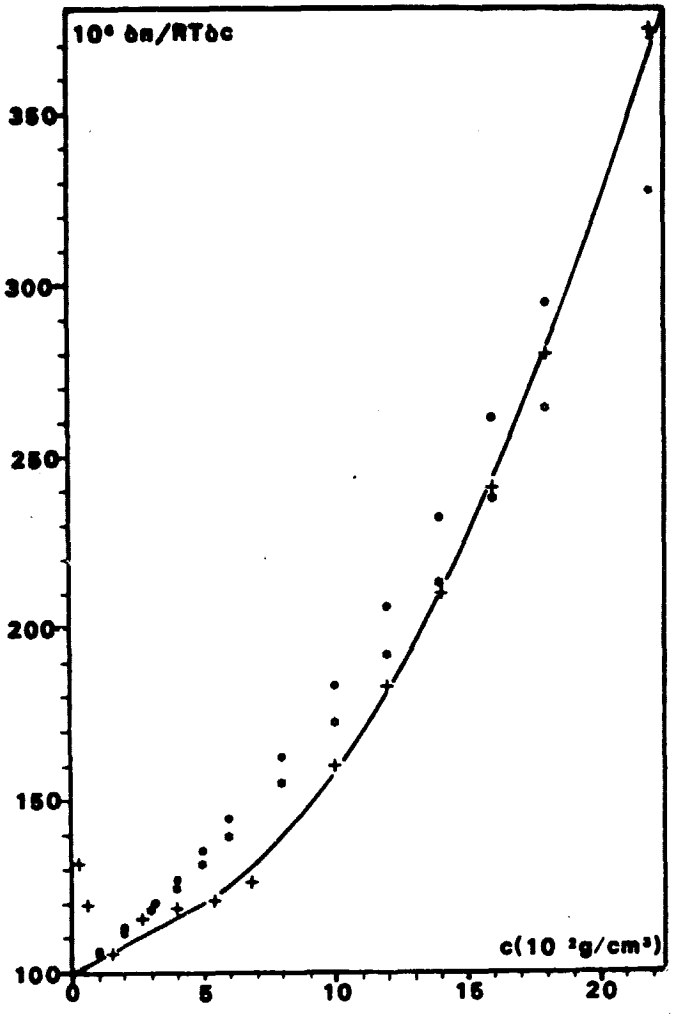

Figure II.12. Curve of $\frac{\partial n}{RT\partial c}$ as a function of the concentration of ester solutions in hexane: /69

+ experimental curve

✡ theoretical curve for R_{hs} of 28 A

• theoretical curve for R_{hs} of 29 A

Then where we extract an experimental value of σ_{Hs}:

$$\sigma_{Hs} = \left(\frac{3b}{2\pi}\right)^{1/3} = 25.7 \text{ Å}$$

Then this value of the hard sphere diameter is somewhat slightly different from that calculated by considering the compact polymer particle: /70

$$\sigma_c = \left(\frac{6M}{\pi \mathcal{N} d}\right)^{1/3}$$

with σ_c = diameter of the compact sphere
M = mass of the particle = 10000
$\mathcal{N}$ = Avogadro number
d = density of the polymer = 0.964
T_c = 32 Å

The disagreement observed between σ_{Hs} and σ_c can be due to the existence of an attractive type interaction potential. This is confimed also by the examination of the network of curves $\frac{\partial \pi}{RT \partial c}$ as a function of the concentration (figure II.12).

Indeed, no calculated curve gives satisfactory agreement with the experimental curve, the best result being obtained for σ_{Hs}=29 Å. In order to take into account the attractive interaction potential, Vrij has considered this last as a perturbation of the hard sphere potential.

If we select a function of the Van der Waals type:

$$F_2(r) = -A \left(\frac{\sigma_{Hs}}{r}\right)^6$$

or its equivalent expression as a function of C:

$$F_2(c) = -a \frac{\mathcal{N}^2}{M^2} c^2 \qquad (2\text{-}22)$$

the analytical expression of the osmotic pressure by taking into account (7) becomes:

$$\pi = \left(\frac{cRT}{M}\right) F_1(c) + F_2(c) \qquad (2\text{-}23)$$

or
$$\frac{\partial \pi}{RT \partial c} = \frac{(1-2qc)^2 - q^3c^3(4-qc)}{M(1-qc)^4} - \frac{2\mathcal{N}^2 a}{RT M^2} c \qquad (2\text{-}24)$$

where
$$\frac{(1+2qc)^2 - q^3c^3(4-qc)}{M(1-qc)^4} - \frac{\partial \pi}{RT \partial c} = 2\frac{\mathcal{N}^2 a c}{RTM^2} \qquad (2\text{-}25).$$

We thus observe that, in the case of an attractive perturbation, the difference between the theoretical values calculated from the hard sphere theory and the experimental values must be linear as a function of the concentration, the slope of the straight line allowing us to know the amplitude of the attractive function. Figure II.13 presents the curves $\frac{(1+4qc)^2 - q^3c^3(4-qc)}{M(1-qc)^4} - \frac{\partial \pi}{RT\partial c}$ as a function of the concentration for different values of σ_{Hs}. The best straight lines are obtained for values of σ_{Hs} between 31 and 32 Å, thus very close to the diameter σ_c of the compact sphere previously calculated (σ_c=32 Å). It is nevertheless necessary to remark that the attractive potential can not be treated as a perturbation on the set of concentrations. Indeed, for c >10%, it interferes by one third in the value of $\frac{\partial \pi}{RT\partial c}$, which is not a negligible quantity in the face of the contribution due to the hard sphere potential. It is also interesting to note that we discover a value of σ_{Hs} of the same order of magnitude as previously ($\sigma_{Hs} \simeq 29 \rightarrow 31$ Å).

II.4.3.4.2. Quasi-Elastic Diffusion (QELD)

The auto-correlation curves have been compared with simple exponentials, the various having been found lower than .1 in all our tests (this corresponds to polydispersity on the order of 1.4). The values of the diffusion coefficient obtained for solutions of different concentrations are grouped in table II.4, presented in chapter II.3.1. In order to determine the value of the hydrodynamic radius (R_{Hy}) of particles, we have shown on figure II.13b the values of the coefficent of diffusion as a function of the concentration. By extrapolating the linear portion of this curve (Zone $10^{-2} \rightarrow 7 \cdot 10^{-2}$ g/cm^3) to zero concentration we extract the value D_o. The hydrodynamic radius is then calculated from the expression:

$$R_{Hy} = \frac{kT}{6\pi\eta D_o}$$

where T = 298 K /74
k = Boltzmann constant
η = hexane viscosity
η = 0.294 cp
D_o= coefficient of diffusion extrapolated at zero concentration

we find R_{Hy} = 30 ± 2 Å.

II.4.3.5. Conclusion on the Results

The value of the radius of particles found by the freezing fracturing technique is in good agreement with that found by QELD ($R_p \simeq R_{Hy} \simeq 30$ Å).

On the other hand, the value of the hard sphere radius found from measurements of mean diffused intensity is not completely in agreement with the preceding ones ($R_{Hs} \simeq 14$-16 Å).

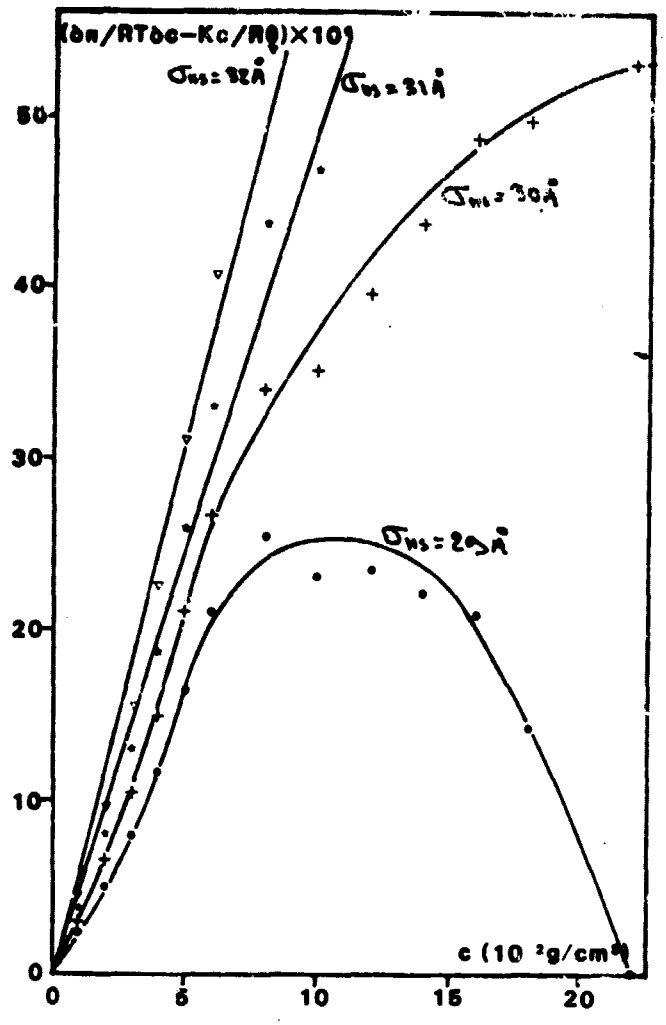

Figure II.13. Difference between the value of the osmotic compressibility $\frac{\delta\pi}{\delta c}$ calculated by the solution of Carnahan and Starling and the experimental value, both divided by RT as a function of the concentration c in ester for different values of the diameter of the hard sphere.

The difference $R_{Hy} - R_{Hs}$ is on the order of 15 Å, which corresponded well enough with the unfolded chain length of the C36 diacid and the C13-C15 alkyl radicals situated at the end of the chain.

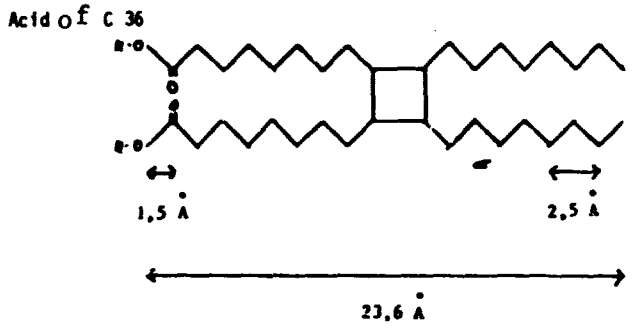

Alcohol of C_{13}

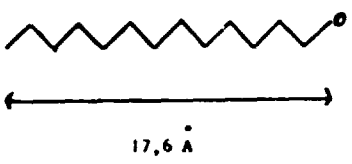

Alcohol of C_{15} l = 20,1 Å

/73

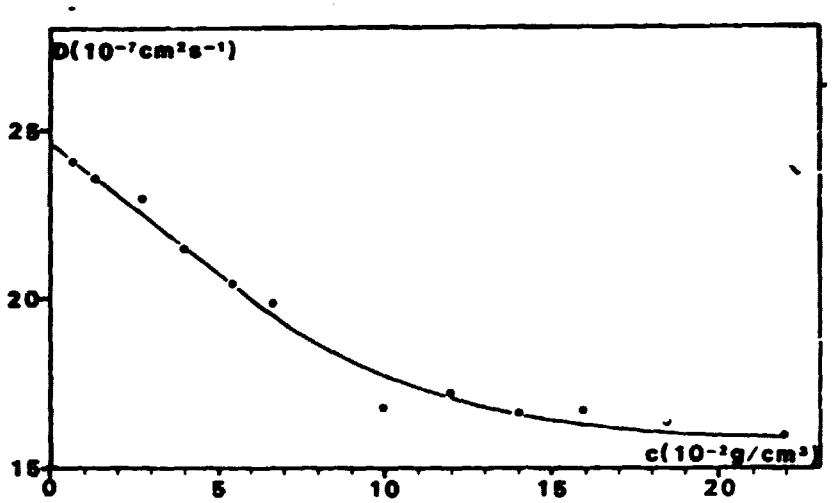

Figure II.13b. Variation of the coefficient of diffusion as a function of the concentration of the solutions in esters.

/75

Then in fact, if we observe that the chains of the alkyl diacid and alcohols situated on the end of the chain have random strengths and are not completely unfolded, it is then possible to propose a micellar structure. The diagram presented in figure II.14 represents the ester micella.

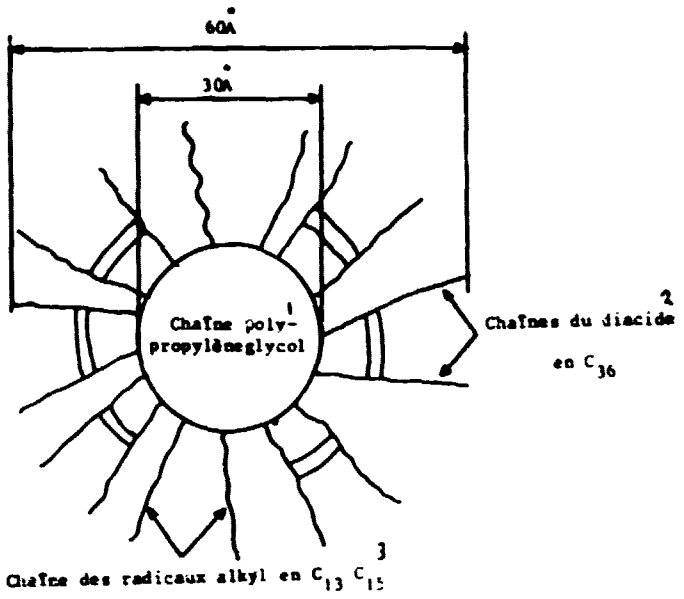

Figure II.14. Structural model of the ester micella (bimolecular here)

Key: 1-Poly-propyleneglycol chain; 2-C36 diacid chains; 3-C13 C15 alkyl radical chain.

With the density of polypropylene glycol being 0.964 and the mass of this in the molecule being 3000, the nucleus will have for a radius:

$$R_{Pro} = \frac{1}{2}\left(\frac{6M}{\pi d N}\right)^{1/3} = 14.2\ \text{Å}$$

This value is approximately that of the hard sphere radius ($\frac{\sigma_{Hs}}{2}$ ≃16 Å).

II.4.4. Study of the Adsorption of the Additive at a Solid-Liquid Interface

Among the techniques allowing us to study adsorption of the polymers at a solid/liquid interface, two types are largely used:
-Hydrodynamic techniques based on capillary viscosimetric measurements (Orhm, 1965; Fleer, 1972) or derivatives on porous filters (Gramain, 1976), as well as measurements of electrophoresis (Fleer, 1971).
-Ellipsometry based on the analysis of the reflection of a beam of polarized light by a polymer film adsorbed on a surface (Killmann et al., 1970, 1974, 1977; Takahasi et al., 1980).

For the study of the adsorbed film of the additive, we have used the technique of ellipsometry. Preferably, we have carried out tests of measurement of the thickness of a monomolecular ester film at the liquid/gas interface by the Bac method of Langmuir (1932) which has only allowed us to form conclusions in relation to the parameter studied. Indeed, when the liquid phase is water or a saturated solution of potassium nitrate in water, the polar portions of the molecule (polypropylene glycol chains) "plunge"into the liquid during compression of the film, not allowing us to determine the value of the specific area of the molecule in a dense monomolecular film.

II.4.4.1. Summary Description of the Experimental Method and Device

This method is based on the analysis of change in polarization which are subjected to a luminous wave at the time of its reflection by an interface.

In general, the two orthogonal components of the electrical field of the polarized incident wave are modified by reflection; thus, with the assistance of an adequate model (Malin and Vedam, 1976) by using relative variations of phase and amplitude of the two components of the /77
electrical field. It is then possible to determine, with the assistance of a single measurement, certain physical properties of a system such that the real and imaginary portions of the complex refraction index, dielectric constant of a substrate, or even the thickness and the index of refraction of a transparent film deposited on a substrate whose characteristics are known.

The measurements which we have carried out have been made with the assistance of an ellipsometer whose diagram is presented in figure II.15.

II.4.4.2. Experimentation

For practical reasons, the measurements of the thickness of the film adsorbed have been carried out at the air/gold interface, the support being constituted of a polished glass plate covered with a 1000 Å layer of gold, this choice being guided by the necessity of having very polished and reproducible surfaces. Measurements have to be made in air, the difference in index between the ester and the solution of this in the dodecane being very low. The experimental process has thus been the following: the mirror, previously cleaned with hot hexane (sohxlet) and immersed into a solution filtered through 0.1 millipore of 1% ester /79
in dodecane. The mirror is retreated with the solution at specified intervals, rinsed with RPE hexane, then placed in the ellipsometer It is necessary to note that, at the start of a test carried out in situ on a stabilized polymer film, we have seen that desorption of the polymer in the presence of pure hexane was very slow. Consequently, rinsing of the substrate with hexane does not result in appreciable desorption of the product.

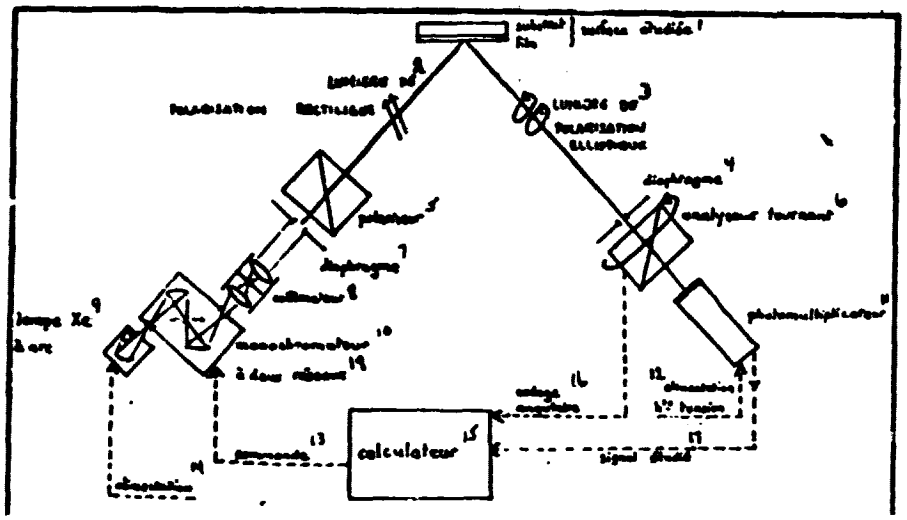

Figure II.15. Diagram of the ellipsometer used.

Key: 1-Substrate/film: surface studied;2-rectilinear polarization light;3-elliptical polarization light;4-Diaphragm;5-polarizer;6-turning analyzer;7-diaphragm; 8-Collimator;9-Xe arc lamp;10-Monochromator;11-Photomultiplicator;12-High pressure supply;13-Command;14-supply;15-Calculator;16-Angular coding;17-Signal studied; 18-With two diffraction gratings.

II.4.4.3. Results and Discussion

Figure II.16 presents values of the thickness of film adsorbed from measurements carried out on a mirror at time t_o (mirror alone) and 5 mn, 30 mn, 60 mn, and 120 mn. We note that the thickness of the stabilized film is on the order of 17 ± 1 Å, duration corresponding to one hour. Taking into account these results and different models of adsorbed layers of polymers on the one hand (Silberberg, 1962; 1968; Hoeve et al, 1965; 1970; 1971; Weber et al, 1976), and fatty acids on the other hand (Hardy, 1936; Bailey and Courtney-Pratt, 1955; Trillat, 1925; Bragg, 1925; Muller, 1928; Germer and Storks, 1939; Brummage, 1947) we can propose a possible structure of the adsorbed additive film. This is presented in figure II.17.

The length of lipophilic chains is on the order of 20 to 23 Å (see II.4.3.5). The PPG chains are connected at the surface by several sites forming rings developing within the liquid and constituting a film of mean thickness on the order of several Å (Silberberg, 1971). With these conditions, the mean thickness of the entire film will be less than the unfolded length of the alkyl chains. Moreover, this is in good agreement with the mean thickness found of 17 ± 1 Å. /80

We will estrapolate these results to the case of 100C6 steel.

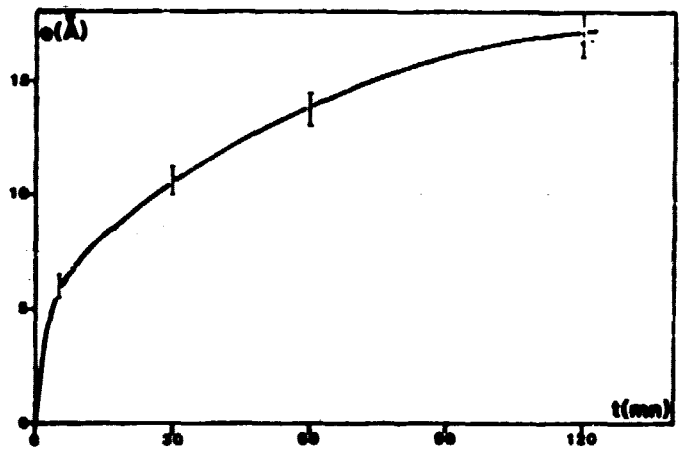

Figure II.16. Variation of the thickness of film adsorbed of ester on a metallic surface (gold) as a function of time from a 1% solution of ester in dodecane at 298 K.

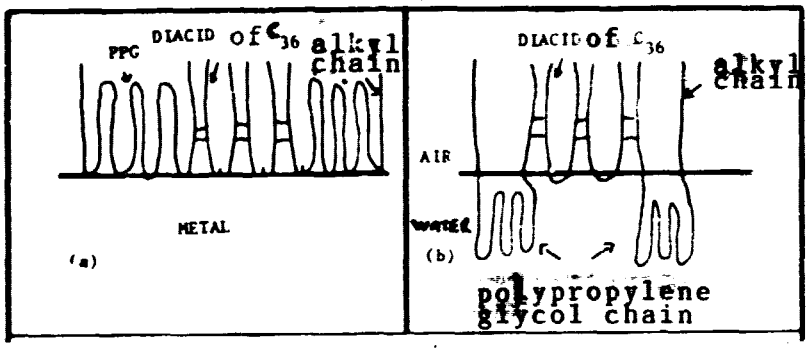

Figure II.17. Structure proposed for the adsorbed film.

a) on metallic surface
b) water/air interface (Langmuir)

II.5. Influence of the Lubricant Structure on its Anti-Friction Properties

II.5.1. Experimental Device and Conditions

The sphere/plane tribometer used for our tests is described in detailed fashion in Appendix A, as well as the response of this system to a known stress in order to avoid errors of interpretation. The tribological parameters relative to our tests have been given in paragraph II.2.6 within table II.1. Manipulaitons are carried out in the following fashion. The sphere and plane are placed in static contact in the presence of the lubricant. The plane is then induced with uniform

rectilinear movement (V=50 μm/s) over a distance of 0.5 mm (≃3 hertzian diameters). During the sliding of the pieces on each other, the friction force and the electrical resistance to contact are measured.

II.5.2. Description of Measurements Carried Out in a Test

During our friction tests on a sphere/plane simulator, two measurements are carried out:
-measurement of the friction force which allows us to obtain the coefficient of friction through the relationship:

$$\mu = \frac{\vec{T}}{\vec{W}}$$

where μ = coefficient of friction
$\vec{T}$ = unit of friction force
$\vec{W}$ = unit of normal force applied at contact

-measurement of electrical resistance to contact which we will attempt to interpret in chapter III. /81

In the graphs presented in figure II.18, three zones can be considered:
-Zone 1 corresponding to the placement under stress of the measurement chain (transitory state of contact-c.f. II.2.4) during which sliding propagates annularly from the periphery of the contact up to the center of this, and where we do not record the relative macroscopic displacement of the pieces in frictional contact.
-Zone 2 during which the friction force increases up to a maximum $\vec{T}_{max}$ /82
while simultaneously the electrical resistance to contact passes from a value on the order of 1 Ω to approximately 10^3 Ω, then decreases slowly to attain a minimum value when $\vec{T}$ is maximum. This part of the graph will be studied in chapter III.
-Zone 3 where the friction force $\vec{T}$ decreases to a stable value which we will call the dynamic friction force ($\vec{T}_{dy}$). The electrical resistance to contact then has a low value ($R_c \leq 1\,\Omega$).

In what follows in this chapter, we will only concern ourselves with the value of $\vec{T}_{dy}$, this being measured after a displacement of three hertzian diameters. We will study the significance of the thickness of the adsorbed film and presence of micella within the lubricant on the value of the dynamic friction force, this at the temperature at which we have carried out the tests of light diffusion and ellipsometry.

II.5.3. Variation of the Dynamic Friction Force as a Function of the Adsorption Time of the Ester on Pieces in Frictional Contact

The sphere and plane are placed in the presence of the lubricant (1% solution of ester in dodecane) for a given time. The pieces in frictional contact are then placed in static contact, then the friction test is carried out in the presence of the lubricant.

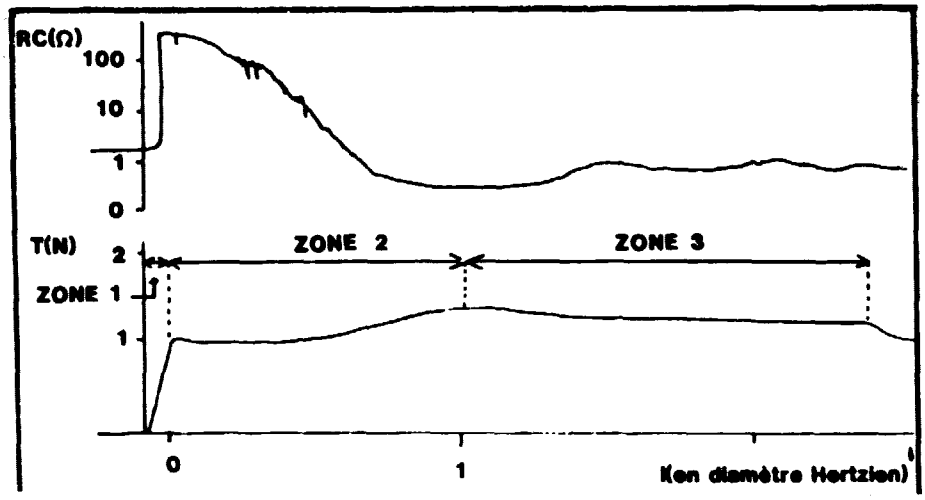

Figure II.18. Graph of the electrical resistance to contact R_c and of the friction force as a function of the distance travelled l by the sphere on the plane.

Key: 1-K in Hertzian diameter.

Figure II.18 presents the curve of development of the coefficient of dynamic friction ($\mu_{dy}=\frac{T_{dy}}{W}$) as a function of the time during which the pieces have been placed in the presence of the ester solution.

We have superimposed on this curve the isotherm of adsorption of the ester at the gold/solution interface obtained in paragraph II.4.4.3. We thus see that the coefficient of dynamic friction passes from a value on the order of 0.19 obtained at the end of an adsorption time of 30 seconds to a value of 0.11 after 120 minutes of adsorption. The decrease is very rapid at the start (after 30 mn of adsorption, μ_{dy} is not greater than 0.12), corresponding to the rapid increase of the mean thickness of the adsorbed film, then decreases, the coefficient of friction passing from 0.12 to 0.11 for respective adsorption times of 30 and 120 minutes, corresponding to a portion of the adsorption isotherm where the increase of the film adsorbed is slow. /84

Figure II.18 shows us that the mean thickness of the adsorbed film influences the coefficient of dynamic friction, although the two curves presented are not completely in agreement.

Figure II.19 presents the developments of the electrical resistance of contact and the friction force in zone 2 as a function of the time during which the pieces in frictional contact have been placed in the presence of the lubricant before carrying out the sliding. We see that the extent of zone 2 varies as a function of the adsorption time (lengthening of the signal of electrical resistance of contact), while the maximum value of the friction force decreases. The thickness of the adsorbed film thus also influences this zone.

/83

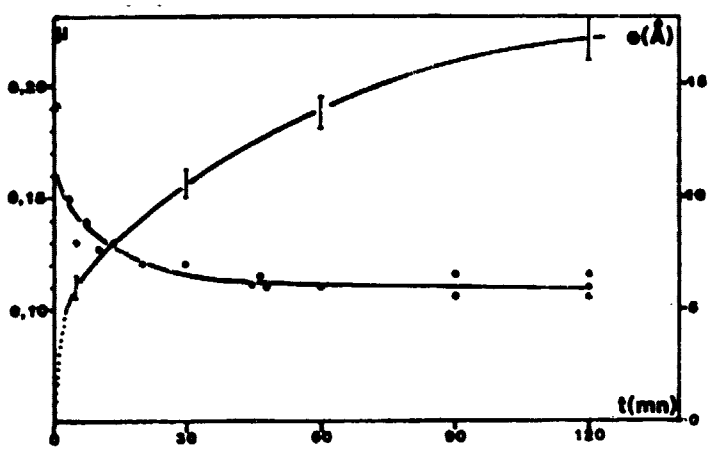

Figure II.19. Development of the coefficient of friction and thickness of adsorbed film of ester as a function of the contact time of the surfaces with the lubricant (1% solution of ester in dodecane, T=298 K).

II.5.4. Importance of the Micellar Aspect of the Lubricant in the Reduction of Friction

/85

In order to carry out this study, the sphere and plane are placed in the presence of a 30% solution of ester in dodecane for 30 min, so that the adsorbed film has attained its equilibrium thickness. The friction test is then made in the presence of the solution. The pieces are then rinsed with the next solution, of lower ester concentration, and the friction test is carried out in the presence of this. The operation is then repeated for 30, 20, 10, 1 and 0.1% solutions of ester in dodecane. Figure II.20 groups the values of the coefficient of dynamic friction as a function of the concentrations of the ester solutions.

We see that the effect of concentration is very low on the value of the coefficient of friction (approximately 10% of the mean value). We always observe an appreciable variation when we pass from the concentration of 1% to 0.1% of ester, this last corresponding to the critical micellar concentration which we had discovered during light diffusion tests (c.f.II4.3.4.1). It thus appears, from our tests, that the presence of micella in the solution contributes very slightly to the reduction of friction.

II.5.5. Microscopic Appearance of Surfaces After Frictional Contact

II.5.5.1. Experimental Method

Examination, through transmission electron microscopy, of the surfaces having frictional contact was carried out on platinum-carbon replicates with the friction scars obtained at the time of the test on

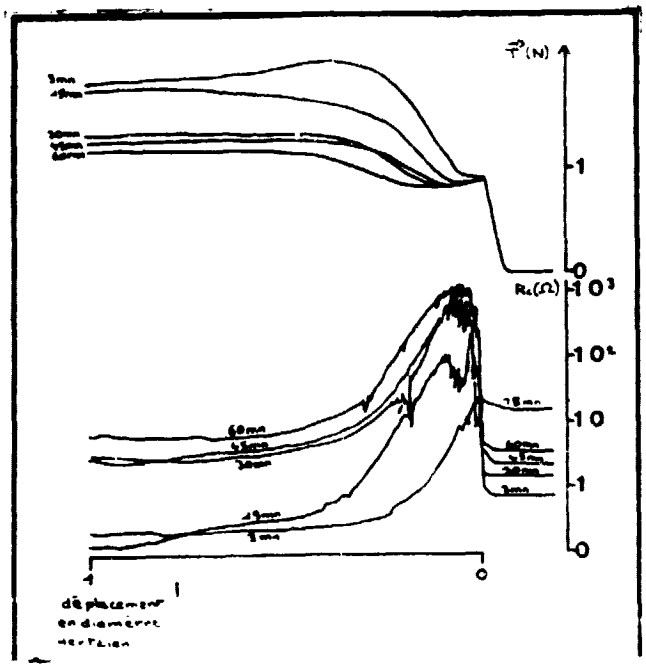

Figure II.20. Development of the graphs of the friction force and electrical resistance of contact as a function of the adsorption time of the ester on the surfaces.

Key: 1-Displacement in Hertzian diameters.

the plane with treated 100C6.

For this, the plane is rinsed after the test in a hexane bath with ultrasonics, then introduced intothe vacuum chamber for cryo-fracturing (c.f. I.2.2). After having achieved the vacuum (10^{-6} mmHg), the replica is made through pulverization with a 30 Å layer of platinum according to an incidence of 45°, then with a 300 Å thick carbon layer with an incidence of 90° (c.f. I.3.3). The plane is then reduced to atmospheric pressure. The replica is detached with the assistance of a 1% solution of Teepol in water, then rinsed in three baths of twice distilled water. It is then deposited on a support grid and examined by transmission electron microscopy. /87

II.5.5.2. Results and Discussion

Figure II.22 presents transmission electron microscopy plates carried out on the friction marks obtained, on the one hand, during a simple advance unidirectional test (which we have studied during this chapter), and, on the other hand, during an alternative test, the sphere having then carried out several advances-returns on the plane.

In the first case (figure II.22a), we observe almost no degradation of the lubricant of cluster type or tribochemical film (Martin

/86

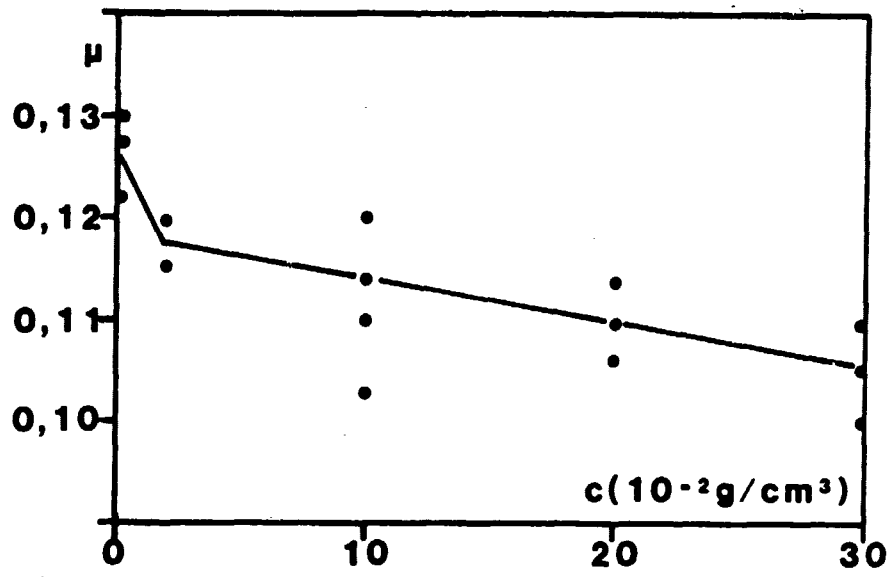

Figure II.21. Development of the coefficient of dynamic friction as a function of the ester concentration in the lubricant solutions.

1978); on the other hand, in the second case (figure II.22b) the surface is littered with cylindrical particles,arranged on the average perpendicularly to the friction scar, composed of degradation products of the additive formed during friction. Figure II.22c shows the detail of debris, this having the form of a roll formed by rolling up of a fine skin of degraded product (the thickness of the skin is estimated at 100 Å taking into account the overshadowing).

Formation of the tribochemical film constituting the rolls can be explained by in situ polymerization (Reda, 1975; Furey, 1975) through homo- or heterolytic fragmentation of the ester when this is subjected to a high rate of shearing (De Gennes, 1974) or to photoactivator radiation which can constitute the exo-electrons emitted by the metal during sliding (Basset, 1982). Polymerization can occur according to the type of fragmentation, in ionic or free radical fashion. /89

II.6. Conclusion

During this chapter, we have been able to define several significant points:
-Study of the solution, by freezing fracturing and light diffusion techniques, has allowed us to collect a significant amount of data on the behavior of the ester in solution with dodecane, and has revealed the existence of molecular aggregates for which we have been able to propose a structure in agreement with the results obtained.
-We have been able, with the assistance of ellipsometry, to have access to the thickness of the ester film adsorbed at a metal/solution interface, as well as at its adsorption isotherm.

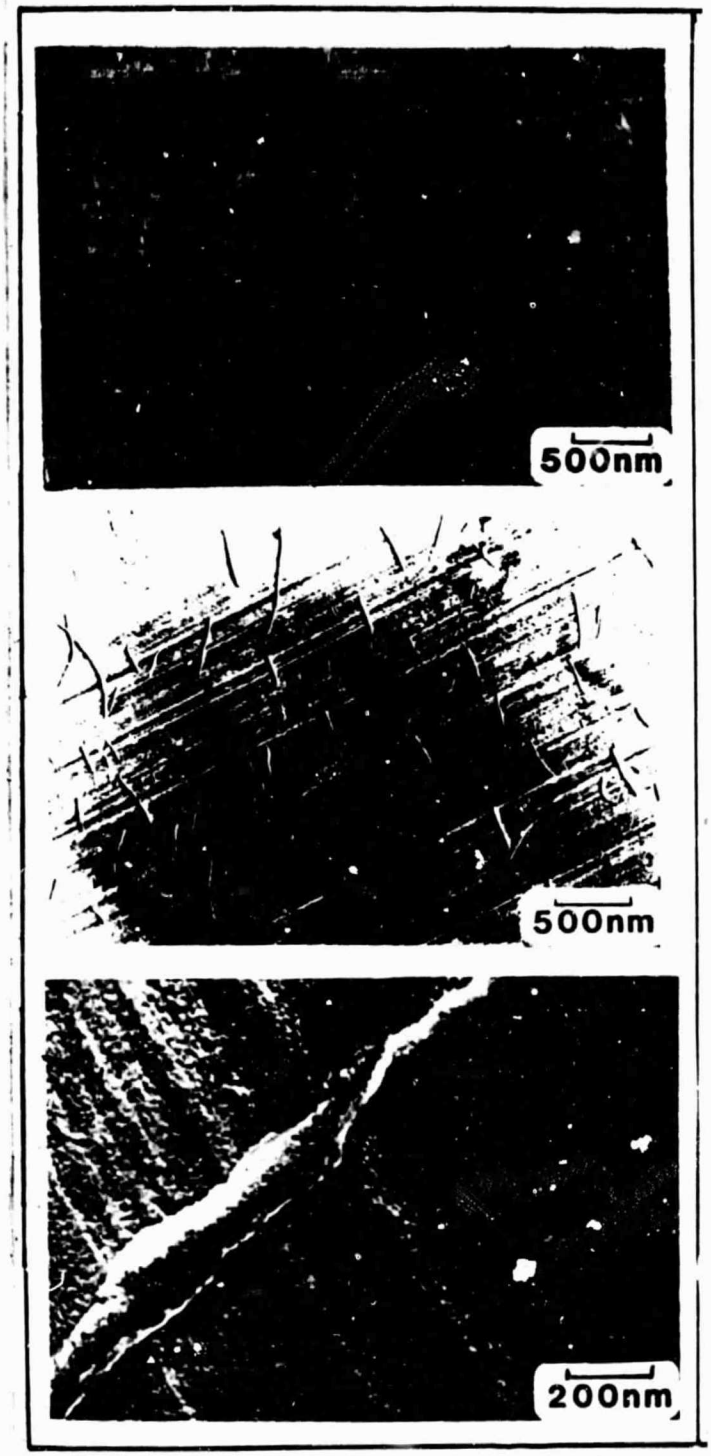

Figure II.22. TEM plates obtained from replicates of platinum/carbon surfaces.

a) on a unidirectional friction scar simply going.
b) and c) on a friction scar obtained after several advance-returns of the piece on the plane.

-The friction tests which we have carried out allow us to see that the coefficient of dynamic friction, as well as the friction force and electrical resistance to contact and the friction force in zone 2, depends in significant fashion on the mean thickness of the adsorbed ester film on the pieces in frictional contact. On the other hand, with stablized adsorbed film, the effect of the concentration of lubricating solutions, and the presence of micella within these, very slightly affects the coefficient of dynamic friction (10% of the mean value).

The figure below summarizes the results obtained: /90

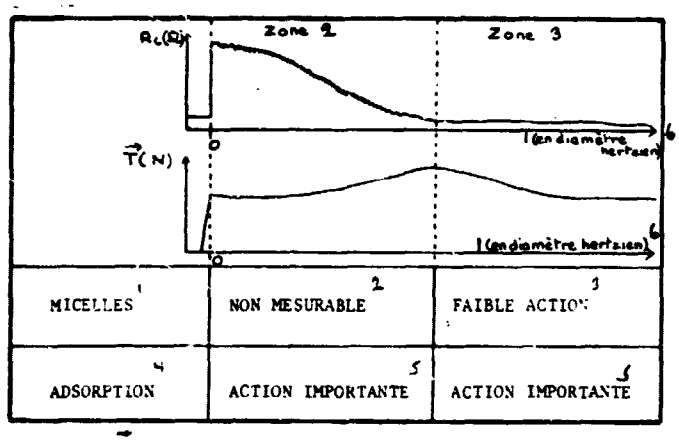

Key: 1-Micella; 2-Not measurable; 3-Slight action; 4-Adsorption; 5-Significant action; 6-In hertzian diameters.

-Finally, microscopic examination of the friction scars has revealed that at the time of a simple advance unidirectional test, degradations of the additive are not discernible, and that, on the other hand, in the case of alternative tests, the additive undergoes significant transformations, resulting in the presence of "rolls" in the friction scar.

A certain number of tests were necessary to complete this study, in particular by varying the parameters such as load and temperature. In the case of this latter parameter, this would prescribe the use of a less volatile base than dodecane (squalane), which would give rise to a certain number of changes in the structure of the solutions and would pose problems for studies by light diffusion and by ellipsometry of the behavior of the additive in solution.

Chapter III /91

Reduction of Boundary Friction by Monomolecular Films

III.1. Use of Electrical Measurements of Contact

III.1.1. Electrical Conduction Within an Interface by Monomolecular Lubrication

III.1.1.1. Description of the Measurement Circuit of Resistance of Contact

III.1.1.2. Demonstration of the Phenomenon of Electrical Conduction in an Interface by Monomolecular Lubrication During the Critical Instants of Sliding

III.1.1.3. Study of Some Characteristics of the Electrical Contact Phenomenon

III.1.1.4. Hypothesis Published to Interpret the Development of the Electrical Resistance of Contact

III.1.1.4.1. Method of Construction in the Interface is Standard

III.1.1.4.2. Electrical Transports in the Interface Made Through Tunnel Conduction

III.1.2. Electrical Transports Through the Monomolecular Layers

III.1.2.1. Electrical Transports Through Monolayers of Langmuir-Blodgett Type

III.1.2.2. Electrical Transports in Adsorbed Monolayers

III.1.2.3. Demonstration of Tunnel Conduction in the Case of Adsorbed Ester Complex Layer of Polypropylene Glycol

III.1.2.4. Demonstration of Tunnel Conduction with Hertzian Contact of a Normally Loaded Sphere-Plane Lubricated Monomolecularly /92

III.2. Interpretation of the Relationship Between the Electrical Contact Resistance and the Coefficient of Friction

III.2.1. Experimental Curves

III.2.2. Separation Hypothesis

III.2.3. Determination of the Analytical Expression of the Function

III.2.4. Estimation of the Variation of Thickness

III.2.5. Estimation of the Exponent

III.3. Conclusion

Chapter III /93

Reduction of Boundary Friction by Monomolecular Films

III.1. Use of Electrical Measurements of Contact

III.1.1. Electrical Conduction Within an Interface by Monomolecular Lubrication

III.1.1.1. Description of the Measurement Circuit of Resistance of Contact (Figure III.1)

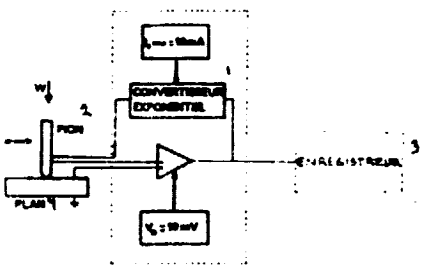

Figure III.1. Diagram of the sphere/plane principle of tribometry and the measurement circuit of the electrical resistance of contact (RC).

Key: 1-Exponential converter;2-Piece;3-Recorder;4-Plane.

The measurement circuit of the resistance of contact which we have used has already been described in the literature (Tonck, 1979).

Contact is supplied by a feedback loop such that the fall of pressure between the materials in contact remained constant and continuously equal to 10 mV. The feedback loop acts as an exponential current generator which gives a logarithmic scale of discharge for the values of electrical resistance to contact. Limitation of the current to 10 mA preserves the contact from any deterioration during measurement. The complete system furnishes a logarithmic response for resistance values of 1 Ω to 10 MΩ. For the low resistances to contact, the current regulator modifies the response of the circuit which becomes practically linear between 0 and 1 Ω. The common method of rejection is sufficiently great to avoid noise. The response in the frequency of the circuit depends on the amplitude of the signal. In the most favorable case (R_C=10 Ω), the upper limit is approximately 100 KHz. This pressure control circuit has the advantage of not involving the condenser, formed by the interface, in the measurement of the intensity and thus allows us to observe instantaneous variations of the electrical resistance to contact. /94

III.1.1.2. Demonstration of the Phenomenon of Electrical Conduction in an Interface by Monomolecular Lubrication During the Initial Instants of Sliding

The tests were carried out with the same conditions as in chapter II. The lubricant present in the form of a monomolecular film during contact is the complex ester of polypropylene glycol studied in chapter II.

Figure III.2 presents simultaneous recordings of the development of the friction force and the electrical resistance to contact at the time of sliding of the sphere on the plane.

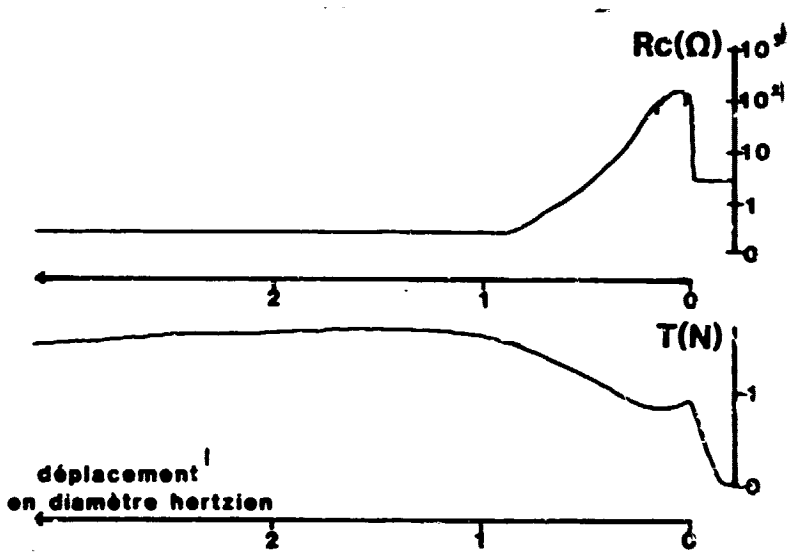

Figure III.2. Simultaneous recordings of the development of the electrical resistance to contact and the friction force as a function of displacement of the sphere on the plane.

Key: 1-Displacement in Hertzian diameters.

A great number of recordings jointly grouping the developments of the resistance to contact and the friction force as a function of the displacement have allowed us to conclude that these two parameters are correlated. In all cases, we note that total sliding (c.f. II.2.5) is obtained for a value of tangential force on the order of 1 N, corresponding to a shearing concentration on the order of 40 N/mm^2 (for a loaded contact at 10 N) and that this increases up to a maximum value F (on the order of 2 N) at the end of a sliding distance equal to approximately one Hertzian diameter. Jointly, we note from the start of sliding (the sensitivity of our measurement devices does not allow us to locate the start of the phenomenon in the transitory or dynamic zone), an increase of the value of the resistance contact by a factor /96

greater than or equal to 10^5. The resistance value then decreases slowly up to a minimum value (on the order of 0.1 to 0.01 Ω) in the majority of cases, when the friction force is maximum. In order to eliminate the possibility of an electromotive force phenomenon created at the time of frictional contact and already observed as well in the literature (c.f. II.2.4), we have been induced to reverse the polarities of the measurement system (the F_{em} adding to the pressure applied to the boundaries of contact would avoid [illegible] when we reverse the polarities of the measurement system, thus radically modifying the recording). This has allowed us to immediately reject the F_{em} hypothesis, the recordings not being affected by modification of the electrical measurement system.

III.1.1.3. Study of Some Characteristics of the Electrical Phenomenon of Contact

Figure III.3 demonstrates the sensitivity of the phenomenon to micro-deteriorations of the surfaces during sliding. Indeed, the curve recorded is practically smooth when we do not note any deterioration of the surfaces in the contact area (figure III.3a). On the other hand, we observe that the signal is very much affected when the contact area allows a scratch to appear (figure III.3b), created by unevenness of one of the surfaces or abrasive particles present during the contact. In the case where the surfaces have deteriorated in significant fashion (figure III.3d), the increase of resistance of contact is non-existent. /98
This demonstrates well the sensitivity of the electrical measurements of contact to local deteriorations inthe hertzian zone, sudden drops of this being theoretically explainable besides, the resistance of conduction at the level of the deterioration (metallic contact) being low (0.01 Ω) for junctions of diameter greater than 0.1 µm.

It is for this reason that it is necessary to work with hyper-polished surfaces ($R_a \leq 100$ Å) and eliminate as much as possible abrasive particles caught on the surfaces (ultrasonic bath).

Figure III.4 presents recordings obtained at different sliding velocities.

The reproducibility of the signal obtained allows us to conclude that the phenomenon is independent of this tribological parameter in the zone of velocity studied. The recording of the development of the resistance of contact presented in figure III.5 is characteristic. Indeed, the sphere is set to sliding, then stopped at the end of several microns displacement, then after several seconds, it is again set to sliding.

We note on this recording that the resistance of contact does not drop to a low value at the stop of sliding, thus eliminating the hypothesis of a purely dynamic phenomenon. Nevertheless, the slow decrease of the resistance of contact over time (10 in 3 sec), accompanied by a slight decrease of the friction force, tends to demonstrate that a relaxation phenomenon is produced in the interface. This is confirmed by the fact that, at the resumption of sliding, the resistance and friction force recover the values which were found at the stop of sliding,

/97

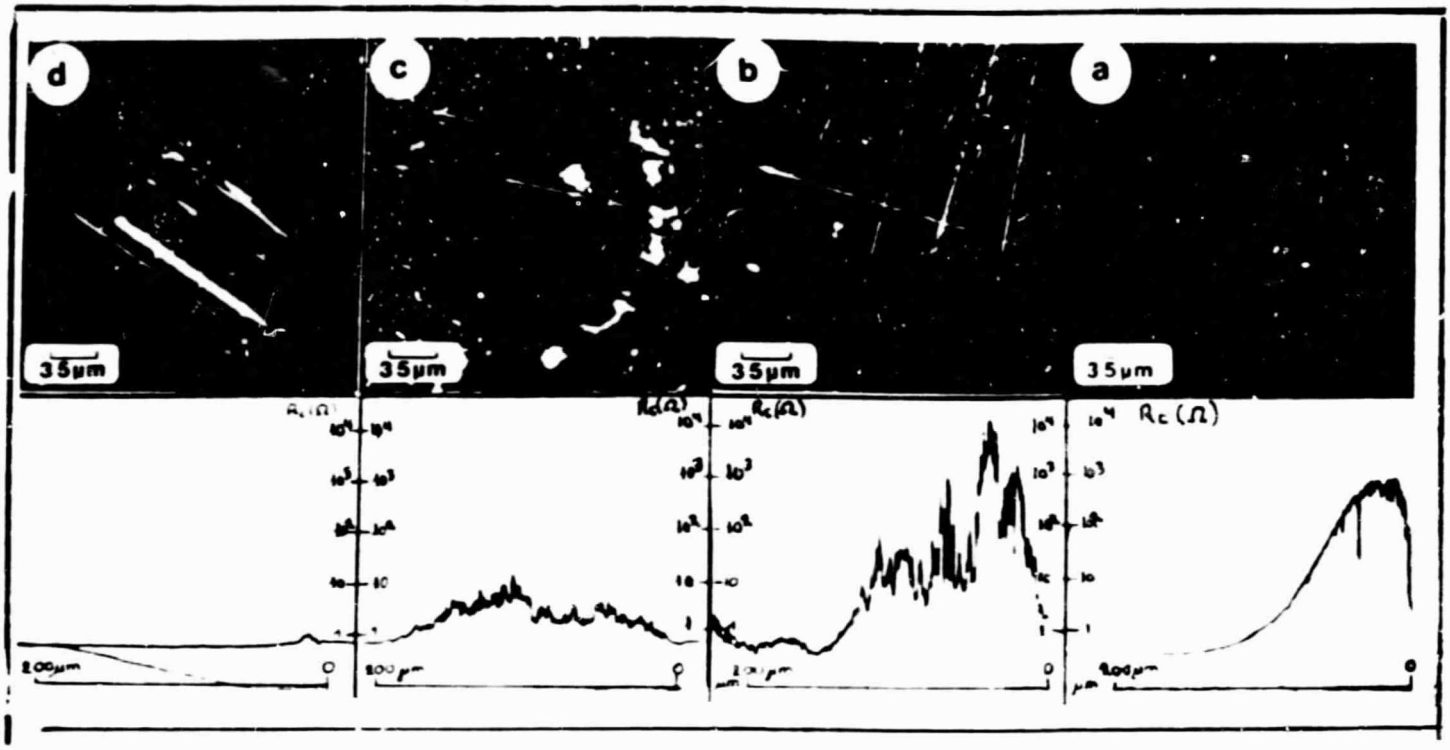

Figure III.3. Degradation of the recordings of electrical resistance to contact as a function of the scratches undergone by the surfaces during sliding in the contact zone.

the remainder of the recording not demonstrating any difference with standard recording.

On the other hand, from II.5.3, the resistance of contact is correlated with the previous adsorption time of the ester molecules on the pieces in frictional contact (figure II.20).

Several observations allow us to conclude that the phenomenon described by the developments of the friction force and the contact resistance is characteristic of the behavior of the monomolecularly lubricated interface during the initial instant of sliding.

III.1.1.4. Hypothesis Published to Interpret the Development of the Electrical Contact Resistance /101

III.1.1.4.1. Method of Conduction in the Interface is Standard

In the simple case of a sphere/plane hertzian contact in the presence of a very narrow isolating layer (h=0.1 µm), homogeneous, of thickness h and electrical conductivity C, in which the type of conduction is standard (ohmic film), the expression of total resistance is

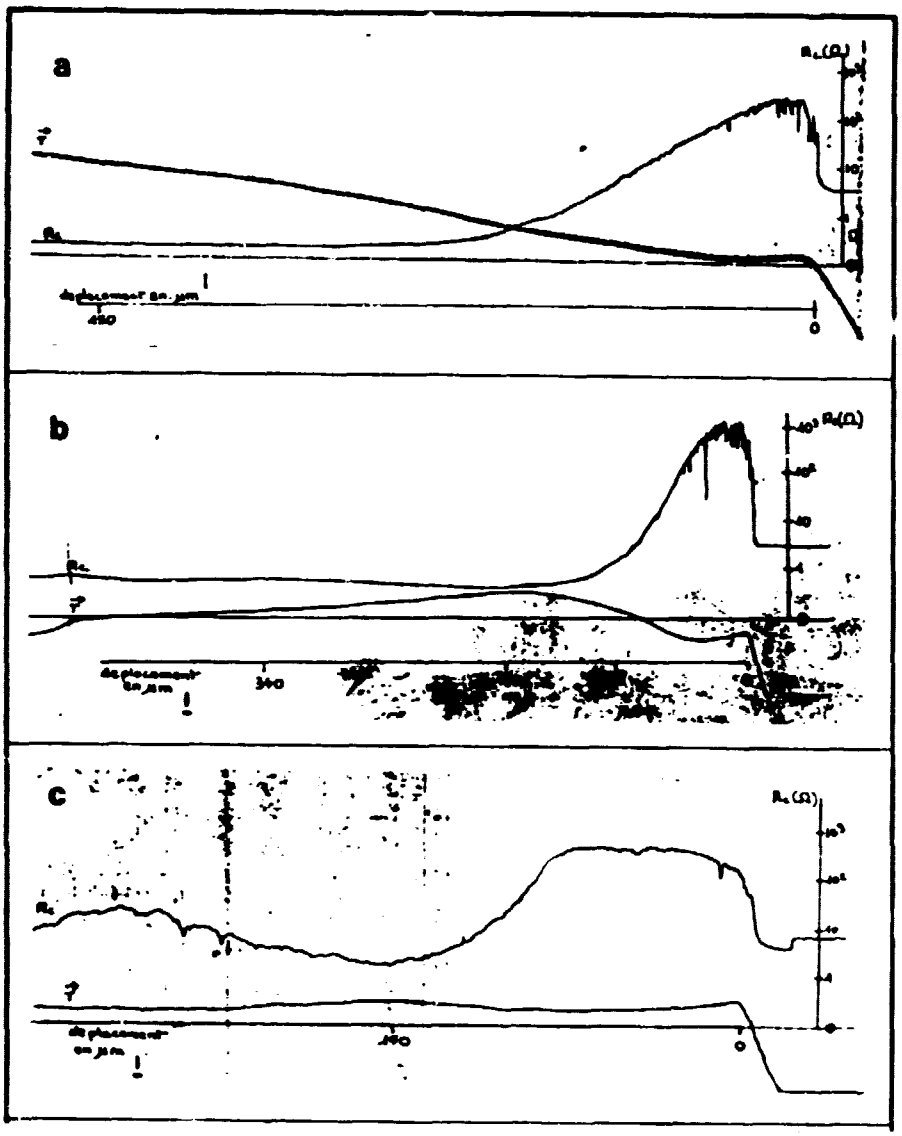

Figure III.4. Recordings of the electrical contact resistance at different sliding velocities.

a) 20 μm/s b) 50 μm/s c) 200 μm/s

Key: 1-Displacement in μm.

after Holm (1967):

$$R_T = \frac{\rho}{2a\sigma} + \frac{h}{\sigma\pi a^2} + \Sigma R_t \qquad (3-1)$$

σ = electrical resistance of the materials constituting the sphere and plane;
R_t = transitional resistance of insulator/metal (negligible) at radius of the contact area calculated from the Hertz theory.

/100

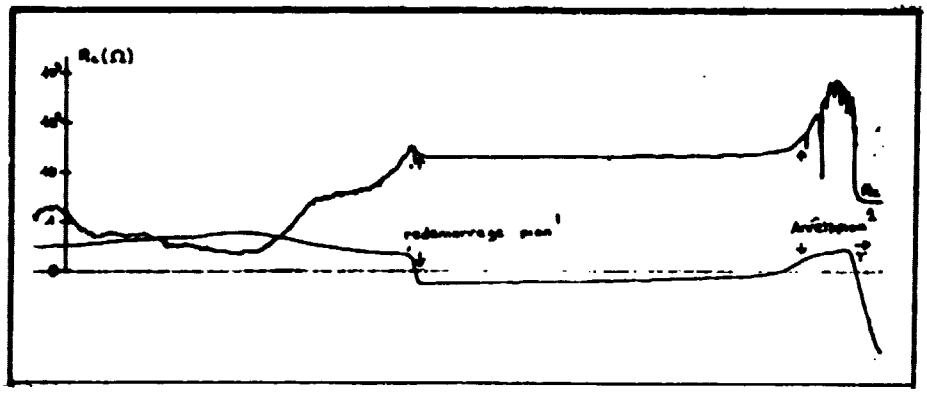

Figure III.5. Recording of the electrical contact resistance during a test where the peice is stopped after several microns of displacement, then in movement at the end of several seconds.

Key: 1-Restarting of piece;2-Stop of piece.

The first term of expression 3-1, due to constriction of the current lines with contact, always has a sufficiently low value (it is on the order of 10^{-2} Ω in our case); we can thus write, for resistances greater than 1 Ω:

$$R_T = \frac{h}{\zeta \pi a^2} \qquad (3\text{-}2)$$

With these conditions, an increase of the contact resistance by a factor of 10^3 was accompanied either by an increase of the thickness, by a decrease of the contact area, or finally by a variation of the electrical conductivity.

As we have seen in paragraph II.2.4, the contact area increases very slightly at the time of sliding, which goes to counter the increase of contact resistance.

An increase of thickness, in the case of a thickness of separation of 3 nm (taking into account the results of ellipsometry presented in chapter II.4.4.3) results in a thickness of 3 μm. To verify this we /103
have proceeded to place an inductive pick-up into position on the measurement face of friction in order to record the variation of thickness of the interface. The recording presented in figure III-6 presents simultaneous developments of the friction force, thickness of the interface, and contact resistance. The slope of the recording of the thickness is due to the absence of parallelism of the plane; however it is necessary to note that it does not present at the start any significant variation of the thickness. The smallest measurable variation with this apparatus being 30 nm, we have carried out an even finer manipulation. The recording presented in figure III.7 has been accomplished with the assistance of a Talystep roughometer of 2 nm height which we have modified into a tribometer by replacing the diamond with

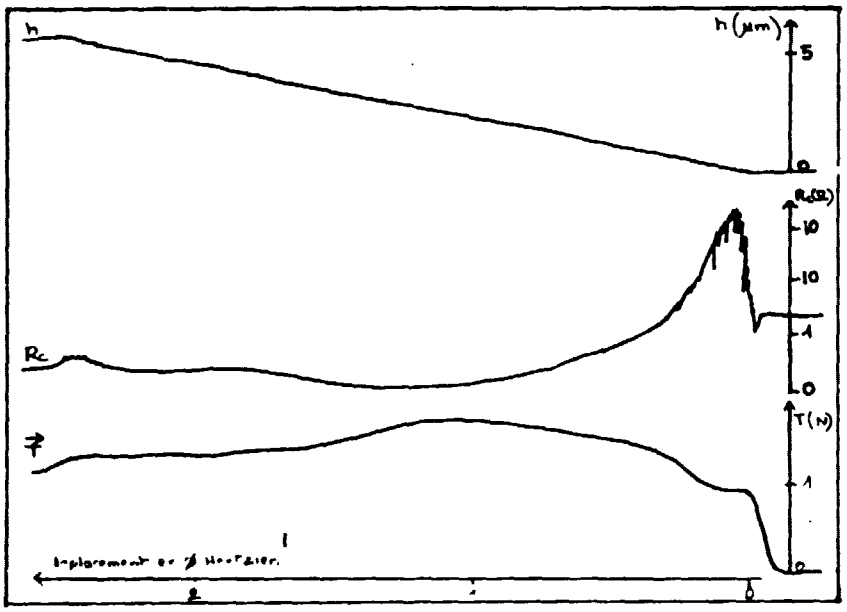

Figure III.6. Simultaneous recording of the friction force of the electrical contact resistance and the variation of thickness of the interface during a friction test in the presence of a 1% ester solution in dodecane.

Key: 1-displacement in Ø hertzian.

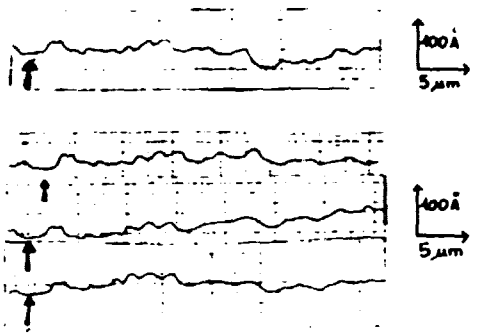

Figure III.7. Friction tests carried out on a plane of 100C6 steel with a roughometer (Talystep) whose diamond has been replaced by a 100C6 steel ball of 3 mm diameter.

a) recording of variations of dried thickness;
b) and c) recording of variations of thickness in the presence of the ester solution.

a hyperpolished 100C6 steel ball of 3 mm radius. The plane is constituted of a flame-polished thin glass plate covered with a 1000 Å layer of cobalt. Sliding of the sphere on the plane is carried out in the presence of the lubricant (solution of ester complex in dodecane).

The recording of the development of the thickness of the interface during sliding does not reveal any appreciable variation of this. It is thus possible that the thickness of the interface varies, but with a very low proportion, the increase occurring below the resolution of the roughometer. The hypothesis of an increase of the thickness of the interface by a factor on the order of 10^3 can thus be rejected. Thus, it only remains to invoke a variation of the electrical conductivity of the interface to explain, in the case of an ohmic film, the variation of resistance.

The decrease of the electrical conductivity of the interface can be due to changes of physical or chemical states occurring in the interface at the start of sliding (transition phase, orientation, crystallization, ..., degradation of the lubricant, ...). However, taking into account the factor involved in the change of conductivity, it seems to us unlikely that these types of phenomena occurring in the interface themselves alone explain the variation of contact resistance.

III.1.1.4.2. Electrical Transports in the Interface Made Through Tunnel Conduction /104

The thickness of the interface being less than 10 nm, we find ourselves in the range of distance where tunnel conduction can occur.

This hypothesis has already been proposed by certain authors (Tripp, Snowball and Williamson, 1966). We will see in the following chapter that a slight variation of thickness, on the order of several angstroms, can be at the origin of a significant variation of the tunnel resistance which could explain the fact that we do not observe significant increase of the thickness of the interface during sliding with the roughometer equipped with tribometer.

III.1.2. Electrical Transports Through the Monomolecular Layers

III.1.2.1. Electrical Transports Through Monolayers of Langmuir-Blodgett Type

A certain number of authors (B. Mann and H. Kuhn, 1979; K.H. Gundlach and J. Kadlec, 1973; E. Polymeropoulos, 1978) have demonstrated that electrical transports through monomolecular layers deposited by the Langmuir-Blodgett method operate by a tunnel conduction process.

Application of a low pressure to the boundaries of a monolayer ($h \simeq 20$-30 Å) contained between two electrodes induces the passage of a tunnel current through this. This current, due to the presence of free

electrons in the metals, have a current density of j. The conductivity (continuous current) then decreases exponentially with the thickness l of the insulating layer. It is given by the equation of Bethe (1930):

$$\sigma=\left(\frac{jl}{v}\right)_{v\to 0} = \frac{e^2}{h^2}(2m\varphi)^{\frac{1}{2}} \exp\left(-\frac{1}{\hbar}(2m\varphi)^{\frac{1}{2}}\right) \qquad (3\text{-}3)$$

obtained from an ideal barrier model of the following potential (figure III.8) with:

e=electron charge
m=electron mass
h=Planck constant

Energy of electron extraction from the metal toward the insulator:

$$\varphi=\tfrac{1}{2}(\phi_1+\phi_2)-\kappa$$ /105

ϕ_1, ϕ_2 of metals 1 and 2 in vacuum
κ=electron affinity of the insulator

Equation 3.3 can be rewritten more simply in the form:

$$\sigma=\left(\frac{jl}{v}\right)_{v\to 0} = b \exp(-2\alpha l) \qquad (3\text{-}4)$$

with $$b=\frac{e^2(2m\varphi)^{\frac{1}{2}}}{h^2} \qquad \alpha=\frac{(2m\varphi)^{\frac{1}{2}}}{\hbar}$$

The resistance of the junction having for expression:

$$R=\frac{V}{j\pi a^2} \qquad (3\text{-}5)$$

V=pressure at the boundaries of the junction
j=tunnel current density
a=radius of the junction

By combining 3.4 and 3.5:

$$R=\frac{1}{b\pi a^2}\exp(2\alpha l) \qquad (3\text{-}6)$$

We thus observe that the value of the resistance of a junction /106
constituted by two electrodes separated by a monolayer of Langmuir-Blodgett type depends on the thickness of this and that a slight variation of l induces a significant variation of this resistance, taking into account the exponenet intervening on l.

III.1.2.2. Electrical Transports in Adsorbed Monolayers

Polymeropoulos and Sagiv (1978) have demonstrated, by graphing the characteristics of I=f(V) at 77°K of junctions constituted of two aluminum electrodes, separated by an adsorbed fatty acid layer, that electrical transports in the adsorbed monolayers are carried out by a tunnel conduction process. However, they have had problems in graphing

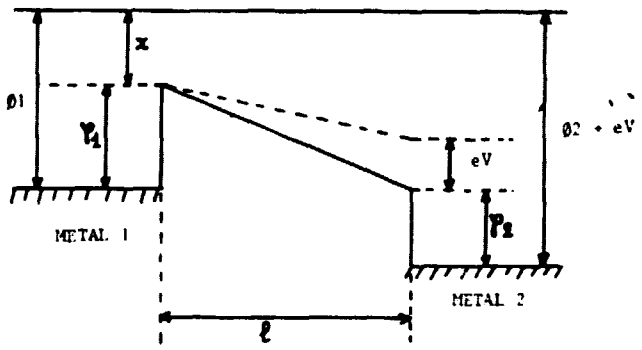

Figure III.8. Idealized barrier potential by Bethe representing two electrons of different metals separated by a thick steel monolayer subjected to low pressure.

the tunnel characteristics of such junctions at ambient temperature (295°K), a phenomenon of conduction through the impurities contained in their adsorbed layers superimposing on the tunnel conduction at this temperature, thus capable of being due to the presence of impurities in the separation products or even to the operational method used by the authors.

III.1.2.3. Demonstration of Tunnel Conduction in the Case of an Adsorbed Ester Complex Layer of Polypropylene Glycol

In order to verify that, inthe case of an adsorbed ester complex monolayer of polypropylene glycol, electrical transports occur through tunnel conduction; we have graphed the characteristic I=f(V) of a 100C6 steel adsorbed layer junction measurement. Figure III.9 presents the diagram of the principle of the installation used to graph the characteristic of the junction.

/107

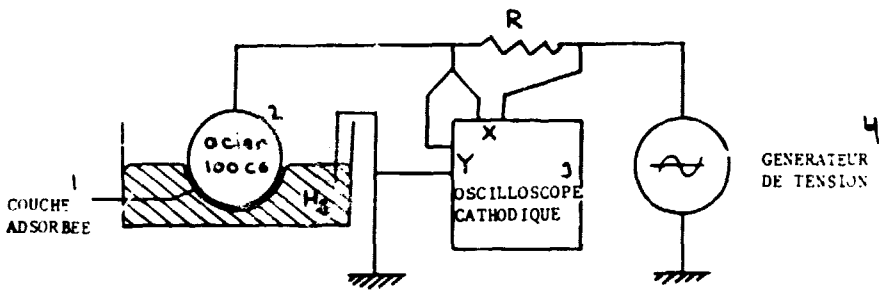

Figure III.9. Installation used to graph the characteristic I=f(V) of a mercury/adsorbed layer junction of ester/100C6 steel.

Key: 1-Adsorbed layer;2-Steel;3-Cathode oscilloscope;4-pressure generator.

The measurements are carried out in the following fashion: The 100C6 steel ball is soaked for 15 mn in a 5% ester solution in dodecane, then rinsed in RPE acetone. It is then deposited at the surface of the mercury (junction area $\simeq$ 1 cm^2). We then apply to the boundaries of the junction a pressure rise of -0.3 to +0.3 v. The characteristic I=f(V) is recorded on a cathode oscilloscope and the curve is photographed.

Figure III.10 presents a recording of the characteristics. /108

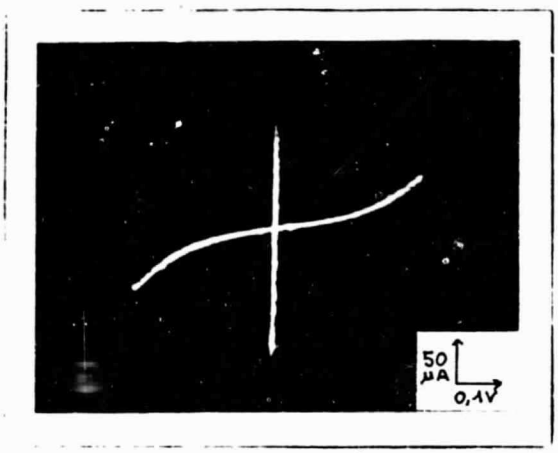

Figure III.10. Characteristic I=f(V) of a 100C6 steel/mercury junction (vertical line) and a 100C6 steel/adsorbed ester complex/mercury junction.

We observe that the metal/mercury junction has an almost zero resistance, while the 100C6 steel/adsorbed layer/mercury junction presents a characteristic I=f(V) corresponding to a tunnelconduction process. Indeed, the resistance is very high for low pressures ($R \simeq 10^4 \Omega$) and decreases progressively and with measurement when we increase the pressure at the boundaries of the junction ($R \simeq 10^3 \Omega$ for V=0.3 v). The recording presented in figure III.10 is in good agreement with tunnel conduction through the ester complex monolayer of polypropylene glycol.

III.1.2.4. Demonstration of Tunnel Conduction with Hertzian Contact of a Normally Loaded Sphere-Plane Lubricated Macromolecularly

The difficulties encountered during tests of recording of the characteristics I=f(V), in the case of a junction constituted by hertzian contact of a sphere-plane lubricated molecularly by an adsorbed ester layer are connected to the contact parameters:

-low surface of junction (0.03 mm^2);
-possibility of metallic contacts, as well as hyperpolished surfaces;
-low resistance of the junction in the case of static contact;
-instability of the resistance of the junction with time when the interface is sheared (see chapter II.1.1.3).

Despite these different problems, we have been able to record characteristics I=f(V) of such junctions. The installation used is presented in figure III.11.

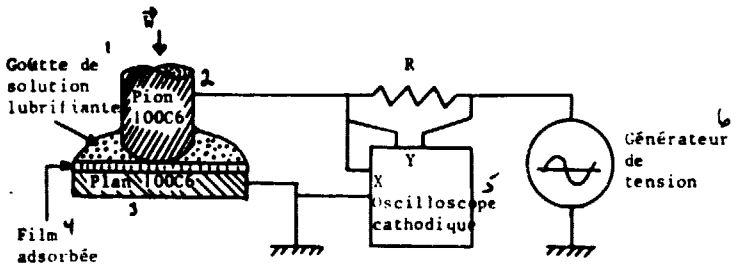

Figure III.11. Installation used for recording of j characteristics I=f(V) of junctions constituted by a sphere/adsorbed layer/plane Hertzian contact.

Key: 1-Drop of lubricating solution;2-Piece;3-plane;4-Adsorbed film;5-Cathode oscilloscope;6-Pressure generator.

The measurements were carried out according to the following process. The piece and the plane are placed in the presence of a 5% ester solution in dodecane for 15 mn, then they are placed in contact under a load of 10 daN. Recording of the characteristic is made as in chapter III.1.2.3. /111

Figure III.12a represents a recording of the characteristic of a sphere-plane static contact. The resistance for low applied pressures to the boundaries of contact is on the order of 0.2 Ω. We note a slight inflexion of the curve beyond 0.15 v tending to demonstrate that we are in the presence of an I/V tunnel characteristic.

The recording presented in figure III.12b is that of the same contact which has slid over tens of microns. The characteristic has been graphed immediately after the stop of sliding. We note that the resistance for low values of applied pressure is on the order of 50 Ω, this higher than in the case of static contact. The curve presents an inflexion beyond 0.2 v demonstrating a decrease of the resistance measured while the pressure at the boundaries of the junction is increased.

This thus confirms, at the start of these tests, that the conduc-

/110

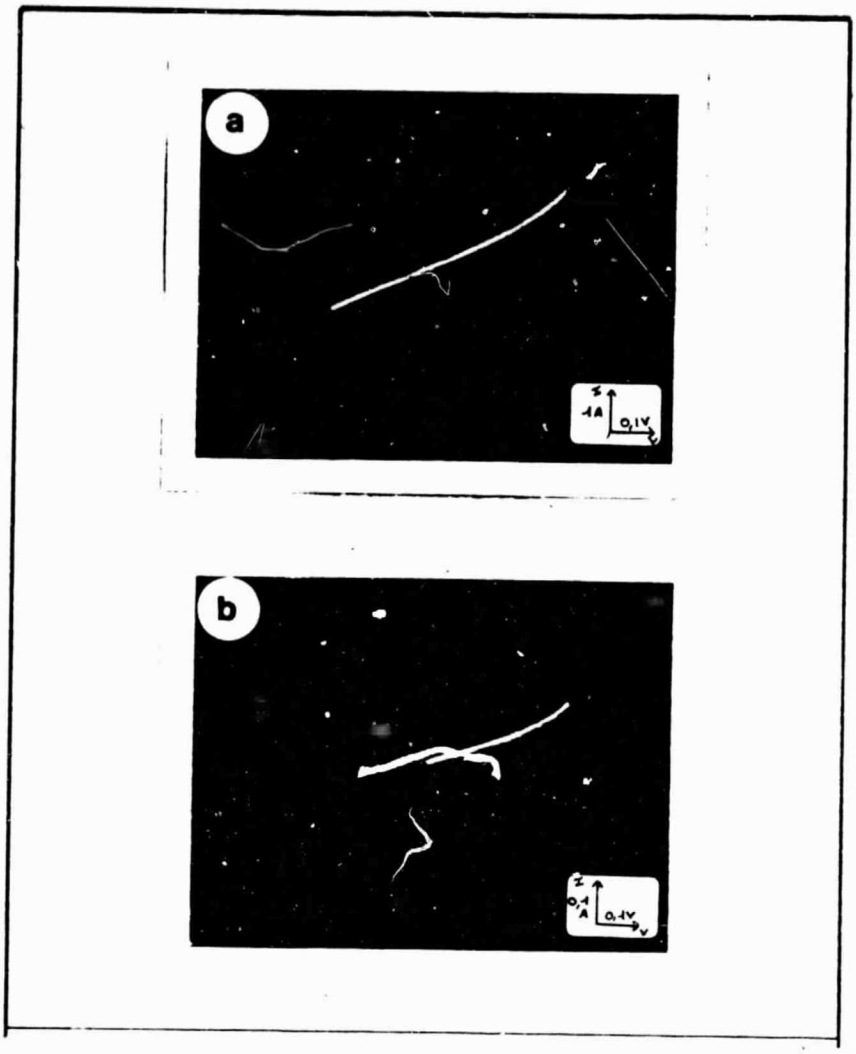

Figure III.12. Recording of I/V characteristics of Hertzian contact.

a) static contact; b) contact having some sliding.

tion involved in a loaded and monomolecularly lubricated sphere-plane hertzian contact is of tunnel type. However, it is necessary to note that the characteristics I=f(V) are unstable over time at ambient temperature (contact developed c.f. III.1.1.3), but it has not yet been technologically possible for us to carry out the standard tests at low temperature in order to eliminate the processes of conduction by impurities and avoid modifications of the interface due to passage of a significant current in this (0.1 to 2 Å).

III.2. Interpretation of the Relationship Between the Electrical Contact Resistance and the Coefficient of Friction

/112

III.2.1. Experimental Curves

Tunnel resistance varying as a function of the thickness of the interface in almost exponential fashion (III.1.2.1), we have taken the values of the coefficient of friction as a function of the logarithm of the correpsonding electrical contact resistance (thus to a close factor of the thickness). Figure III.13 presents a network of curves taken from recordings of the same type as those presented in figure III.2.

/113

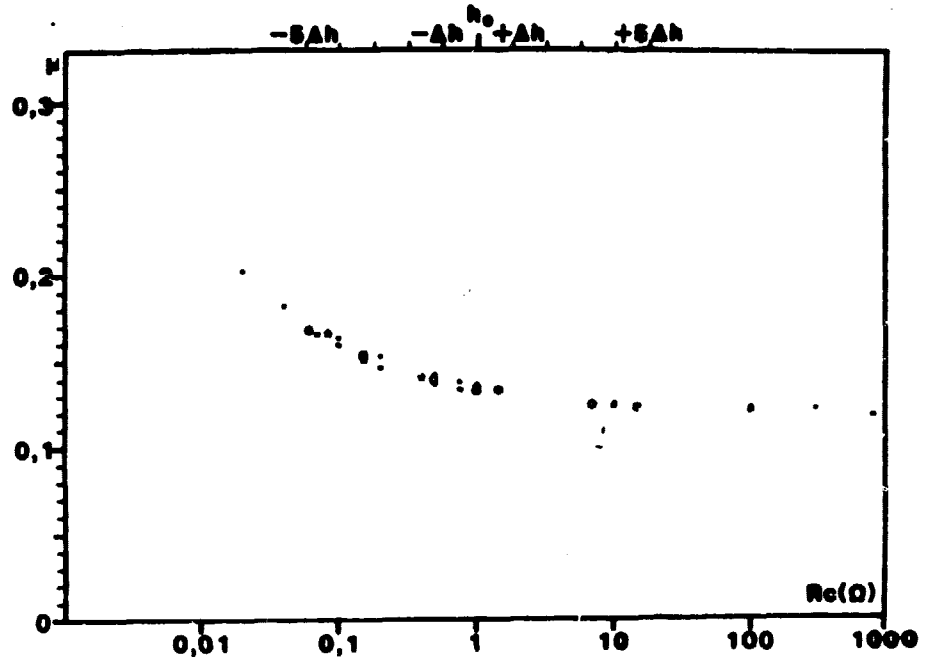

Figure III.13. Curve $\mu = f(\log R_c)$ obtained from several tests.

We see that the development of the coefficient of friction as a function of the logarithm of electrical contact resistance is well reproducible.

In the following part of this work, we will interest ourselves in a mean curve presented in figure III.14.

III.2.2. Separation Hypothesis

By representing expression 3.6 of the tunnel electrical resistance of a junction of thickness h:

$$R = \frac{\rho}{b\pi a^2} \exp(2\alpha h)$$

we then have:

$$\log R = A + \log \rho + \beta h \qquad \beta = 2\alpha \qquad (3\text{-}7).$$

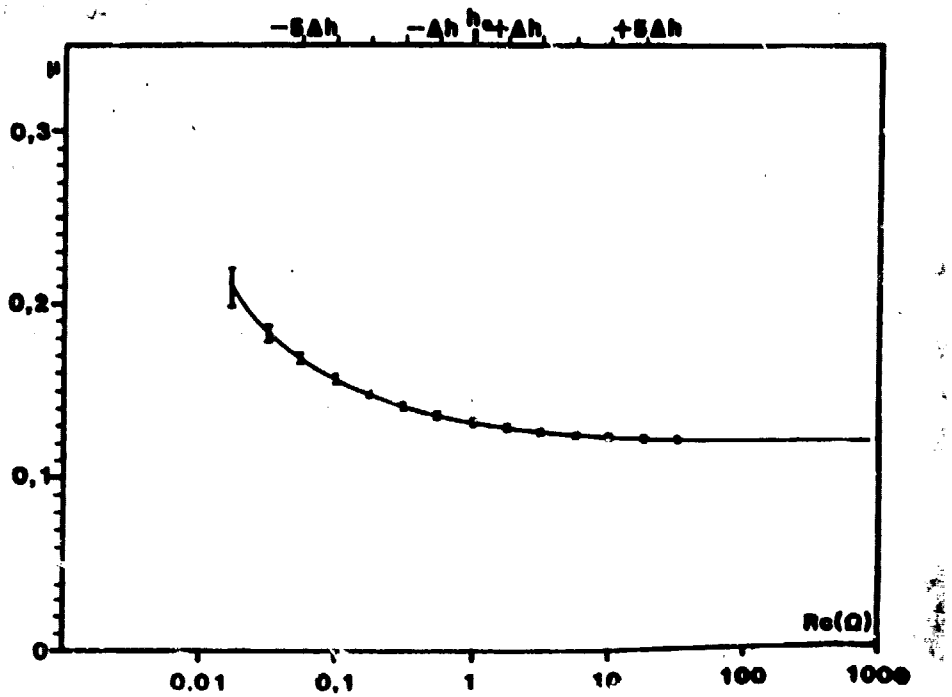

Figure III.14. Mean curve μ-f(log R_c drawn from values of figure III.13.

As the network of curves obtained by Polymeropoulos (1978) presented in figure 3.15 shows us, variation of the value of the conductivity (thus of the resistance) by a factor of 10 corresponds to a relative variation in thickness comprised between 0.01 and 0.05, according to the type of junction studied. With these conditions, the resistance of the junction R_0 corresponding to a thickness h_0 and the variation of thickness h corresponding to a variation of R by a factor n, we have: /115

$$\log R_0 = A + \log h_0 + \beta h_0 \qquad (3\text{-}8)$$

$$\log R_1 = \log nR_0 = A + \log(h_0+\Delta h) + \beta(h_0+\Delta h) \qquad (3\text{-}9)$$

$$\Delta h \ll h_0 \Rightarrow \log nR_0 = A + \log h_0 + \beta h_0 + \log\left(1+\frac{\Delta h}{h_0}\right) + \beta\Delta h$$

$$= \log R_0 + \log\left(1+\frac{\Delta h}{h_0}\right) + \beta\Delta h$$

$$\frac{\Delta h}{h_0} \ll 1 \Rightarrow \log\left(1+\frac{\Delta h}{h_0}\right) \simeq \frac{\Delta h}{h_0}$$

$$\log n = \beta\Delta h + \frac{\Delta h}{h_0} \qquad (3\text{-}10)$$

where (3-11)

With Δh_x ($\Delta h_x \ll h_0$), the variation of thickness corresponding to an increase of resistance R_0 by a factor of n^x. By redoing the preceding calculation, we obtain:

$$x \log n = \frac{\Delta h_x}{h_0} + \beta\Delta h_x \qquad (3\text{-}12).$$

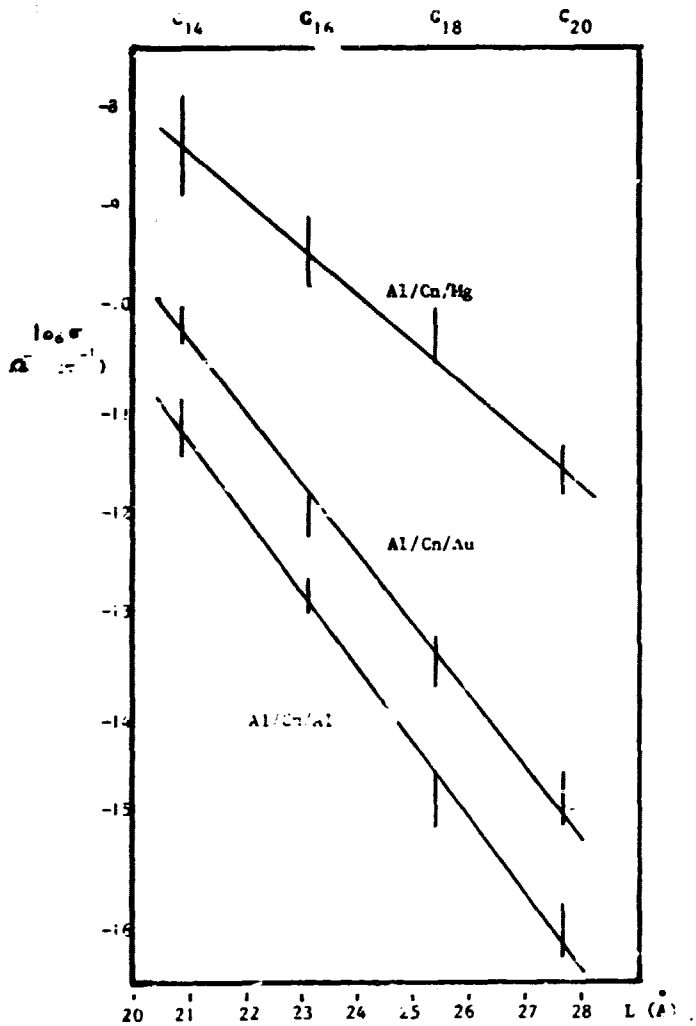

Figure III.15. Network of curves obtained by Polymeropoulos (1977) representing the logarithm of tunnel conductivity as a function of the thickness of the insulating monolayer l.

a) Al/Cn,Al junction
b) Al/Cn/Au junction
c) Al/Cn/Mg

By combining 3.11 and 3.12 we obtain:

$$\Delta h_x = x\,\Delta h \qquad (3\text{-}13).$$

We thus see that if for a given resistance R_o, the thickness of the interface h_o for increases of R_o by factors n, n^2, n^3, n^x correspond to increases of thickness Δh, $2\Delta h$,..., $x\Delta h$; it is for this reason that, besides the logarithmic scale of the electrical contact resistance, we have taken on figure III.14 an arbitrary scale of thickness, the thickness h_o corresponding to log R_c=1, Δh are taken in such

a fashion that the approximation 3.10 $\log\left(1 + \frac{\Delta h}{h_o}\right) \simeq \frac{\Delta h}{h_o}$ remains valid.

The function $\mu = f(\log R_c)$ can be written in the form of a sum of two functions: /116

$$\mu = f_1 + f_2\,(h) \qquad (3\text{-}14)$$

f_1 being a constant for a given test corresponding to the asymptotic value of the coefficient of friction toward which the curve approaches (3.14);
f_2 (h) is a more complex function for which we will determine the form

For f_1 we have taken the value of the coefficient of friction established at the end of five advance-returns of the sphere on the plane at the time of the execution of the manipulation which has allowed us to obtain curve 3.14.

$$f_1 = 0.11.$$

We will return to this hypothesis in the conclusion of this chapter.

III.2.3. Determination of the Analytical Expression of the Function

The curve $\mu_2 = f_2$ (h) presented in figure III.16 not being identifiable by a simple exponential, we have been induced to identify it with another type of function. For this, we refer to the literature. A certain number of theoretical friction models influence the thickness of the interface in the expression of the coefficient of friction (Lifshitz, 1960; Deryagin, 1934) in particular in the form $\mu = \frac{k}{h^n}$ with $1 \leq n \leq 6$.

We thus are going to attempt to identify f_2 (h) with a function of the type:

$$f_2\,(h) = \frac{k}{h^n} \qquad (3\text{-}15)$$

We observe that for h_o we have: /117

$$f_2(h_o) = \frac{K}{h_o^n} \qquad (3\text{-}16)$$

for $h_o + x\,\Delta h$ with $\frac{x\,\Delta h}{h_o} \ll 1$ we will have:

$$f_2(h_o + x\,\Delta h) = \frac{K}{(h_o + x\,\Delta h)^n} = \frac{K}{h_o^n} \cdot \frac{1}{\left(1 + x\frac{\Delta h}{h_o}\right)^n}$$

with

$$f_2(h_o + x\,\Delta h) = f_2(h_o) \cdot \frac{1}{\left(1 + x\frac{\Delta h}{h_o}\right)^n} \qquad (3\text{-}17)$$

we have: $\left(1 + x\frac{\Delta h}{h_o}\right)^n = 1 + n\,x\frac{\Delta h}{h_o} + C_n^2\,x^2\left(\frac{\Delta h}{h_o}\right)^2 + C_n^n\left(x\frac{\Delta h}{h_o}\right)^n$

since $\frac{x\,\Delta h}{h_o} \ll 1$, we can neglect the terms of degree greater than 2, we then obtain:

$$f_2(h_o + x\Delta h) = f_2(h_o) \cdot \frac{1}{1 + n\frac{x\Delta h}{h_o} + p\left(\frac{x\Delta h}{h_o}\right)^2} \qquad (3\text{-}18)$$

with $p = C_n^2$.

By expressing $f_2(h_o + y\Delta h)$ we also obtain:

$$f_2(h_o + y\Delta h) = f_2(h_o) \cdot \frac{1}{1 + n\frac{y\Delta h}{h_o} + p\left(\frac{y\Delta h}{h_o}\right)^2} \qquad (3\text{-}19)$$

from 3.18 and 3.19 we derive:

$$1 + n\frac{x\Delta h}{h_o} + p\left(\frac{x\Delta h}{h_o}\right)^2 = \frac{f_2(h_o)}{f_2(h_o + x\Delta h)} \qquad (3\text{-}20)$$

and

$$1 + ny\frac{\Delta h}{h_o} + p\left(\frac{y\Delta h}{h_o}\right)^2 = \frac{f_2(h_o)}{f_2(h_o + y\Delta h)} \qquad (3\text{-}21)$$

By multiplying both sides of 3.20 by the factor $-y^2/x^2$ then by adding the expression obtained in 3.21 we arrive at:

$$n\frac{\Delta h}{h_o} = \frac{f_2(h_o)\left\{\left[f_2(h_o + y\Delta h)\right]^{-1} \frac{y^2}{x^2}\left[f_2(h_o + x\Delta h)\right]^{-1}\right\} - \left(1 - \frac{y^2}{x^2}\right)}{\left(y - \frac{y^2}{x}\right)}$$

where $\left(1 - \frac{y^2}{x^2}\right) + n\frac{\Delta h}{h_o}\left(y - \frac{y^2}{x}\right) = f_2(h_o)\left\{\left[f_2(h_o + y\Delta h)\right]^{-1} - \frac{y^2}{x^2}\left[f_2(h_o + x\Delta h)\right]^{-1}\right\}$ (3-22) /118

The values of $f_2(h)$ for h_o, $h_o + x\Delta h$, $h_o + y\Delta h$, x et y being fixed, can be seen on graph 3.14.

We can thus calculate the product $n\frac{\Delta h}{h_o}$ for different values of x and y. The exponent n and the variation of thickness being constants, to verify if we also have a law of $\frac{k}{h^n}$ it suffices to verify over a large portion of the curve the constancy of the product $n\frac{\Delta h}{h_o}$.

Table III.1 groups the values calculated of $n\frac{\Delta h}{h_o}$ in the interval $[h_o - 6\Delta h, h_o + 5\Delta h]$ determined on the scale of the abscissa of curve 3.14, as well as the absolute uncertainties on the results. We observe that the values of the product are relatively constant over the portion of the curve studied. The mean value calculated from the results presenting a relative uncertainty lower than 15% is:

$$\boxed{n\frac{\Delta h}{h_o} = 0.15 \pm 0.02.}$$

TABLE III.1. VALUES OF THE PRODUCT $n \frac{\Delta h}{h_o}$ CALCULATED IN THE INTERVAL $[h_o - 5\Delta h, h_o + 5\Delta h]$.

h / h		$-5\Delta h$	$-4\Delta h$	$-3\Delta h$	$-2\Delta h$	$-\Delta h$
	$f_2(h)$ / $f_1(h)$	0,061 ± 0,002	0,047 ± 0,002	0,036 ± 0,001	0,031 ± 0,001	0,026 ± 0,001
$+5\Delta h$	0,012 ± 0,001	0,15 ± 0,02	0,15 ± 0,02	0,15 ± 0,02	0,15 ± 0,02	0,16 ± 0,06
$+4\Delta h$	0,014 ± 0,001	0,14 ± 0,03	0,14 ± 0,02	0,14 ± 0,02	0,14 ± 0,02	0,15 ± 0,006
$+3\Delta h$	0,015 ± 0,001	0,15 ± 0,03	0,15 ± 0,03	0,15 ± 0,03	0,15 ± 0,02	0,15 ± 0,06
$+2\Delta h$	0,017 ± 0,001	0,14 ± 0,05	0,14 ± 0,05	0,14 ± 0,04	0,15 ± 0,03	0,15 ± 0,05
$+\Delta h$	0,019 ± 0,001	0,15 ± 0,09	0,15 ± 0,09	0,15 ± 0,08	0,15 ± 0,07	0,16 ± 0,05
$-\Delta h$	0,026 ± 0,01	0,16 ± 0,09	0,16 ± 0,09	0,16 ± 0,01		
$-2\Delta h$	0,031 ± 0,001	0,16 ± 0,05	0,16 ± 0,05	0,16 ± 0,06		
$-3\Delta h$	0,036 ± 0,001	0,16 ± 0,03	0,16 ± 0,05			
$-4\Delta h$	0,047 ± 0,002	0,15 ± 0,05				

To calculate the mean nalue of $n \frac{\Delta h}{h_o}$ we only take into account the values whose relative uncertainty is less than 0.15.

III.2.4. Estimation of the Variation of Thickness

When h_1 and h_2 are two thicknesses corresponding to two values of electrical contact resistance R_{c1} and R_{c2}. We select h_2 such that $h_2=h_1+\Delta h$, it then suffices to observe by taking into account 3.7 that:

$$\log R_{c_2} - \log R_{c_1} = \delta h \left(\frac{1}{h_1} + \beta\right)$$

with

$$\lim_{\delta h \to 0} \frac{F_2(h_2) - F_2(h_1)}{\log R_{c_2} - \log R_{c_1}} = \frac{1}{\left(\frac{1}{h_1} + \beta\right)} \cdot F_2'(h_1)$$

or

$$F_2'(h_1) = -n \frac{K}{h_1^{n+1}} = -\frac{n}{h_1} F_2(h_1)$$

where

$$\lim_{\delta h \to 0} \frac{F_2(h_2) - F_2(h_1)}{\log R_{c_2} - \log R_{c_1}} = -\frac{n}{\left(\frac{1}{h_1} + \beta\right) h_1} \cdot F_2(h_1) \qquad (3\text{-}23)$$

/120

if we select two thicknesses h_3 and h_4 corresponding to two values R_{c3} and R_{c4} such that $h_4=h_3+\Delta h$, we will have in the same fashion:

$$\lim_{\delta h \to 0} \frac{F_2(h_4) - F_2(h_3)}{\log R_{c_4} - \log R_{c_3}} = -\frac{n}{\left(\frac{1}{h_3} + \beta\right) h_3} \cdot F_2(h_3) \qquad (3\text{-}24)$$

if we take:

$$h_3 = h_1 + m\,\Delta h \qquad (m\Delta h \ll h_1)$$

we have:

$$\frac{\left(\frac{1}{h_1} + \beta\right)}{\left(\frac{1}{h_3} + \beta\right)} \simeq 1$$

by dividing member to member 3.24 by 3.23 we obtain:

$$\lim_{\delta h \to 0} \frac{\frac{F_2(h_4) - F_2(h_3)}{\log R_{c_4} - \log R_{c_3}}}{\frac{F_2(h_2) - F_2(h_1)}{\log R_{c_2} - \log R_{c_1}}} = \frac{h_1}{h_3} \cdot \frac{F_2(h_3)}{F_2(h_1)}$$

if we take $h_1=h_0$ and $h_3=h_0+m\,\Delta h$:

$$\frac{\Delta h}{h_0} = m^{-1} \left(\lim_{\delta h \to 0} \frac{\frac{F_2(h_2) - F_2(h_1)}{\log R_{c_2} - \log R_{c_1}}}{\frac{F_2(h_4) - F_2(h_3)}{\log R_{c_4} - \log R_{c_3}}} \cdot \frac{F_2(h_3)}{F_2(h_1)} - 1 \right)$$

The mean value calculated from four points of the curve is

$$\boxed{\frac{\Delta h}{h_o} = 0.04 \pm 0.01}$$

III.2.5. Estimation of the Exponent n

The value of the product $n \frac{\Delta h}{h_o}$ found in chapter III.2.4 being $n \frac{\Delta h}{h_o} = 0.15 \pm 0.02$ with $\frac{\Delta h}{h_o} = 0.04 \pm 0.01$. We can calculate n. We find:

$$\boxed{n = 4 \pm 2}$$

III.3. Conclusion /121

At the time of shearing of an interface of sliding by monomolecular lubricant, we have demonstrated that the electrical transports in this were made by tunnel conduction. With these conditions, taking into account the results derived from the literature and certain hypotheses, we have been able to make a quantitative approach of the variations of thickness of the interface during sliding and define one of the aspects of the reduction of friction. The hypothesis according to which we have broken down the coefficient of friction in the form of two functions:

$$\mu = f_1 + f_2 (h) \text{ with } f_1 = 0.11$$

has been suggested to us by the results obtained by Hirst and Moore (1978) in E.H.D. These authors have demonstrated, from the model of viscosity of liquids of Eyring (1940), which in a contact subjected to a high rate of shearing (10^3-10^5 s^{-1}), the coefficient of traction T/W ($\equiv$coefficient of friction) due to the fluid contained in the interface has for an expression:

$$\frac{T}{W} = \frac{V_p}{V_\tau} - \frac{\tau_o}{p} \ln \left(\frac{\tau_o}{2\eta\dot{\gamma}} \right)$$

T = tangential force
W = normal load
τ_o = characteristic shearing stress of the product
V_τ = activation volume of the product under shearing
V_p = activation volume of the product under pressure
η = viscosity of the fluid
$\dot{\gamma}$ = rate of shearing.

For high pressures ($\simeq$1 GPa), the ratio T/W tends toward a limit value ($\lim_{p \to 0} \frac{T}{W} = \frac{V_p}{V_\tau}$) depending solely on the activation volumes V_p and V_τ of the product studied. In the majority of the cases studied by Hirst and Moore, $0.07 \leq \frac{T}{W} \leq 0.13$. The value $f_1 = 0.11$ which we have fixed /122 with the hypothesis is thus not aberrant, taking into account the results of Hirst and Moore, and would thus correspond, with the coefficient of limited friction, to a purely molecular contribution of the additive.

The contribution $f_2(h)$ which we have been able to identify for a function of the type $\frac{k}{h^n}$ with $z \leq n \leq 6$ can be reconciled with certain elementary friction theories (Lifshitz, 1960; Akmatov, 1966; Postnikov, 1978) involving interactions between condensed phases (electrodynamic interactions of $\frac{k}{h^n}$). This becomes significant when the surfaces in frictional contact are only separated by a very small thickness. As we have seen above, the ratio V_p/V_z is approximately 0.1 for a great number of products. This would thus signify that for a reducer of friction to be effective and produce coefficients of friction on the order of 0.1, this is capable of reducing the electrodynamic forces either by its physical properties (dielectric constant, ...) or by separating the pieces in frictional contact in sufficient fashion. This would appear to be in agreement with the results of Zisman (1957) and Hardy (1936), these having demonstrated for the series of linear fatty acids that coefficients of friction on the order of 0.1 were obtained from C12-C14 molecules, the coefficient of friction being greater than 0.1 for shorter hydrocarbon chains of acids ($T/W \simeq 0.3$ for a C8 acid(Hardy) and equal to 0.1 for longer chains $T/W=0.1$ for C12-C14... C18 acids (Hardy).

General Conclusions /123

During the work presented here, having the objective of the study of the reduction of friction by boundary lubrication, we have been able to define a number of significant points.

Application of the freezing fracturing technique to the study of the microscopic structure of lubricants has allowed us to obtain interesting results, particularly the forms in which the additives are dispersed within the base.

We have been able to demonstrate the influence of the physicochemical properties of the additive in solution in a pure base, such that the adsorption at the liquid-solid interface, constituted by friction pieces in contact with the lubricating solution, or the micellar dispersion of the additive within the base, on the reducing properties of friction of this.

Finally, we have been able to demonstrate specific properties of the interface in frictional contact studied:
-The electrical conduction of which this is the center has been able to be assimilated by non-standard conduction of tunnel type. This has allowed:
-on the one hand, with the hypothesis of the model of Bethe to study the relationship existing between the coefficient of friction and the variation of thickness of the interface;
-on the other hand, this type of electrical transport occurring at the level of the interface by sliding would theoretically allow us to study molecular transformations of the additive during frictional contact (inelastic tunnel electron spectroscopy).

REFERENCES

Akhmatov, A.S., "Molecular physics of boundary lubrication", Israel program for Scientific Translations, Jerusalem (1966). /124

Anderson, F.W., R.C. Nelson, and F.F. Farley, NLGI Spokesman 31, 252-254 (1967).

Archard, J.F., J. Appl. Phys. 24, 291 (1953); Proc. Roys Soc., series A 243, 190-205 (1957).

Bailey, A.I. and J.S. Courtney-Pratt, Proc. Roy. Soc., series A 227, 500-515 (1955).

Basset, D., "Etudes dès propritétés de frottement d'additifs fluores soluble dans les lubricants", [Studies of the friction porperties of fluoride additives soluble in lubricants], C.N.A.M. Thesis (1982) in press.

Benedetti, E.L. and P. Favard, "Freeze-etching techniques and applications", Société française de microscopie electronique (1973).

Bragg, W.L., Nature 115, 269 (1925); Proc. Roy. Inst. 24, 481 (1925).

Briscoe, B.J. and D. Tabor, Trans. Am. Soc. Lub. Engrs. 17, 158 (1974).

Brummage, K.G., Proc. Roy. Soc. 188, 414 (1947).

Calje, A.A., W.G.M. Agterof, and A. Vrij, "Micellization, solubilization and microemulsions", Volume 2, edited by K.L. Mittal, Plenum Press, 1977, pp. 779-790. /125

Candau, F., J. Boutillier, J.C. Wittmann, and S. Candau, "Physiochimie des composés amphiphiles", [Physicochemical amphiphilic compounds], CNRS INternational Colloquium, No. 938, Bordeaux-lac (1978).

Carnahan, N.F. and K.E. Starling, J. Chem. Phys. 51, 635 (1969).

Cazabat, A.M. and D. Langevin, "Light scattering in liquids and macromolecular solutions", pp. 139-155, edited by D.M. Corti and M. Giglio (1980).

Cazabat, A.M., D. Langevin, and A. Pouchelon, J. Coll. and Interf. Sci. 73 (1), 1.12 (1980).

Courtney-Pratt, J.S. and E. Eisner, Proc. Roy. Soc. Lond., series A, 238, 529-549 (1956-1957).

De Gennes, P.G., J. Chem. Phys. 60, 12 (1974).

Deryagin, B.V., Zh Fkh, 5, (9) (1934).

Desporte, J.H., (1982) in press.

Einstein, A., Ann. Physik 33, 1275 (1910). /126

Eyring, H., J. Chem. Phys. 4, 283-291 (1936).

Fleer, G.J., PhD Thesis, Wagenmyen, Netherlands (1971).

Fleer, G.J., L.K. Koopal, and J. Lyklema, Kolloid. Z. Z. Polym. 250, 689 (1972).

Furey, M.J., Wear 26, 369-392 (1973).

Furey, M.J., "Polymères et lubrification", [Polymers and lubrication], CNRS International Colloquium, No. 233, pp. 393-404 (1975).

Georges, J.M. et al, Wear 42, 217-228 (1977); J. Mech. Appl. 2, 231-266 (1978).

Germer, L.H. and K.M. Storks, Phys. Rev. 55, 648 (1939).

Goldblatt, I.L., Contract Report (1978).

Gramain, Ph., Makrom. Chem. 176, 1875 (1975).

Greenwood, J.A. and J.M. Tripp, Proc. Inst. Mech. Eng. 185, 625-631 (1970).

Greenwood, J.A. and J.P.B. Williamson, Proc. Roy. Soc., series A, 295, 300-319 (1966).

Gruner, F. and Lehmann, "Light scattering in liquids and macromolecular solutions", pp. 51-69, edited by D.M. Corti and M. Giglio (1980). /127

Gundlach, K.H. and J. Kadlec, Chem. Phys. Letters 25 (2), 293-295 (1973).

Hardy, W.B., Collected Scientific Papers, Cambridge University Press (1936).

Hertz, H., J. Reine Angew., Math. 92, 156 (1882).

Hirst, W. and A.J. Moore, Proc. Roy. Soc. Lond. A 365, 537-565 (1979).

Hoeve, C.A.J., J. Polym. Sci. 30, 361 (1970); J. Polym. Sci., part C, 34, 1 (1971).

Hoeve, C.A.J., A. Dimarzio, and P. Peyser, J. Chem. Phys. 42, 2558 (1965).

Holm, R., Electric contacts, Springen-Verlag (1967).

Israelachvilli, J. and D. Tabor, Wear, 24, 386-390 (1973).

Kawaguchi, M., K. Hayakawa, and A. Takahashi, Polym. J. 12 (4), 265-270 (1980).

Killmann, E., J. Eisenlauer, and M. Korn, J. Polym. Sci., Polym. Symp. 61, 413 (1977). /123

Killmann, E. and M.V. Kuzenko, Angew. Makrom. Chem. 35, 39 (1974).

Killmann, E. and G. Wiegand, Makrom. Chem. 132, 239 (1970).

Koppel, D.E., J. Chem. Phys. 57, 4814 (1972).

Langmuir, I., Met. Chem. Eng. 15, 468 (1916); J. Am. Chem. Soc. 39, 1848 (1917).

Lifshitz, E.M., "Electrodynamics of continuous media", Pergammon Press, 1960, pp.368.

Malin, M. and K. Vedam, Surface Science 456, 49 (1976).

Mann, B. and H. Kuhn, J. Appl. Phys. 42 (11), 4398-4405 (1970).

Mann, B., H. Kuhn, and L.V. Szentpaly, Chem. Phys. letters 8(1), 82-84 (1970).

Martin, J.M., State Doctoral Thesis, Lyon, No. 7827 (1978).

Menold, R., B. Luttge, and W. Kaiser, Adv. Coll. Interf. Sci. 5, 281-335 (1976). /129

Mindlin, R.D., J. Applied Mechanics, 259-268 (1950).

Moor, H., Z. Zellforsch 62, 546-580 (1964); Phil. Trans. Roy. Soc. Lond. B 261, 121-131 (1971).

Muller, Q., Proc. Roy. Soc. A 120, 437 (1928).

Ohrn, O.E., J. Polym. Sci. 17, 65 (1965).

Pefferkorn, E., R. Varoqui, and Ph. Dejardin, J. Coll. Interf. Sci. 63 (2), 353 (1978).

Peyrot, J. and J. Du Parquet, Mécanique, matériaux, électricité 316, 46-51 (1976).

Polymeropoulos, E.E., J. Appl. Phys. 48 (6), 2404-2407 (1977); Solid state communications 28, 863-885 (1978).

Polymeropoulos, E.E. and J. Sagiv, J. Chem. Phys. 69 (5), 1836-1847 (1978).

Postnikov, S.N., "Electrophysical and electrochemical phenomena of friction, cutting and lubrication"; Van Nostraud Reinhold Co., Chapter III, 1978, pp. 113-114.

Pusey, P.N., "Light scattering in liquids and macromolecular solutions", edited by D.M. Corti and M. Giglio, pp. 1-29 (1980); J. Phys. A (G.B.) 8, 1433 (1975).

Rash, J.E. and C.S. Hudson, "Freeze fracture: methods, artifacts and interpretations", Raven Press (1979).

Reda, A.A., Wear 32, 115-116 (1975).

Rigelhuth, R.D. and R.C. Watkins, J. Inst. of Petroleum 58 (562), 188-192 (1972).

Riehle, U., Dissertation No. 4271, Eigden. Tech. Hochschule, Zurich (1968).

Schilling, A , "Motor oils and engine lubrication", Scientific publications (G.B.) Ltd. (1968).

Silberberg, A., J. Phys. Chem. 66, 1872-1883 (1962); J. Phys. Chem. 66, 1884-1909 (1962); J. Chem. Phys. 46 (3), 1105-1114 (1966); J. Chem. Phys. 48 (7), 2835-2851 (1967); "Polymers et lubrication, [Polymers and lubrication], CNRS International Colloquium, No. 233, 81-86 (1975).

Sjostrand, F.S., J. of Ultrastructure Research 69, 378-420 (1979).

Smoluchowski, M., Ann. Physik. 25, 205 (1908); Phil. Mag. 23, 165 (1912).

Sommerfeld, A. and H. Bethe, "Handbuch der Physik", [Handbook of Physics], edited by H. Geiger and K. Schal, Vol. 24/2, 1933, pp. 450.

Strazielle, C. and G. Weill, Technique de l'Ingénieur, P 1065, 1-22.

Tabor, D., "Surface and colloid science", edited by E. Matijevic, Vol. 5, John Wiley (1972).

Takahashi, A., M. Kawaguchi, H. Hirota, and T. Kato, Macromolecules 13, 884-889 (1980); "Adhesion and adsorption of polymers", edited by Leing Huang Lee, part B., 1980, pp. 729-749.

Thiele, E.J., J. CHem. Phys. 39, 474 (1963).

Timoshenko, S. and J.N. Goodier, "Theory of elasticity", McGraw Hill Book Company (1951).

Trillat, J.J., C.R. Acad. Sciences, Paris No. 180, 280 (1925).

Tripp, J.H., R.F. Snowball, and J.B.P. Williamson, J. APpl. Phys. 38 (6), 2439-2441 (1966-67).

Tonck, A., J.M. Martin, Ph. Kapsa, and J.M. Georges, Tribology international, 209-213 (1979).

Vanhelden, Thesis (1980).

Weber, T.A. and E. Helfand, Macromolécules 9 (2), 311 (1976).

Wilson, R.W., Proc. Phys. Soc. B 68, 625 (1955). /132

Zisman, W.A., "Friction and Wear", edited by E. Davies, pp. 110-148 (1957).

Appendix A

/133

A-1 Description of the Sphere-Plane Simulator

Figure A-1 demonstrates the installation necessary to carry out measurements of electrical contact resistance and friction force.

The system for measurement of the friction force is detailled in figure A-2. It is composed:
-of a movable portion constituted by the plane-support P, being able to be propelled by a uniform rectilinear movement, on which is attached the plane P_a used for the experiment;
-of an attached portion constituted by arm b on which is attached the piece with the front hemispheric end P serving for frictional contact.

Measurement of the friction force is carried out during sliding, by deformation of the force pick-up q (piezo-electric quartz of stiffness 50 N/μm). The stiffness of the measurement system is 1 N/μm.

A-2 Response of the Measurement System to a Known Impulse

The objective of this study is to see if the chain of measurements faithfully reproduces that which occurs in the interface, this in order to avoid making improper interpretations. To study the response of the system to a known impulse, two methods were possible:
-mechanically modelling of the arms and simulation;
-experiment.

Taking into account the complexity of the chain of measurements, we have preferred to study its response experimentally. For this, it is necessary to apply between the piece and the plane an impulse of known form and value.

A-2.1 Description of the Experiment

/136

Figure A-3 demonstrates the assembly of the installation which has necessitated this experiment.

In order to apply a known impulse between the plane and the piece, we have had recourse to a cylindrical magnet A, of the same size as the pieces used, attached to the base, and to an electromagnet B, of the same mass as the cuvette-plane system, attached on the plane support P (see figure A-4).

The force which we would like to apply between the two parts of the system (arm + piece and plane + plane support) is produced by passage of a current in the coil of electromagnet B. The generator assembly of frequency + power amplifier (g + A figure A-3) allows us to send into the coil a known and modulated current i (in our case we will use a square signal).

/134

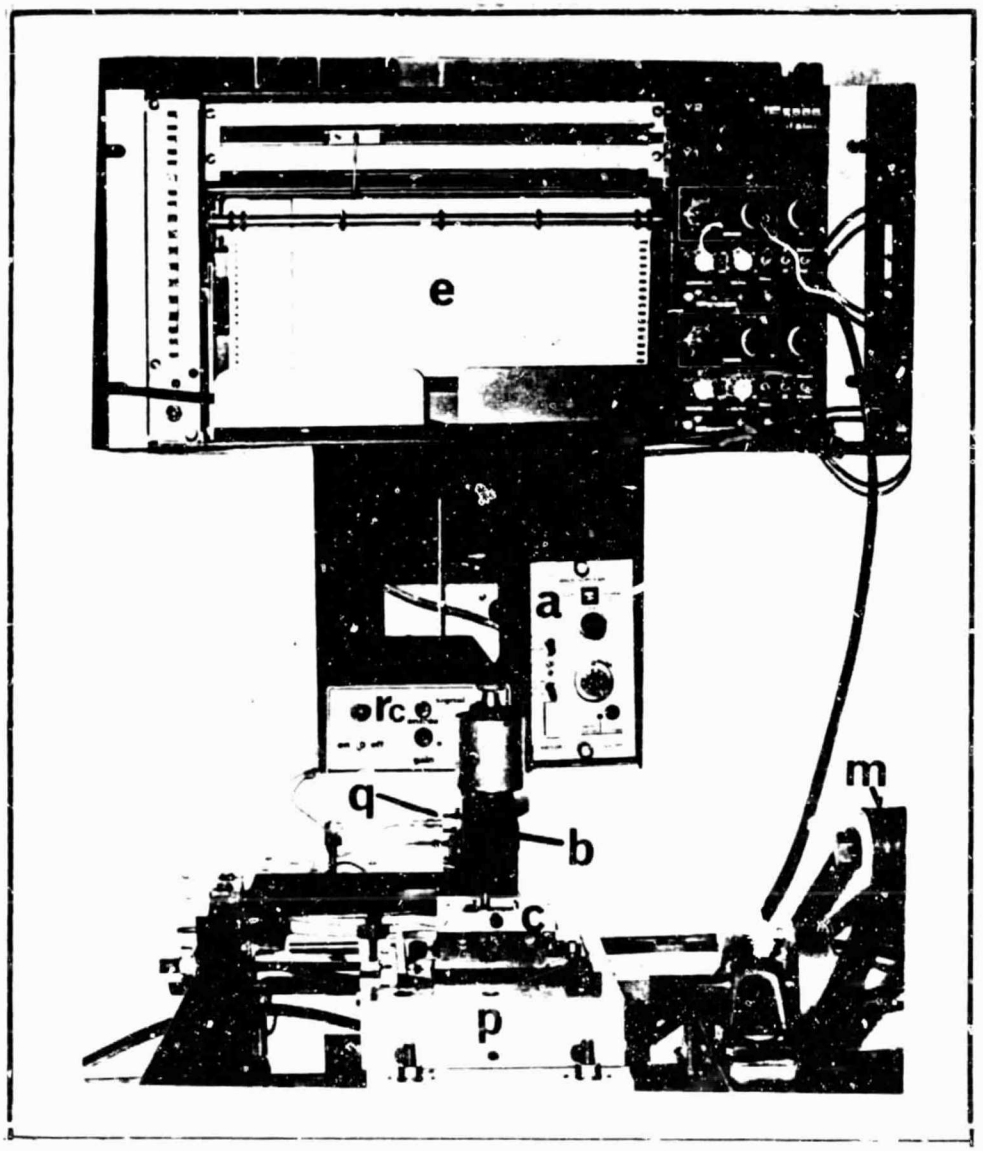

Figure A-1. Photograph of the installation used for our friction tests.

p=movable plane support; m=drive motor of the plane; e=recording;
c=cuvette containing the plane and lubricant; a=load amplifier;
b=measurement arms of the friction force;
q=force pick-up constituted by a piezo-electric quartz;
rc=measurement circuit of electrical contact resistance.

/135

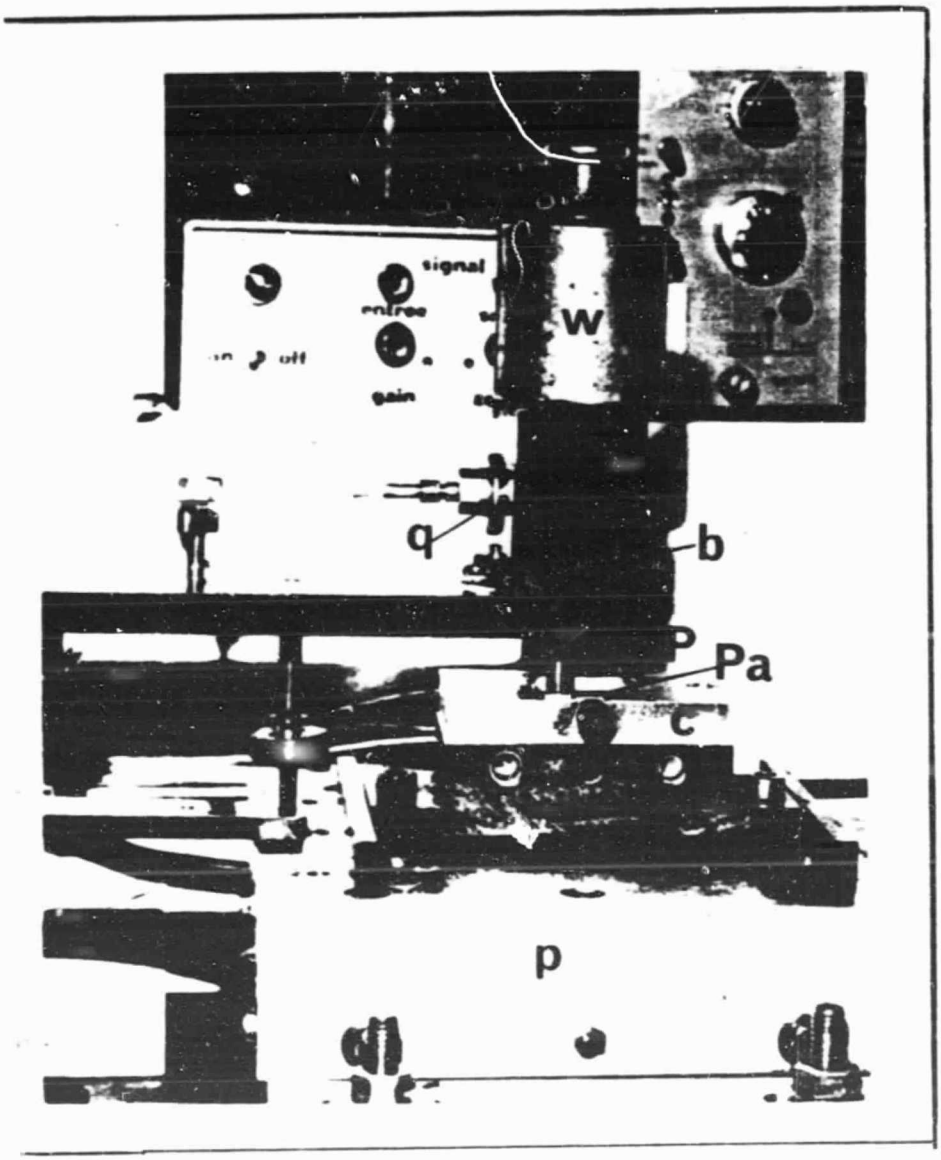

Figure A-2. Detail of the measurement arm and plane.

w=normal load applied on the contact; P_a=100 steel plane;
b=measurement arm; a=piezo-electric quartz;
c=cuvette containing the plane and lubricant;
P=100 steel piece with hemispheric end;
p=movable support of the plane.

C-2

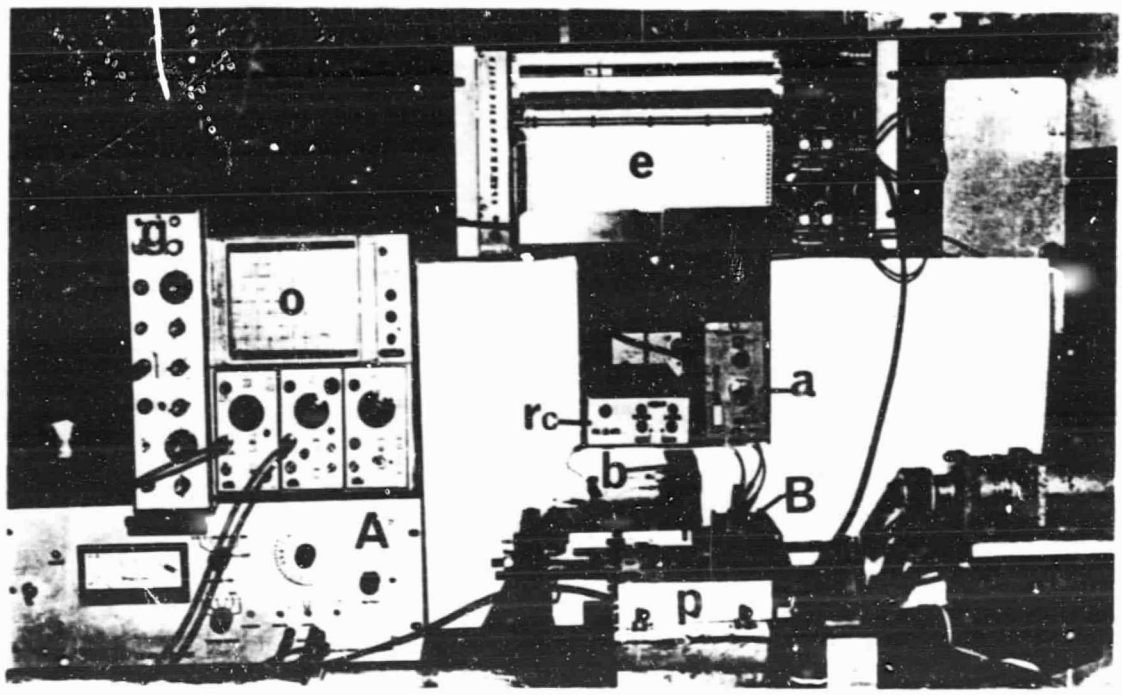

Figure A-3. Installation necessary for the study of the impulse response of the measurement system. /137

g= frequency generator ; a=load amplifier ; A=power amplifier;
b=measurement arm of friction force; o=cathode oscilloscope;
B=coil constituting the electromagnet; c=recorder;
p=movable support of plane.

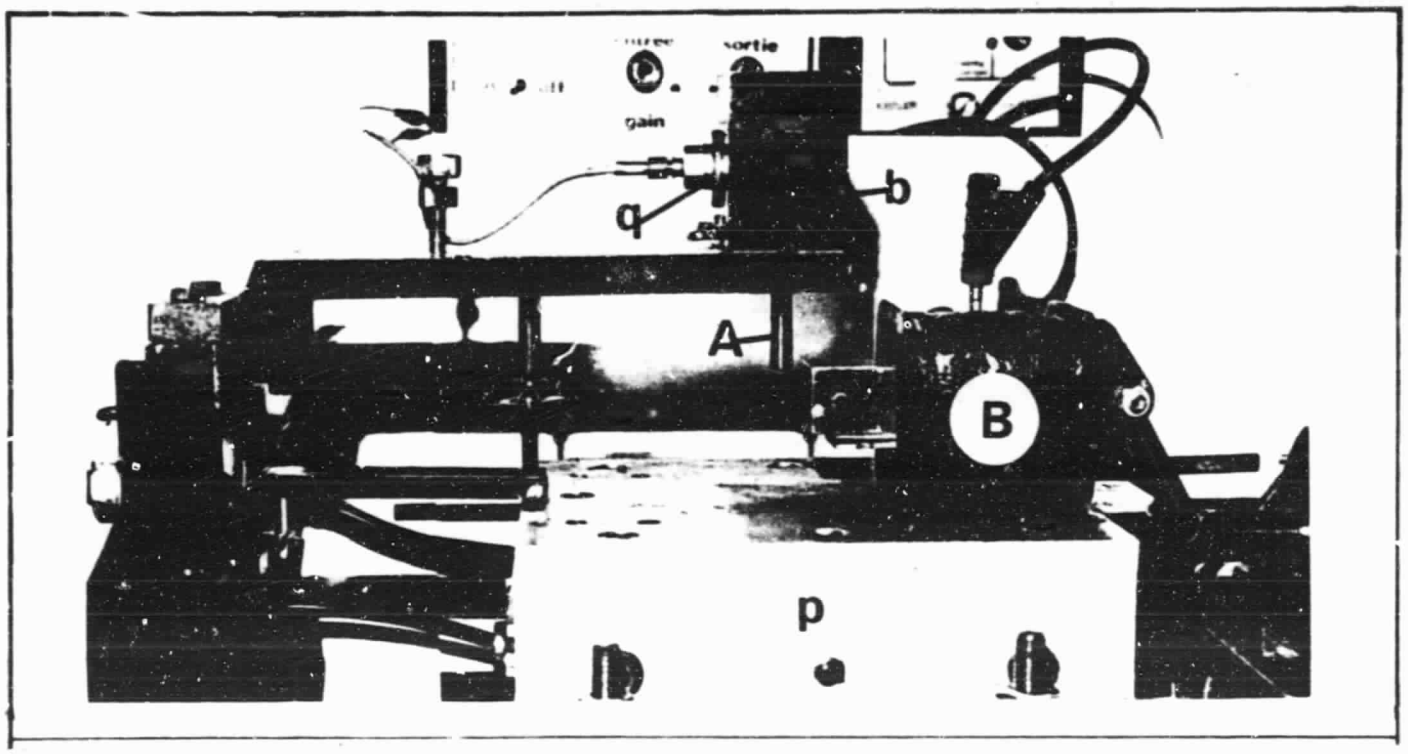

Figure A-4. Detail of the system allowing the study of the impulse response of the chain of measurements. /138

b=measurement arm of the friction force;
q=force pick-up: piezo-electric quartz;
A=cylindrical magnet in place of the piece;
B=coil of the electromagnet;
p=movable support of the plane.

The force F exerted between the two parts of the system is a function of the intensity I of the current passing into the coil:

$$F = 10^{-7} \pi n I S$$

B=intensity of magnetic induction
S=cross section of the piece subjected to the attraction of the electromagnet
n=number of spirals per meter of the coil
I=intensity of current passing into the coil.

During our tests, we will thus record the intensity of the current passing into the coil and the signal delivered by the force pick-up.

A-2.2. Results and Discussion

Figure A-5 presents the recordings on cathode oscilloscope of the current passing into the coil and the signal delivered by the quartz.

We see on the assemblage of plates that the response of the measurement system follows very well the impulse applied between the arm and the plane represented by the current passing into the coil (response of the arm > 1 kHz). This thus allows us to eliminate with our conditions the possibility of deformation of the original signal by the measurement system. /140

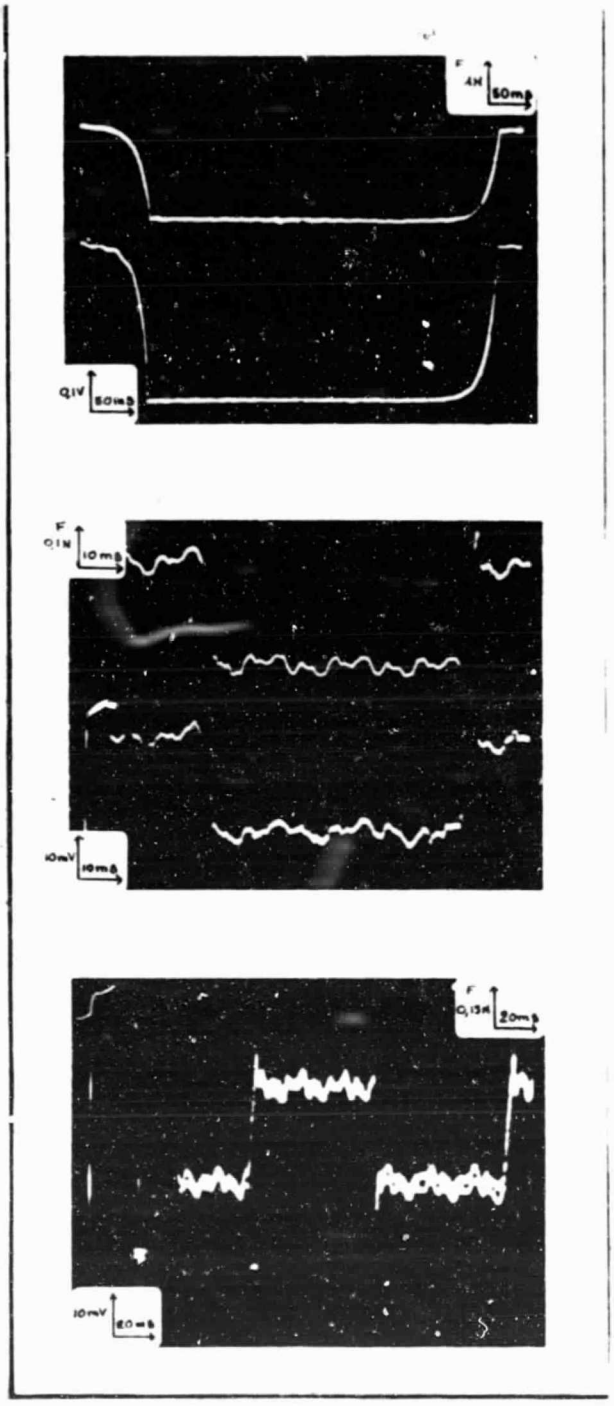

Figure A-5 Simultaneous recordings of the current passing into the coil (thus of the force applied) and the signal furnished by the force pick-up.

a) the amplifier at the exit of the generator amplified by pressure:
-the graph above corresponds to the signal furnished by the quartz;
-that of the bottom corresponds to the current passing in electromagnet.
b) the amplifier at the end of the frequency generator amplified current:
-graph above corresponds to the signal furnished by the quartz;
-graph below corresponds to the current passing into the coil.
c) superimposition of the current passing into the electromagnet and the signal furnished by the quartz.